The Structure and Kinematics of the Nankai Trough Accretionary Prism, Japan

By

Joe D. Kington IV

A dissertation submitted in partial fulfillment of
the requirements for the degree of

Doctor of Philosophy
(Geoscience)

at the
UNIVERSITY OF WISCONSIN–MADISON
2012

Date of final oral examination: 6/22/12

The dissertation is approved by the following members of the Final Oral Committee:
Harold J. Tobin, Professor, Geoscience
Laurel B. Goodwin, Professor, Geoscience
Herbert F. Wang, Professor, Geoscience
Clifford H. Thurber, Professor, Geoscience
David J. Hart, Associate Professor, Wisc. Geological and Natural History Survey

"If you don't care where you are, then you ain't lost."

—`/usr/bin/fortune`

ACKNOWLEDGMENTS

I would like to thank the many people who have aided me with this work:

- My advisor Harold and my committee members (Laurel Goodwin, Cliff Thurber, Herb Wang, and Dave Hart).
- My research group (Matt Knuth, Carolyn Streiff, Joanne Tudge, Kyle Federicks, Susanna Webb, and Tamara Jeppson) for reading many early drafts and for many helpful discussions.
- My mother for constantly encouraging my curosity and providing moral support through twelve years of college and grad school.
- Most of all, my wife, JoAnn Gage for many helpful discussions about geomechanics and structural geology, reading (and greatly improving) several drafts, and constant moral support.

This work was funded by NSF award OCE-0800653.

TABLE OF CONTENTS

Page

Page

Page

LIST OF FIGURES

Figure Page

ABSTRACT

Subduction zone frontal prisms are among the most tectonically dynamic environments on Earth. Accretionary frontal prisms contain a fold and thrust belt comprised of sediments transferred from the subducting plate. 3D seismic data acquired as a part of the Nankai Trough Seismogenic Zone Experiment provides a unique opportunity to study accretionary prism processes at a type locality for sediment-dominated accretionary prisms. My research focuses on three aspects of the structure of the outer wedge fold and thrust belt using 3D seismic imaging.

In Chapter 2, I investigate the structural evolution of the outer wedge. Based on the geometry of thrust sheets in the outer wedge, the décollement has ramped up and then back down within the incoming sedimentary section. This has resulted in an unusually thick underthrust sediment volume, which has caused uplift and mass wasting $\sim$30 km landward of the deformation front. I hypothesize that changes in the depth of the décollement are due to the subduction of a basement high beneath the outer wedge $\sim$25 km to the east of the study area. This suggests that basement features may be associated with anomalously thick underthrust sediments for a significant distance along-strike.

In Chapter 3, I estimate the shortening accommodated by a zone of out-of-sequence thrusting within the outer wedge. Bed-length balancing of the structures in the outer wedge suggest that the outer wedge has accommodated 99$\pm$10 km of shortening in the last $\sim$2.3 myr, 34$\pm$17 km of which has been accommodated by a zone of out-of-sequence thrusting. Kinematic modeling of syn-kinematic sediments in the forearc basin indicates

that the landward-most structure in the out-of-sequence thrust zone has accommodated 14.6±1.8 km of the total shortening within the zone. However, our results demonstrate that uplift of the forearc and activity on the landward out-of-sequence thrust must have began at ∼0.9 Ma and continued until sometime younger than 0.5 Ma. This timing of forearc uplift matches the timing of the passage of a nearby basement high beneath the outer wedge. This suggests that out-of-sequence thrusting on the landward branch of the out-of-sequence thrust zone may have initiated in response to the subduction of the basement high.

In Chapter 4, I examine the variability in the stress state of the outer wedge. Previous work has inferred an extensional stress state near a series of IODP drillholes using borehole breakouts and core-based observations. However, borehole-based methods cannot assess the spatial or temporal variability in stress state. Arrays of small (<100 m throw) faults imaged by 3D seismic provide a constraint on how the stress state varies throughout the outer wedge. Paleo-stress inversions based on these faults demonstrate that most sets of faults are compatible with the same orientations, but not relative magnitudes, of the principal stress axes. Based on the distribution of strike-slip and normal faults, most of the wedge has been dominated by transpressional failure, while normal faults are restricted to discrete regions. Furthermore, normal faulting is locally coeval with strike slip faulting. This suggests that the temporal variability in the stress state is larger than the difference between the two smallest principal stresses. Therefore, normal faulting is a result of local perturbations to the average transpressional stress state, rather than due to collapse of the outer wedge, as has been previously suggested.

Chapter 1

Introduction

1.1 Motivation

Subduction zones account for 90% of global seismic moment release [*Pacheco and Sykes*, 1992]. Furthermore, subduction zone earthquakes on the plate boundary megathrust often produce damaging tsunamis. Frontal prisms, whether accretionary or non-accretionary, lie updip of the seismogenically locked zone. However, their structure influences coseismic slip in two ways: 1) The structure of the frontal prism controls the updip extent of coseismic rupture, which plays a key role in tsunamigenesis. 2) Frontal prisms influence the input material for the deeper, seismogenic portions of the subduction zone via underthrusting of sediments and subduction erosion [*e.g. von Huene and Scholl*, 1991; *Tobin and Saffer*, 2009].

Recent events have highlighted the role that frontal prisms play in the seismic cycle. Frontal prisms were traditionally thought to be aseismic and to form the up-dip limit of coseismic slip due to the strain-strengthening properties of frontal prism rocks [*e.g. Byrne et al.*, 1988]. However, *Ito and Obara* [2006a] have detected very-low-frequency earthquakes within the Nankai Trough accretionary prism, suggesting that this type of earthquake may initiate within the frontal prism. Furthermore, recent observations of coseismic rupture to the surface along the trench axis during the 2004 Sumatra-Andaman Islands earthquake [*e.g. Henstock et al.*, 2006] and the 2011 Tohoku-Oki earthquake [*e.g. Lay et al.*, 2011] demonstrate that coseismic slip may propagate into and through frontal prims. Additionally, *Park et al.* [2002] and others have suggested that the 1944 Tonankai earthquake may have ruptured to the surface along a steeply-dipping splay fault within the Nankai Trough accretionary

prism. The updip limit of coseismic slip influences the amount of seafloor displacement and the tsunamigenic potential of an earthquake. Therefore, detailed investigations of the shallow structures on which coseismic slip may propagate into frontal prisms increases our understanding of the tsunami hazard along convergent margins.

In addition to potentially slipping during seismic rupture, frontal prisms influence the structure and composition of the seismogenic zone. Accretionary prisms typically contain a well-developed fold and thrust belt composed of sediments from the subducting plate [*e.g. von Huene and Scholl*, 1991]. The structure of this fold and thrust belt controls which sediments reach the seismogenic zone and which sediments are accreted to the upper plate [*e.g. Byrne and Fisher*, 1990]. Furthermore, the deformation processes operating within the accretionary prism influence the structure and composition of the material that is subducted to seismogenic depths [*e.g. Moore and Saffer*, 2001]. In erosional prisms, material from the frontal prism is directly subducted and likely influences seismogenesis [*von Huene et al.*, 2004]. Therefore, parameters thought to play an important role in seismogenesis such as the pore pressure, thickness, and composition of sediments in the seismogenic zone are strongly influenced by the development of the frontal wedge [*Byrne and Fisher*, 1990; *Bangs et al.*, 2009b; *Tobin and Saffer*, 2009; *Saffer*, 2010].

For these reasons, the structure, kinematics, and deformation processes of fold and thrust belts within frontal prisms are key research topics at the intersection of geology and geophysics. In this work, I focus on the structure and kinematics of the Kumano Basin region of the Nankai accretionary prism in southwestern Japan.

1.2 Nankai Trough

The Nankai Trough in southwestern Japan has a 1300 year historical record of damaging earthquakes [*Ando*, 1975] and long history of scientific investigation. The Nankai accretionary prism is often used as a type example of a sediment-dominated accretionary prism. Therefore, the Nankai Trough and provides an excellent natural laboratory to study subduction zone processes.

The Nankai accretionary prism has been the focus of three Ocean Drilling Program (ODP) and Integrated Ocean Drilling Program (IODP) transects: the Ashizuri transect in the 1980's and 2000, the Muroto transect in 1990 and 2000-2001, most recently, the Nankai Trough Seismogenic Zone Experiment (NanTroSEIZE) transect (2007-present) in the Kumano Basin region of the Nankai Trough [*Moore et al.*, 1990; *Screaton et al.*, 2002; *Tobin et al.*, 2009] (Fig 2.1). The Kumano Basin region lies offshore of the Kii Peninsula in southwestern Japan, where the Philippine Sea plate subducts beneath the Amur Plate at 6 cm/yr at an azimuth of 300°, roughly 30°oblique to the trench [*DeMets et al.*, 2010]. Seven IODP expeditions have been completed in the area as a part of NanTroSEIZE—an ongoing multiyear project to characterize and instrument the seismogenic zone of a plate boundary fault in a subduction zone [*Tobin and Kinoshita*, 2006]. This study focuses on the region of the NanTroSEIZE transect.

The roughly 100 km wide, sediment-dominated accretionary prism and forearc basin in the Nankai Trough can be divided into three regions: 1) the active fold and thrust belt, termed the outer wedge, 2) the older, inactive fold and thrust belt, termed the inner wedge, and 3) the forearc basin overlying the inner wedge. In the Kumano basin region, the outer and inner wedges are divided by a zone of out-of-sequence thrusting. Coseismic rupture inversions for the Mw 8.2 Tonankai earthquake in 1944 event suggest that slip extended to exceptionally shallow depths, roughly coincident with the zone of out-of-sequence thrusting [*Tanioka and Satake*, 2001a; *Ichinose et al.*, 2003; *Baba and Cummins*, 2005]. *Park et al.* [2002] suggested that a fault within the zone of out-of-sequence thrusting may have slipped coseismically and NanTroSEIZE was designed, in part, to investigate this possibility [*Tobin and Kinoshita*, 2006].

As a precursor to IODP drilling as a part of NanTroSEIZE, a 3D reflection seismic survey was conducted by a Japan/US team through commercial contract in 2006 over a 12 by 56 km area from the trench axis back into the foreland basin [*Moore et al.*, 2007, 2009]. After an initial pre-stack time migration, a velocity model was developed at the Japan Agency for

Marine Earth Science and Technology Institute for Research and Earth Evolution (JAMSTEC-IFREE), using constraints from ocean bottom seismometers in the area [*Park et al.*, 2010]. A pre-stack depth migration was then applied to the data [*Moore et al.*, 2009]. This depth-migrated 3D seismic volume is the primary observational dataset for this work, aided by regional 2D seismic lines and data from IODP drilling in the area.

1.3 Problem Statement

Most of the previous work on the structure and kinematic history of the outer wedge in the Kumano Basin region has focused on either broad, regional interpretations [*e.g. Park et al.*, 2002; *Moore et al.*, 2007, 2009] or highly detailed studies focused near IODP drilling locations [*e.g. Screaton et al.*, 2009; *Gulick et al.*, 2010]. There is a need to use the wealth of available reflection seismic data to bridge the two scales of observation and provide an integrated interpretation of the structure and kinematic history of the outer wedge. This provides context for ongoing and future work by numerous researchers as a part of NanTroSEIZE.

In addition to site-specific concerns, the outer wedge of the Nankai Trough provides an excellent natural laboratory to study general accretionary prism mechanics. The highly detailed 3D reflection seismic volume represents a unique opportunity to investigate fold and thrust belt kinematics, accretionary prism morphology, and sedimentation in slope, trench, and forearc basin environments.

In this dissertation I: 1) investigate the structural evolution of the outer wedge fold and thrust belt and develop a model for its formation, 2) estimate the shortening accommodated by the zone of out-of-sequence thrusting and examine its role in the development of the outer wedge, and 3) constrain the spatial and temporal variability in the stress state of the outer wedge.

Chapter 2

Along-strike Influence of Subducting Basement Topography: Structural Evolution of the Nankai Trough Accretionary Prism in the Kumano Basin Region

Abstract

Reflection seismic interpretation in the vicinity of the NanTroSEIZE transect in the Nankai Trough, Japan documents features of the accretionary prism's outer wedge, shedding light on the structural development of this convergent margin. The thickness of the thrust sheets within the fold and thrust belt systematically varies from 2 km to less than 1 km. We interpret this to be a consequence of changes over time in the depth of the décollement in the incoming stratigraphic sequence. These changes in the décollement depth have resulted in an up to 1 km thick volume of sediments underthrust beneath the active décollement, thinning updip and along-strike to the southwest. The underthrust package is currently located near the landward end of the outer wedge, beneath a piggyback slope basin. The northeastern side of this piggyback basin has undergone recent uplift which has a magnitude and extent that is inconsistent with movement on any nearby structures. However, the extent and geometry of the underthrust sediment body is consistent with that of the uplifted region of the piggyback basin. Therefore, we infer that uplift resulted from the décollement riding up and over the thickened underthrust sediments. A basement high is not present beneath the thin thrust sheets' restored position. Therefore, the change in the depth of the décollement cannot have resulted from a local basement topographic feature. Similarly, the presence of thick underthrust sediments beneath this same location suggests

that the change in thickness of the thrust sheets cannot be explained by a rapid thinning of the incoming stratigraphic sequence. We ascribe the temporary upward ramping of the décollement to the along-strike effects of the nearby western end of the paleo-Zenisu ridge passing beneath the outer wedge of the accretionary prism. As the paleo-Zenisu ridge would have impacted the trench axis approximately 25 km northeast of this area given present-day plate motions, this implies that a buried topographic feature may be associated with a large region of thick underthrust sediments, potentially affecting the extent and structure of the seismogenic zone.

2.1 Introduction

As a part of the Nankai Trough Seismogenic Zone Experiment (NanTroSEIZE), substantial recent work has focused on the Kumano Basin region of the Nankai Trough, particularly on whether an out-of-sequence fault system at the rear of the outer wedge is still active and may have slipped coseismically in historic events [e.g., *Park et al.*, 2002; *Moore et al.*, 2007, 2009; *Strasser et al.*, 2009] (Fig 2.1). The development of an out-of-sequence fault system and other structural features observed in the outer wedge need to be evaluated in the context of the kinematic history of the fold and thrust belt and the regional tectonic history. Otherwise, it is difficult to decouple the influence of unique events in the evolution of the accretionary prism from ongoing processes that may be generic to accretionary prism evolution. For this reason, an accurate understanding of the kinematic evolution of the outer wedge is a prerequisite for using this locality as a model for other, less well studied regions.

Active fold and thrust belt systems in accretionary prisms, while generally aseismic, influence the input material for the deeper, seismogenic portions of the subduction zone via underthrusting of sediments and subduction erosion [e.g. *von Huene and Scholl*, 1991; *Tobin and Saffer*, 2009]. Parameters such as the pore pressure, thickness, and composition of underthrust sediments are strongly influenced by the development of the fold and thrust belt and are thought to play an important role in controlling seismogenesis [*Byrne et al.*,

1988; *Byrne and Fisher*, 1990; *Bangs et al.*, 2009b; *Saffer*, 2010]. Additionally, the structure of the outer wedge may influence the geometry and extent of the updip limit of coseismic slip [*Cummins and Kaneda*, 2000; *Park et al.*, 2002; *Nakanishi et al.*, 2008]. Therefore, understanding the structural history and deformation processes in the outer wedge provides important constraints on the structure and composition of the seismogenic zone at depth.

This study aims to 1) document the structural evolution of the Kumano outer wedge, 2) illustrate the effects of past and ongoing tectonic events, and 3) provide geologic context for other studies in the area. To accomplish this, we use 3D reflection seismic data to illuminate the present-day structure of the outer wedge domain of the Nankai accretionary prism seaward of the Kumano Basin and investigate the kinematics that led to its formation. We present a new 3D structural interpretation of the outer wedge. Then, by correlating this regional-scale structural interpretation with the stratigraphy of slope basins in the outer wedge, we are able to infer both the past and recent kinematics of the outer wedge fold and thrust belt.

2.2 Tectonic Setting and Previous Work

2.2.1 Nankai Trough

The Nankai Trough is one of the most thoroughly investigated subduction zones in the world and provides an excellent natural laboratory to study subduction zone processes and accretionary prisms. The ∼100 km wide, sediment-dominated accretionary prism and forearc basin in the Nankai Trough have been the focus of three Ocean Drilling Program (ODP) and Integrated Ocean Drilling Program (IODP) transects: the Ashizuri transect in the 1980's and 2000, the Muroto transect in 1990 and 2000-2001, and most recently, the NanTroSEIZE transect (2007-present) in the Kumano Basin region of the Nankai Trough [*Moore et al.*, 1990; *Screaton et al.*, 2002; *Tobin et al.*, 2009] (Fig 2.1). The Kumano Basin region lies offshore of the Kii Peninsula in southwestern Japan, where the Philippine Sea plate subducts beneath the Amur Plate at a rate of ∼6 cm/yr with an azimuth of ∼300°, roughly 30°oblique to the trench [*DeMets et al.*, 2010] (Fig 2.2). Seven IODP expeditions have been

completed as a part of NanTroSEIZE—an ongoing multiyear project to characterize and instrument the seismogenic zone of a plate boundary fault in a subduction zone [*Tobin et al.*, 2009]. These expeditions provide data from thirteen drilling locations (Fig 2.2).

2.2.2 Paleo-Zenisu Ridge

The subducting Philippine Sea Plate has irregular basement topography and contains numerous basement ridges and isolated seamounts (Fig 2.1). The influence of basement topography on the development of the Nankai Trough accretionary prism has long been recognized, and a subducted seamount has been imaged beneath the accretionary wedge in the Muroto region, ∼200 km west of our study area [*Park et al.*, 1999]. To the east of the Kumano Basin area, a thrust within the oceanic crust forms the Zenisu Ridge: a basement-cored uplift with approximately 1-2 km of topographic relief [*Lallemant et al.*, 1989] (Fig 2.2). Magnetic anomalies and regional 2D seismic lines indicate that a similarly sized basement high, referred to as the paleo-Zenisu ridge, has been subducted and currently lies approximately 30 km landward of the trench axis at around 6-8 km depth [*Le Pichon et al.*, 1996; *Park et al.*, 2003; *Kodaira*, 2003]. The western tip of this ridge can be clearly identified in regional 2D reflection seismic lines and comes within 10 km of the NanTroSEIZE transect (Fig 2.2) [*Park et al.*, 2003].

2.2.3 Recent Megathrust Earthquakes and the Megasplay

The most recent great subduction zone earthquakes in the Nankai Trough ruptured adjacent plate-boundary segments in the 1944 Mw 8.2 and 1946 Mw 8.4 events (Fig 2.1) [*Ando*, 1975; *Tanioka and Satake*, 2001a, b]. Coseismic rupture inversions for the 1944 event suggest that slip extended to exceptionally shallow depths, causing extensive uplift of the forearc basin, and produced a large tsunami [*Cummins and Kaneda*, 2000; *Tanioka and Satake*, 2001a, b; *Ichinose et al.*, 2003; *Baba and Cummins*, 2005]. The structure of the plate boundary fault at the updip end of the seismogenic zone is hypothesized to have played a major role in producing anomalously shallow coseismic slip [*Park et al.*, 2002].

In the Kumano Basin region, a thrust fault branching from the interpreted plate interface reflector, termed the megasplay, is inferred at depth based a prominent reflector in reflection seismic data dipping around $\sim$15°and intersecting the primary plate boundary fault at around 10 km depth [*Park et al.*, 2002; *Moore et al.*, 2007; *Bangs et al.*, 2009a]. At $\sim$7 km depth, the megasplay is interpreted to bifurcate into two out-of-sequence thrust (OOST) splays which reach the surface at the rear of the outer wedge (Figs 2.3 & 2.4) [*Moore et al.*, 2007]. The seaward terminus of coseismic slip is approximately coincident with the seaward-most OOST splay based on geodetic and tsunami inversions [*Cummins and Kaneda*, 2000; *Baba and Cummins*, 2005]. This suggests that the megasplay fault and the OOSTs it connects to may have slipped coseismically and contributed to forearc uplift, potentially affecting the magnitude of the resulting tsunami [*Park et al.*, 2002; *Moore et al.*, 2007; *Bangs et al.*, 2009a]. The NanTroSEIZE study area spans the updip terminus of slip for the 1944 earthquake, and NanTroSEIZE was partly designed to investigate the possibility of coseismic slip propagating onto the OOSTs that divide the inner and outer wedge [*Tobin and Saffer*, 2009].

Out-of-sequence motion on the seaward OOST is thought to have initiated around 1.95 Ma, based on dates from IODP coring (Fig 2.4) [*Strasser et al.*, 2009]. This fault's tip is covered by undeformed sediments dating to $\sim$1.24 Ma, leading [*Strasser et al.*, 2009] to conclude that it has been inactive since that time. However, based on the subtle deformation of sediments above the tip of the thrust post-dating 1.24 Ma, *Kimura et al.* [2011] hypothesized that the fault may be acting as a blind thrust. This implies that slip on the fault may still be occurring at depth and is being accommodated as diffuse deformation closer to the surface [*Kimura et al.*, 2011]. Other workers have suggested that activity may have shifted to one of the other, more steeply dipping thrust faults in the hanging wall of the drilled fault (Fig 2.4) [*Moore et al.*, 2007; *Strasser et al.*, 2009].

2.2.4 Low-Velocity Zone in the Outer Wedge

Multiple workers have recognized an approximately 2 km thick low-velocity zone in the landward-most portion of the outer wedge between the oceanic crust and the thrust sheets in the fold and thrust belt [*Nakanishi et al.*, 2008; *Park et al.*, 2010; *Kamei et al.*, 2012]. This zone is interpreted to consist of underthrust or underplated sediments, implying that >1 km of relatively high-porosity sediments are in the process of being subducted to seismogenic depths [*Park et al.*, 2010]. However, the structure of this interval and the tectonic factors that led to its development have not been examined in detail. Similarly, no studies have focused on the effect of underthrust sediments on the subsequent development of the outer wedge. Better understanding of the processes by which these features formed and the events that led to the underthrusting or underplating of this sediment body is needed to evaluate processes that affect the development of the plate boundary décollement.

2.2.5 Piggyback Slope Basin

Much recent work has focused on the region near the updip end of the seaward OOST [*Kimura et al.*, 2011; *Strasser et al.*, 2011]. Seaward of the this thrust, a >1 km thick piggyback slope basin blankets currently inactive thrust sheets in the outer wedge [*Moore et al.*, 2009] (Figs 2.4, 2.5, & 2.6). IODP sites C0004, C0008, C0010, and C0018 penetrate varying thicknesses of slope basin sediments and provide a biostratigraphic and magnetostratigraphic framework for correlating the slope basin stratigraphy with events recognized elsewhere in the accretionary prism and forearc basin [*Expedition 333 Scientists*, 2011; *Tobin and Saffer*, 2009] (Figs 2.2, 2.3, & 2.6).

This piggyback slope basin near the updip terminus of the seaward OOST has undergone recent uplift and numerous mass transport deposits are present within its sediments, including a single deposit approximately 200 m thick [*Expedition 333 Scientists*, 2011; *Strasser et al.*, 2011] (Fig 2.6). Several workers have hypothesized that the history of mass wasting within the slope basin sediments is directly related to slip on the nearby out-of-sequence thrust at the rear of the outer wedge [e.g. *Kimura et al.*, 2011; *Strasser et al.*, 2011]. Additionally,

Strasser et al. [2011] linked the history of mass wasting in the slope basin to periods of movement on the nearby out-of-sequence thrust. However, recent IODP results have shown that the mass wasting post-dates motion on the out-of-sequence thrust [*Expedition 333 Scientists*, 2011]. This supports *Ikari et al.* [2011]'s suggestion that mass wasting may be linked to fluid overpressures, rather than tectonic uplift. Alternatively, *Strasser et al.* [2011] suggested that the uplift of the slope basin is occurring due to activity on an underlying anticline trending roughly east-northeast, parallel to the axis of the basin (Fig 2.3). Further understanding the source of uplift provides key insight into the recent evolution of the outer wedge. In addition, understanding the recent tectonic history of the piggyback slope basin may aid work on mass movement processes in the region. Therefore, this study uses the slope basin stratigraphy to constrain and inform our structural interpretation and kinematic model for the development of the outer wedge.

2.3 Methods

2.3.1 3D Seismic Acquisition and Processing

As a part of NanTroSEIZE, a 3D reflection seismic survey was conducted in 2006 using an industry vessel by a Japan/US team over a 12 by 56 km area from the trench axis back into the forearc basin [*Moore et al.*, 2007, 2009; *Bangs et al.*, 2009a; *Park et al.*, 2010] (Fig 2.2). After an initial pre-stack time migration, a velocity model was developed at the Japan Agency for Marine Earth Science and Technology Institute for Research and Earth Evolution (JAMSTEC-IFREE) using constraints from ocean-bottom-seismometer-based refraction studies, and a pre-stack depth migration (PSDM) was applied to the data (*processing details are given in Moore et al.* [2009]). The 3D volume is binned in 18.7 by 12.5 by 5 meter voxels and has a maximum depth resolution of 5-7 meters, degrading to around 100 meters near the top of the oceanic crust due to attenuation and increased sediment velocity [*Moore et al.*, 2009]. This PSDM seismic reflection volume is the primary observational dataset for this study.

2.3.2 Stratigraphic Correlation Between Thrust Sheets

The correlation of stratigraphy across thrust sheets is necessary to generate an accurate structural interpretation of the outer wedge. While the shallow stratigraphy within the outer wedge is constrained by seven IODP sites (Fig 2.2), these drillholes do not penetrate pre-kinematic sediments in more than one thrust sheet [*Tobin and Saffer*, 2009]. Likewise, geochronologic timing constraints are not available for structures other than the out-of-sequence thrust and the prism toe. Therefore, it is necessary to base the correlation of seismic horizons between thrust sheets on other criteria. Whereas gradual changes in the thickness of the stratigraphic section are expected, we assume that abrupt changes in the thickness of a thrust sheet compared to the immediately adjacent thrust sheets are a result of structural, rather than stratigraphic, changes. Using this simplifying assumption, we can further refine our stratigraphic interpretation by correlating packages of seismic reflectors between thrust sheets.

Using these principles, we correlated five pre-kinematic sediment intervals among thrust sheets (Fig 2.4). Based on their correlation with the undeformed sedimentary section, these intervals are interpreted to consist of the Lower Shikoku Basin sediments identified in IODP sites C0011 and C0012, the Upper Shikoku Basin sediments recognized at C0011 and C0012, and three trench-fill units, not previously subdivided by other workers (Fig 2.4) [*Expedition 333 Scientists*, 2011; *Moore et al.*, 2009; *Underwood et al.*, 2010]. The relatively thin ($\sim$100 meters—similar to the seismic resolution at depth) Middle Shikoku Basin sediments produce a prominent reflector, referred to as the "bright deep reflector" (BDR), between the Lower and Upper Shikoku Basin sections, which can be traced throughout the underthrust section in the outer wedge (Figs 2.4 & 2.5).

Additional complexity arises because approximately half of the stratigraphy within each thrust sheet consists of stratigraphically variable trench-fill sediments that onlap older stratigraphy seaward of the trench axis [*Underwood et al.*, 2010]. Nonetheless, distinct packages of reflectors are correlateable between thrust sheets, even though a detailed, reflector-to-reflector correlation is typically not possible. The three uppermost pre-kinematic

units likely correspond to various proximal vs. distal facies of trench-fill sedimentation. Therefore, we are likely making a lithofacies correlation within the trench-fill section, implying that the correlations of thrust sheet stratigraphy used here are time-transgressive. Despite the lack of a time-equivalent correlation, a time-transgressive, seismic-character-based correlation provides the necessary framework for the structural analysis performed here, as long as comparable units are present in each thrust sheet.

2.3.3 Structural Analysis

2.3.3.1 Balancing of Cross Section

For simplicity, our structural analysis focuses on a single cross section in the eastern portion of the study area (Figs 2.3, 2.4, & 2.7). Bed-length balancing of four units was used to structurally validate this cross section [*Dahlstrom*, 1969; *Woodward et al.*, 1989] (Fig 2.7). This technique explicitly assumes that bed lengths are preserved during deformation. Sediments deformed in accretionary prisms commonly undergo significant (>50%) volume loss, implying that bed lengths are not preserved during deformation [*Bray and Karig*, 1985; *Morgan and Karig*, 1995; *Screaton et al.*, 2002]. In this work we use bed-length balancing only as a method of checking the admissibility of a cross section, and not as a direct measurement of strain. Bed-length balancing will remain a reasonable validation technique as long as deformation processes do not lead to significant differential shortening between vertically adjacent restored units [*Marshak and Mitra*, 1988; *Woodward et al.*, 1989]. Therefore, the assumption of preserved bed lengths may be relaxed as long as bed lengths remain consistent, even if they do not remain constant [*Marshak and Mitra*, 1988; *Woodward et al.*, 1989].

2.3.3.2 Out-of-plane Motion

Another underlying assumption of any 2D structural restoration technique is that there is no significant out-of-plane motion of the thrust sheet. We focus on restoring a cross section along the eastern edge of the study area (Fig 2.4) because this is the only portion of

the seismic volume that is not cut by strike-slip faults (Fig 2.3). However, the plate motion vector between the Philippine Sea Plate and the stable Amur Plate is $\sim$30°oblique to the section in Figures 2.4 and 2.7 [*DeMets et al.*, 2010]. A significant portion of this obliquity is likely partitioned onto two right-lateral strike slip faults: the Median Tectonic Line onshore in central Japan (Fig 2.1), and the Kumano Basin Edge Fault Zone between the Kumano forearc basin and the outer wedge (Fig 2.2) [*Loveless and Meade*, 2010; *Martin et al.*, 2010]. Therefore, the cross section in Figures 2.4 and 2.7 is likely approximately parallel to the average transport direction of the thrust sheets in the outer wedge. Although there may be differences between the transport directions of individual thrust sheets within the outer wedge, we consider these to be minor enough to apply two-dimensional restoration techniques.

2.4 Structural Interpretation

2.4.1 Fold and Thrust Belt

Our large-scale, 3D seismic interpretation of the outer wedge reveals a fanning series of thrusts cut by a major out-of-sequence thrust (the seaward OOST) at the landward boundary of the outer wedge, as noted by previous workers (Fig 2.3) [*Park et al.*, 2002; *Moore et al.*, 2007]. Additionally, two right-lateral strike-slip faults with offsets of approximately 1 km cut the western portion of the wedge within the seismic volume as shown in map view in Figure 2.3 and previously noted by *Moore et al.* [2009]. Coupled with other structural complexity, this produces substantial along-strike variability in the outer wedge, as shown by the depth-structure map in Figure 2.3. However, we focus here on the eastern portion of the seismic survey, and a full discussion of the detailed structure of the outer wedge is beyond the scope of this study.

2.4.1.1 Relative Timing of Motion

As noted by *Moore et al.* [2009], syn-kinematic sediments within the outer wedge display evidence that the majority of offset on major thrusts has occurred in-sequence, with the

exception of the out-of-sequence thrusts connecting to the megasplay and some thrusts at the prism toe (Fig 2.4). However, there is evidence for recent, minor activity on many of the structures of the outer wedge. Additionally, many subsidiary structures in the hanging wall of thrusts in the outer wedge clearly formed after motion on their parent thrusts (e.g. the "broken" hanging wall anticlines near 15 km in Fig 2.4.).

2.4.1.2 Thrust Sheet Thickness Changes

The thrust sheets within the outer wedge fold and thrust belt vary in thickness by more than 1 km in the eastern portion of the seismic volume (Fig 2.4). At the landward edge of the outer wedge (22-28 km on Fig 2.4), the thrust sheets are greater than 2 km thick and appear to include Lower Shikoku Basin stratigraphy at their base that is not present in any of the other thrust sheets (Fig 2.4). Seaward of this, the thrust sheets progressively thin to less than 1 km, and then thicken again to greater than 1 km near the toe of the accretionary prism (Fig 2.4). The thinnest thrust sheets are poorly imaged but appear to form an imbricate fan with $<$1 km spacing between thrusts. We infer that these thrust sheets contain only the uppermost trench-fill stratigraphy present elsewhere based on their thickness and weak reflectivity.

2.4.2 Underthrust Sediments

A 2-3 km thick package of underthrust sediments is present between the uppermost thrust sheets and the oceanic crust at the landward edge of the outer wedge (Figs 2.4, 2.5, & 2.7). This is the same location as a low-velocity zone observed by multiple workers, and is consistent with their interpretation of the low-velocity zone consisting of underthrust or underplated sediments [*Park et al.*, 2010; *Kamei et al.*, 2012]. We interpret that almost half the thickness of this sediment package has been formed by an underplated thrust sheet that lies between the uppermost, inactive décollement and the primary, deepest décollement (Figs 2.4 & 2.5). Beneath this, there is approximately 1 km of Shikoku Basin and trench fill sediments in the footwall of the deepest décollement which appear to conformably contact

the underlying oceanic crust and are truly underthrust, rather than underplated (Figs 2.4 & 2.5). Furthermore, line balancing of Figure 2.4 (Fig 2.7) restores the thinnest thrust sheets directly above the thickest underthrust sediments, supporting the interpretation that the underthrust sediments are in the footwall of the primary décollement.

The underthrust sediments thin along-strike from approximately 2000 meters thickness at the northeast edge of the seismic volume to 700 meters thickness at the southwest edge (Fig 2.5). Additionally, the thin thrust sheets at the toe of the wedge are not present in the western area, and the décollement on which they formed must obliquely ramp down to a deeper stratigraphic level. Although the transition is not imaged within the 3D seismic volume due to missing data near the toe of the wedge, we interpret it to be the hanging-wall equivalent of the oblique ramp shown in Figure 2.5.

2.4.3 Bright Deep Reflector

Within the underthrust sediment interval, there is a prominent reflector above the oceanic crust that has been interpreted as the primary décollement by several previous workers [*e.g. Park et al.*, 2002; *Moore et al.*, 2007, 2009] (labeled "Bright Deep Reflector" in Figs 2.4, 2.8, & 2.9). However, this "bright deep reflector" (BDR) is offset by faults that cut the oceanic crust (Fig 2.4, near the 30 km mark) and generally follows the topography on the top of the oceanic crust except for where it onlaps basement in the western portion of the seismic volume (Figs 2.8 & 2.9). The BDR also has several strike-parallel corrugations, mimicking the underlying oceanic crust, which are inconsistent with dip-slip on a fault (Figs 2.8 & 2.9). Furthermore, at the northeastern edge of the outer wedge there is approximately 1000 meters of section between the BDR and the base of the lowermost thrust sheets above it (the interval labeled "Isopach D" in Figs 2.4 & 2.5). Therefore, interpreting the BDR as the primary décollement requires thickening and shortening of the interval above it and below the lowermost thrust sheets. Although the reflections above the BDR are weak and often incoherent, they are flat-lying where they are present, suggesting that extensive duplexing of the "Isopach D" interval is unlikely (Figs 2.4 & 2.5). We therefore interpret the

underthrust sediments as relatively undeformed sediments lying in the footwall of the main décollement, and the BDR as a stratigraphic reflector corresponding to the Middle Shikoku Basin section in IODP sites C0011 and C0012, not a detachment surface. Nonetheless, based on the geometries of folds in its hanging wall, the primary décollement must be near the BDR in the western portion of the study area (Figs 2.5 & 2.8) and may be at the BDR in areas where the oceanic crust has been locally uplifted by basement thrusting (e.g. near the center of Fig 2.4 and the center of Fig 2.9).

2.5 Discussion of Structural Interpretation

2.5.1 Admissibility of Structural Interpretation

Bed-length balancing (Fig 2.7) shows that our interpretation (Fig 2.4) meets the basic criteria for structural admissibility [*Dahlstrom*, 1969; *Marshak and Mitra*, 1988; *Woodward et al.*, 1989]. All footwall and hanging wall units can be accounted for, and all restored high-angle faults show a consistent, seaward-verging, landward-dipping geometry. While restored pin lines exhibit systematic landward dip, they do not have "jagged" edges [*Marshak and Mitra*, 1988; *Woodward et al.*, 1989]. The systematic dip of the pin lines can be attributed to a combination of several factors, including: a) the regional dip of the section, which is not accounted for in the restoration, b) simple shear, including layer-parallel slip, c) systematic variations in diffuse shortening with depth, perhaps due to preferential volume loss in the upper, relatively un-compacted sediments, d) the time-transgressive nature of the correlations within the trench-fill section, and e) systematic error in tracing folds due to more complex deformation in the shallow section. All of these factors would lead to landward-dipping pin lines, but do not affect the overall admissibility of the interpretation.

Our interpretation requires the décollement to have locally ramped downwards within the sedimentary section. Traditionally, a downward-ramping décollement can never be considered admissible in a convergent tectonic setting [*Marshak and Mitra*, 1988; *Woodward et al.*, 1989]. However, the concept of a locally downward ramping décollement is inherent in many established conceptual models of seamount subduction in accretionary prism settings

[*Lallemand*, 1992; *Park et al.*, 1999; *Dominguez et al.*, 2000; *Bangs et al.*, 2006]. We therefore consider changes in the depth of the décollement to be an admissible interpretation and argue that it is the simplest and most logical explanation for the features we observe in the outer wedge.

2.5.2 Differences from Previous Interpretations

This study represents the most detailed interpretation to date of the structure of the outer wedge in the Kumano Basin region, but focuses primarily on the shallow (<10 km depth) structure seaward of the forearc basin. Previous work investigated the outer wedge in less detail and instead focused on the large-scale structure of the plate-boundary fault [*Park et al.*, 2002; *Moore et al.*, 2007, 2009; *Bangs et al.*, 2009a]. However, the position of the décollement in our detailed interpretation of the outer wedge has key implications for the large-scale structure of the plate-boundary fault.

Park et al. [2002] first interpreted the plate-boundary fault in the Kumano Basin region to consist of two prominent branches–a megasplay and a décollement–that join at a depth of approximately 10 km based on regional 2D reflection seismic data (Fig 2.10B). Subsequent studies based on the PSDM 3D reflection seismic dataset [*e.g. Moore et al.*, 2007, 2009; *Park et al.*, 2010] have followed the bifurcated plate-boundary geometry proposed by *Park et al.* [2002]. However, this geometry requires the décollement beneath the outer wedge to be at or near the "bright deep reflector" (BDR) (Figs 2.4 & 2.10). While all previous workers [*e.g. Park et al.*, 2002; *Moore et al.*, 2007; *Bangs et al.*, 2009a; *Moore et al.*, 2009] have interpreted the BDR as the décollement, as discussed in section 2.4.3, this is unlikely. Instead, we interpret the primary décollement to be $\sim$1 km higher, based on the geometry and thickness of the thrust sheets above it.

Extending our interpretation landward beneath the forearc basin (Fig 2.10C) results in a significantly different plate-boundary fault geometry. The higher décollement position requires the out-of-sequence thrusts connect to directly to the plate-boundary megathrust (Fig 2.10C) instead of connecting to a megasplay fault (Fig 2.10B). We interpret the reflector

identified as the megasplay by *Park et al.* [2002] and *Moore et al.* [2009] as the plane-boundary megathrust, with no décollement beneath it. This results in a simpler fault geometry with thicker underthrust sediments (Fig 2.10C).

2.5.3 Thrust Sheet Thickness Changes

The distinct changes in the thickness of the thrust sheets in the outer wedge could have resulted from three scenarios: 1) Changes in the thickness of the incoming stratigraphic section would result in thinner or thicker thrust sheets. 2) Basement topography could cause the décollement to ramp up and over a topographic high in the basement. 3) The décollement could ramp up and then down within the incoming stratigraphic section. We can distinguish between these three scenarios based on the footwall geometry and composition beneath the restored position of the thin thrust sheets.

2.5.3.1 Stratigraphic Variability

The thrust sheet thickness changes could simply reflect stratigraphic variability. However, if the thin thrust sheet interval was due to anomalously thin stratigraphy, the thin thrust sheets would not be restore over a section of thick underthrust sediments. Furthermore, the underthrust sediments in the restored footwall position of the thin thrust sheets are similar in thickness to the $\sim$1 km of section "missing" from the thin thrust sheets (near the 20 km mark in Fig 2.7). This suggests that there was not an anomalously thin stratigraphic section at the time the thin thrust sheets formed. Additionally, based on *Ike et al.* [2008], the Shikoku Basin and trench-fill sediments only vary in thickness by $>$1 km–the amount necessary to explain the changes in thrust sheet thickness–where they onlap basement topography (See section 2.5.3.2). There is little reason to expect the incoming stratigraphic section to rapidly thin in the absence of a topographic high in the basement, as trench-fill sedimentation would be expected to rapidly fill in topographic depressions. For these reasons, it is unlikely that the interval of thin thrust sheets was formed due to an abnormally thin incoming stratigraphic section. However, it is possible that the lowest

unit (shown in pink in Fig 2.4) interpreted as being in the hanging wall of the unusually thick thrust sheets near the 25 km mark is simply a mis-correlation due to an abnormally thick stratigraphic section. Because the restored footwall of these thick thrust sheets is not imaged, it is not possible to distinguish between the current interpretation of an early phase of décollement down-ramping and up-ramping (near the 75 km mark on Fig 2.7) and an alternate interpretation of an abnormally thick stratigraphic section. Nonetheless, it is apparent that the thin thrust sheet interval cannot be entirely explained by an abnormally thin stratigraphic section.

2.5.3.2 Onlap of Basement Topography

Basement topography in the immediate footwall of the thin thrust sheets could have produced sudden changes in stratigraphic thickness by onlap onto the pre-existing topography [*Ike et al.*, 2008]. If the décollement does not truncate and "decapitate" the basement high, it would ramp up and over it, producing a region of thin thrust sheets in the fold and thrust belt. However, in this scenario, the thin thrust sheets would restore over the basement high. There is no anomalous basement topography at the location over which the thin thrust sheets restore. Instead, there is an abnormally thick section of sediments in the footwall (Figs 2.4 & 2.7). Because the Philippine Sea Plate subducts roughly 30°oblique to the section line in Figure 2.4 [*DeMets et al.*, 2010], the anomalous basement topography could simply lie out of the plane of the cross section. However, there would be a basement high to the west of the section line in this case, and no such anomalous basement topography is observed to the west of the section line (Fig 2.5). Therefore, the thin thrust sheets cannot have formed due to basement topography directly in their footwall.

2.5.4 Mechanism for Thrust Sheet Thickness Changes

For stated above in sections 2.5.3.1 and 2.5.3.2, the changes in thrust sheet thickness cannot be explained by stratigraphic variability or by a basement feature in the footwall of the thin thrust sheets. We therefore interpret the thin thrust sheets to have formed by the

upward ramping of the décollement within a stratigraphic succession of normal thickness. Similarly, we interpret the unusually thick underthrust sediments to be the restored footwall of the thin thrust sheets, and to have formed by the same up-ramping and subsequent down-ramping of the décollement.

If this is true, it requires an explanation of what caused the ramping of the décollement and the formation of the thick underthrust sediments. It is unlikely that the décollement would spontaneously change depths within the incoming stratigraphic section without either stratigraphic changes, along-strike obstructions, or pre-existing structures. In the following sections, we consider the possible causes for the changes in the depth of the décollement.

2.5.5 Influence of the Paleo-Zenisu Ridge

2.5.5.1 Initial Impact of the Basement High with the Trench

The Paleo-Zenisu Ridge is a topographic high within the basement located approximately 10 km east of the edge of the 3D seismic volume [*Park et al.*, 2003] (Fig 2.2). Based on the extent of the ridge determined by *Park et al.* [2003] and present day plate motions from *DeMets et al.* [2010], the edge of this feature would have initially impacted the outer wedge's deformation front approximately 40 km to the east of the study area at approximately 1 Ma, with the southwestern edge of the ridge impacting the deformation front around 25 km to the east of the study area at around 0.8 Ma. However, two major structures likely reduce the obliquity of the local convergence vector: the Median Tectonic Line, a major strike-slip fault onshore in southern Japan, and the Kumano Basin Edge Fault Zone, a potential strain partitioning feature dividing the outer wedge from the forearc basin [*Loveless and Meade*, 2010; *Martin et al.*, 2010]. Therefore, the local convergence vector between the Philippine Sea Plate and the Nankai forearc is likely significantly different than the convergence vector between the Philippine Sea Plate and the Amur Plate. Based on the *Loveless and Meade* [2010] model for the motion of the Nankai forearc block relative to the Philippine Sea Plate, the ridge may have initially impacted the deformation front 35 km to the east of the

study area at around 1.3 Ma, with the southwestern edge impacting the deformation front approximately 20 km to the east of the study area at around 1 Ma.

2.5.5.2 Structural Effects

Due to its close proximity to the study area, it is possible that the Paleo-Zenisu Ridge has affected the development of the outer wedge in this area. We hypothesize that the observed changes in the depth of the décollement may have been the result of the Paleo-Zenisu Ridge impacting the outer wedge to the east of the study area. We envision that the subducting basement topographic high may have caused the décollement to ramp up for some distance along strike, and then ramp down after the passage of the ridge. In areas along-strike from the subducting topography, this would produce thin thrust sheets associated with thick underthrust sediments in the downgoing section, rather than a basement topographic high.

The topographic expression of thrusting supports the correlation of exceptionally thin thrust sheets within the study area with the passing of the Paleo-Zenisu Ridge to the east. There is a distinct change in the spacing of thrusts within the outer wedge that correlates with the change in thickness of the thrust sheets observed within the study area. This change has a prominent topographic expression that can be traced along-strike in regional side-scan bathymetry, forming a wedge of closely spaced thrusts that tapers to the west (Fig 2.11). The wedge of closely-spaced thrusts reaches a maximum width near where the Paleo-Zenisu ridge is projected to have impacted the trench, and its westernmost edge forms the sequence of thin thrust sheets in Figure 2.4. Furthermore, the downward ramping of the décollement after the passage of the ridge would be expected to deform older hanging-wall thrust sheets into a broad syncline above the downward-dipping décollement (Fig 2.12). A similar topographic depression can be traced along-strike in side-scan bathymetry (Fig 2.11), correlating with the broad synclinorium in the cross section shown on Figure 2.4.

2.6 Stratigraphic Interpretation of Piggyback Basin Sediments

2.6.1 Stratigraphic Packages

The sediments within the piggyback slope basin that post-date in-sequence thrusting can be divided into three stratigraphic packages (referred to as Units 1, 2, & 3) based on their seismic character and relationship to the surrounding stratigraphic intervals (Figs 2.6 & 2.13). The basal sequence (Unit 3) consists of a ∼200-300 m thick section of weakly reflective sediments constrained to the center of the basin. Unit 3 onlaps syn-kinematic sediments, but is deformed by late-stage activity on subsidiary thrusts and associated folds (Fig 2.6). Based on correlations with IODP sites C0004 and C0008, the top of this package dates to ∼1.55 Ma [*Moore et al.*, 2009]. Unit 2 consists of a 100-500 meter thick, strongly reflective stratigraphic package containing a well-developed axially-directed channel system (Figs 2.6, 2.13, & 2.14A). However, as noted by several workers, the top of this sequence is scoured and eroded into by a major mass wasting event dating to ∼0.9 Ma, defining the start of the most recent stratigraphic package [*Expedition 333 Scientists*, 2011; *Strasser et al.*, 2011] (Figs 2.6, 2.13, & 2.14B). Unit 1 consists of the major mass wasting event's deposit and other seismically chaotic intervals interwoven with seismically transparent intervals, interpreted as smaller mass transport complexes inter-layered with pelagic sediments and distal turbidite deposits. This unit thins to the north, onlapping Unit 2 and showing consistent internal onlap and thinning indicating continued uplift during its deposition (Fig 2.13). Mass wasting has continued to the present, and several landslide scars are visible on the seafloor, with the corresponding mass transport complexes visible in the 3D seismic data (Figs 2.6 & 2.14C).

2.6.2 Recent Uplift

The northeastern edge of the slope basin is undergoing uplift, as evidenced by the spatially consistent trend in the thickness of the uppermost stratigraphy within the slope basin and the onlap of sediments in the youngest stratigraphic interval onto older sediments (Figs 2.13 & 2.14C). Assuming the sediments at the top of Unit 2 were initially deposited

horizontally, the northeast side of the basin has been uplifted by ∼600 m relative to the southwest side (Figs 2.13 & 2.6).

Based on seismic stratigraphy, the initiation of uplift is roughly correlative with the major mass wasting deposit >200 m thick between Units 1 & 2 (Figs 2.6, 2.13, & 2.14). The deposit from the large mass wasting even was penetrated by C0018 during IODP Expedition 333 and occurred at ∼0.9 Ma based on tephrachronology and biostratigraphy [*Expedition 333 Scientists*, 2011].

Sediments post-dating the large mass wasting event are ∼200 meters thick in the southwestern portion of the slope basin, but onlap the uplifted portion of the basin and thin abruptly to the north and east (Fig 2.14C). This pattern of thinning outlines the uplifted region of the slope basin. However, this pattern of uplift does not match the strike of any of the underlying structures or the seaward OOST. Instead, the uplifted area follows the trend of the underthrust sediments in the footwall of the main décollement beneath it, uplifting most where the underthrust sediment interval is the thickest and not uplifted where it is the thinnest (Fig 2.14D).

2.7 Discussion of Piggyback Basin Stratigraphy

2.7.1 Uplift of Piggyback Basin

The sediments within the piggyback basin constrain the recent kinematics of the landward portion of the outer wedge. Therefore, it is import to understand the cause of uplift within this basin in order to distinguish between different models of the evolution of the outer wedge. Several workers have cited the recent uplift and mass wasting of the slope basin sediments as evidence of motion on the seaward OOST after 1.24 Ma [*Moore et al.*, 2009; *Kimura et al.*, 2011; *Strasser et al.*, 2011]. *Kimura et al.* [2011] have hypothesized that the Paleo-Zenisu Ridge is actively causing minor reactivation of the seaward OOST at the rear of the wedge, in turn causing uplift of the slope basin sediments. Similarly, *Strasser et al.* [2011] have proposed that growth of one of the anticlines (near the 27 km mark on Fig 2.4) underlying the slope basin is causing uplift. However, the extent of the uplifted

region does not match the strike of the seaward OOST or any other structures underlying the slope basin, including the underlying anticline (Fig 2.14B). Given the trend and area of the uplifted region, the uplift of the slope basin cannot be explained by movement on any of the thrusts in the vicinity.

2.7.2 Relationship of Uplift with Underthrust Interval

The thickness of the "excess" underthrust sediments (Isopach D in Figs 2.4, 2.5, & 2.14D) closely matches the pattern of uplift in the slope basin (Fig 2.14B). Therefore, uplift of the piggyback basin likely resulted from features in the footwall of the active décollement or the geometry of its footwall, rather than the out-of-sequence fault or other thrusting in the outer wedge.

The underthrust interval in the landward region of the outer wedge is anomalously thick and is spatially associated with the uplift of the slope basin above it (Figs 2.4, 2.7, 2.5, 2.13, & 2.14). The structure of the interval below the shallowest décollement could influence uplift of the slope basin through two mechanisms: 1) ongoing duplexing of sediments between décollements or beneath the active décollement, or 2) deformation of the hanging wall as the thrust sheet moves over footwall topography.

The reflectors in the sediments beneath the uppermost thrust sheet (5-8 km depth in Fig 2.5) are weak but coherent, despite being poorly imaged (Figs 2.4 & 2.5). These reflectors are predominantly flat-lying and show no unambiguous evidence for large-scale duplexing (Figs 2.4, 2.5, & 2.8). However, the interval between the oceanic crust and the base of the lowermost thrust sheet clearly thickens to the east (Figs 2.5 & 2.14D). Furthermore, the additional thickness of this interval (Isopach D) in the eastern portion of the seismic survey is consistent with the thickness of the "missing" stratigraphy within the thinnest thrust sheets near the toe of the prism. Therefore, the thickness of Isopach D can be explained by the upward-ramping of the décollement that we interpret to have formed the thin thrust sheets. Because there is no clear evidence of internal folding, we interpret Isopach D and the sediments below it to consist of relatively undeformed sediments in depositional contact

with the underlying oceanic crust. This implies that the uplift of the slope basin is due to movement of the thrust sheets over an oblique footwall ramp, rather than due to duplexing within the underthrust sediments.

2.8 Discussion

2.8.1 Model of Kinematic Evolution of the Outer Wedge

The recent kinematics of the study area appear to be dominated by the subduction of the nearby Paleo-Zenisu Ridge even through the ridge did not pass directly beneath the study area. The passage of a buried basement topographic high beneath the outer wedge would force the décollement to locally ramp upwards, producing thin thrust sheets in the hanging wall (Fig 2.12). However, models of seamount subduction (e.g. *Dominguez et al.* [2000]) predict that the portion of the fold-and-thrust belt corresponding to seamount subduction (termed the "suture zone" by *Dominguez et al.* [2000]) should restore over a basement high in the footwall, rather than restoring over an unusually thick interval of underthrust sediments as observed. Restoration of the structures in the study area suggests that they formed from the décollement obliquely ramping upwards within a relatively thick stratigraphic section, rather than due to thin sediments on top of a basement high (Fig 2.7). We hypothesize that this ramping of the décollement within a normal sedimentary section is the along-strike effect of the décollement ramping up and over the Paleo-Zenisu Ridge as it subducted to the east of the study area. The Paleo-Zenisu Ridge would have impacted the trench axis approximately 25-40 km to the east of the study area, as discussed in section 2.5.5.1. This suggests that the décollement ramped upwards by at least 1 kilometer for a minimum of 25 kilometers along strike (Fig 2.12). This is further supported by the bathymetric expression of the "closely-spaced thrust sheets" in Figure 2.11, which can be traced for a similar distance along-strike.

This conceptual model suggests that basement topography may be associated with a laterally extensive region of underthrust sediment, in contrast to sandbox models of seamount subduction, which have suggested that subducted basement features are likely

associated with a "shadow zone" of underthrust sediments only immediately updip of the basement topographic high [*Dominguez et al.*, 2000]. However, laterally extensive zones of thickened underthrust sediment have been observed in the Hikurangi Trench in New Zealand [*Bell et al.*, 2010]. Furthermore, analogue models such as *Dominguez et al.* [2000] focused on basement features with a topographic relief similar to the accretionary prism under which they are being subducted, in which case the outer wedge is locally destroyed and rebuilt [*Dominguez*, 1998; *Dominguez et al.*, 2000]. Different structures may result from cases where the topographic relief of the basement feature is small enough relative to the average incoming sedimentary section that the accretionary wedge can override it without being completely disrupted [*Lallemand and Pichon*, 1987; *Dominguez*, 1998]. As the outer wedge in the study area does not appear to have been completely disrupted by the nearby passage of the Paleo-Zenisu Ridge, we suggest that our conceptual model of the décollement responding to the passage of basement topography along-strike is primarily applicable to the subduction of basement features smaller than those studied by previous workers.

2.8.2 Influence of Pre-Existing Structures

As an alternative conceptual model, the changes in depth of the décollement could be explained by a pre-existing syncline in the incoming stratigraphic section. If the décollement were to cut horizontally across a syncline, the result would be an apparent up-ramping and down-ramping of the décollement relative to the undeformed stratigraphy. This would subsequently produce thin and then thick thrust sheets within the hanging wall of the décollement. Furthermore, the thick underthrust sediments in the footwall of the décollement form a broad, shallow syncline (Figure 2.4). However, this hypothesis does not explain the uplift of the hanging wall concurrent with subduction of the underthrust sediments. If the underthrust sediment body formed due to the décollement cutting across such a syncline, there should not be a topographic high in the footwall. This would not cause uplift and subsidence of the hanging wall as deformation progresses, and would require a second process to explain the uplift of the piggyback basin. It is unlikely that another

process would result in the close match between the "excess" thickness of the underthrust sediments and the uplifted region of the slope basin (Figs 2.14B & 2.14D). For this reason, we prefer the hypothesis that the changes in the stratigraphic level of the décollement were caused by the Paleo-Zenisu Ridge subducting to the east of the study area.

2.8.3 Site-Specific Implications

Our new interpretation of plate-boundary fault structure (Fig 2.10C) has implications for future deep riser drilling at IODP site C0002. We hypothesize that the plate boundary fault in the vicinity of IODP site C0002 may be a single structure, rather than a separate megasplay and basal décollement as previously thought [*Park et al.*, 2002; *Moore et al.*, 2007, 2009; *Bangs et al.*, 2009a]. Our results suggest that future drilling at site C0002 should intersect a single major fault zone at ∼7.5 km below sea level (kmbsl) (∼5.5 km below sea floor), rather than two major fault zones at ∼7.5 kmbsl and ∼8.5 kmbsl, as *Moore et al.* [2009]'s results suggest.

2.8.4 Implications for Seismogenesis

Asperities within the subducting crust have long been thought to play a role in controlling the extent and nucleation of rupture patches during great thrust earthquakes [*Cloos*, 1992; *Das and Kostrov*, 1983; *Bilek et al.*, 2003; *Watts et al.*, 2010]. However, most workers have considered subducting basement topography as an isolated region of uniformly high strength within the footwall [e.g. *Das and Kostrov*, 1983]. The kinematics observed in this region of the Nankai Trough suggest that in sediment-rich accretionary prisms, subducting basement topographic highs could be associated with an "aureole" of underthrust sediment extending for at least 25 kilometers along strike. Because the underthrust sediments are likely to be overpressured and relatively weak, a sedimentary aureole would be expected to produce a contrast in the frictional properties of the footwall. This leads to an isolated point of more competent material surrounded by a 3D ring of material weaker than the rest of the plate interface. Furthermore, the extensive underthrusting of sediments around a

subducted basement feature provides an effective means of material transport into deeper parts of the subduction zone. As dewatering of underthrust sediments is a likely source of fluids at seismogenic depths, subducted basement topography may also be associated with regions of increased pore pressure along the subduction interface. Similar features observed in New Zealand are spatially associated with slow-slip events along the plate boundary fault, and the elevated pore pressure associated with the sedimentary aureole around subducted topography is thought to control the extent of slow slip events along the Hikurangi Trench [*Bell et al.*, 2010].

2.9 Conclusions

The Kumano Basin region of the Nankai Trough accretionary prism shows evidence for a progressive thinning and subsequent abrupt thickening of thrust sheets within the outer wedge accompanied by a thick package of underthrust sediment and recent uplift of the rear of the outer wedge. These three features are interpreted to be a result of the subduction of the Paleo-Zenisu Ridge just to the east of the study area. As this basement topographic high was subducted to the east, the décollement ramped up along strike in the study area, producing a region of anomalously thin thrust sheets and a thick package of underthrust sediment. After the passage of this feature, the décollement ramped downward, and continued subduction of the underthrust sediment package has caused ongoing uplift of the rear of the outer wedge. Our conceptual kinematic model explains the key features of the outer wedge in terms of its structural evolution since $\sim$2 Ma. If similar fold and thrust belt kinematics occur elsewhere in sediment-dominated accretionary prisms, this implies that subducted basement features may produce laterally extensive regions of underthrust sediment, affecting the seismogenic properties of the nearby plate boundary fault.

Acknowledgements

This work was funded by NSF award OCE-0800653. Seismic interpretation was preformed in Geoprobe® Volume Interpretation Software [*Landmark*, 2003], which was generously provided by Halliburton, Inc. To visualize and display the seismic interpretation, including figures in this work, we wrote software in Python [*van Rossum and Drake*, 2006] using Numpy [*Oliphant*, 2007], Matplotlib [*Hunter*, 2007], and SciPy [*Jones et al.*, 2001].

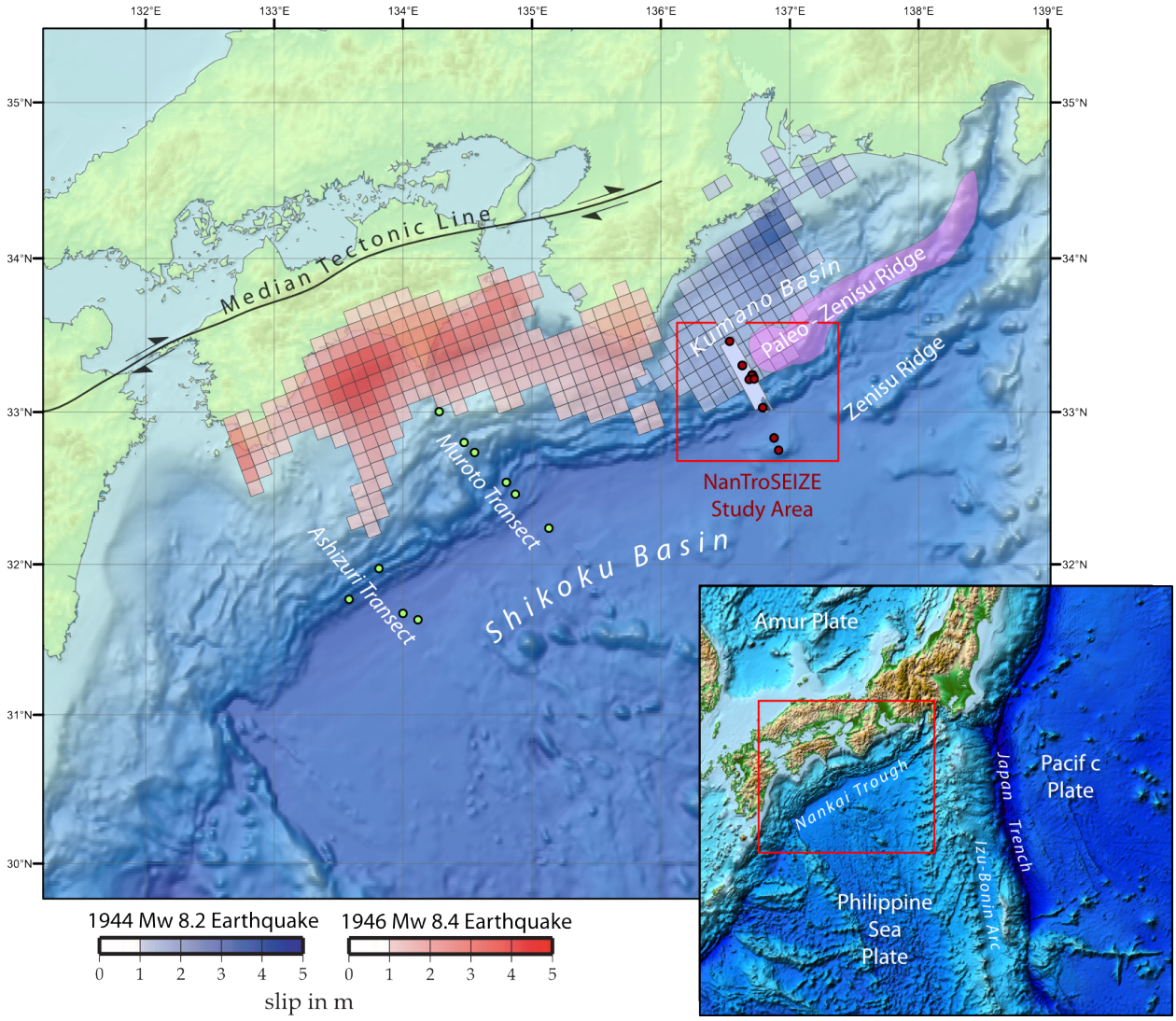

Figure 2.1: Regional location map showing location of study area relative to 1944 and 1946 rupture extents. Slip distributions from *Baba and Cummins* [2005]. Extent of Paleo-Zenisu Ridge from *Park et al.* [2003].

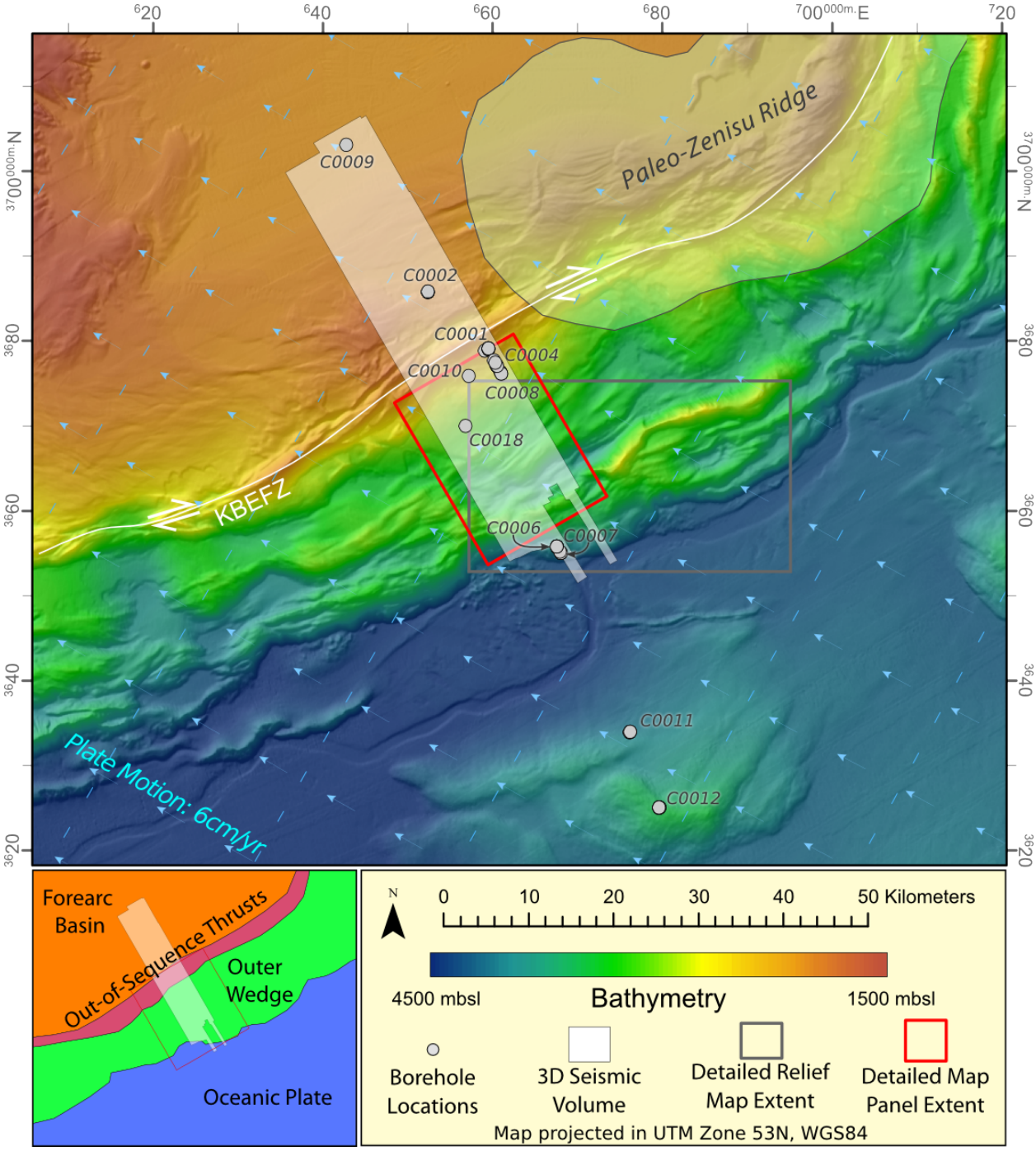

Figure 2.2: Detailed map of study area. Extent of Figures 2.3 and 2.14 shown by red box. The details of the bathymetry within the gray box are shown in Figure 2.11. Convergence vector between Philippine Sea Plate and the stable portion of the Amur Plate from *DeMets et al.* [2010] shown in light blue. Kumano Basin Edge Fault Zone (KBEFZ) shown in white. Note the location of the Paleo-Zenisu ridge (based on *Park et al.* [2003]) relative to the NanTroSEIZE transect.

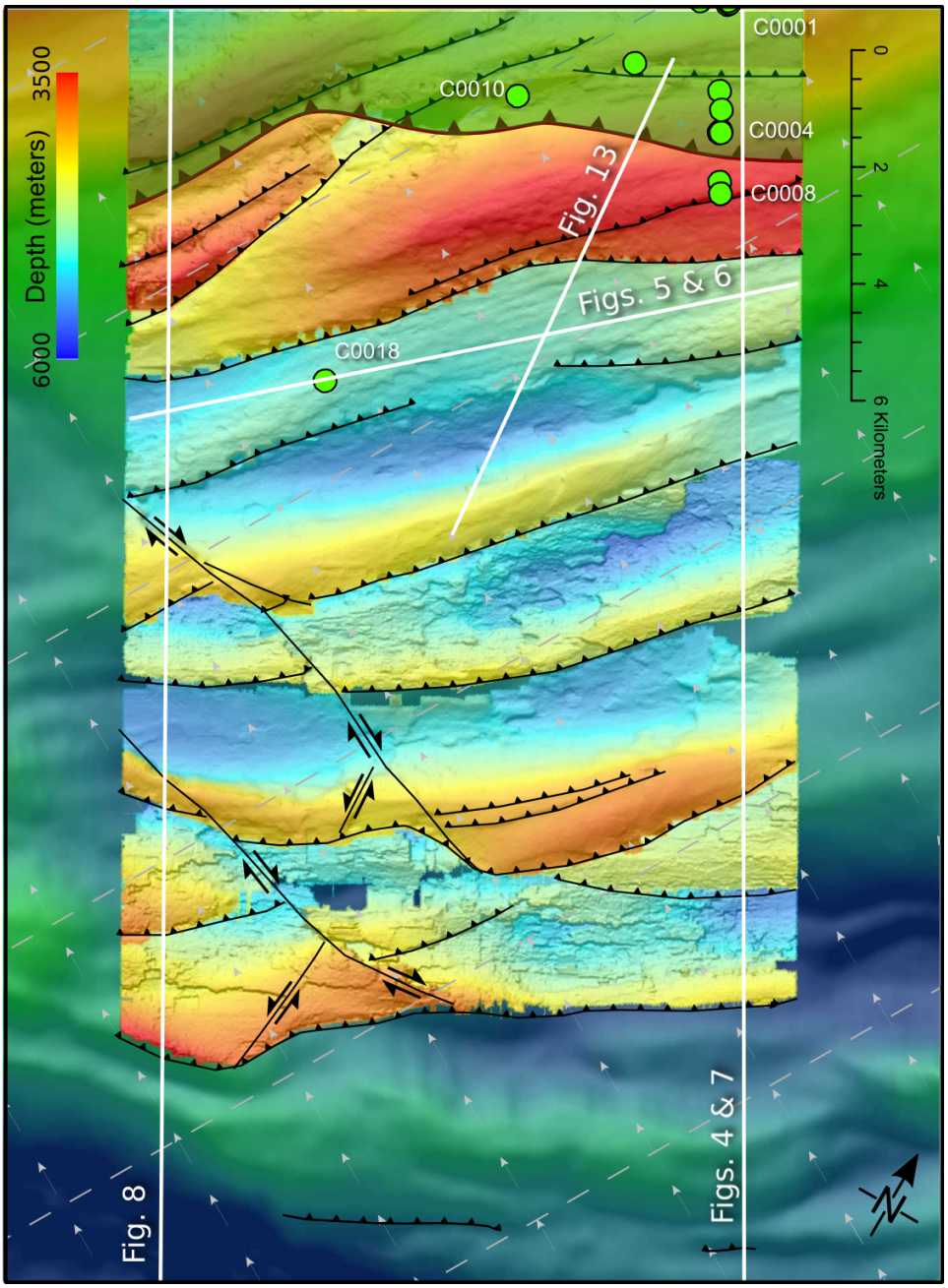

Figure 2.3: Depth structure map of this study's interpretation of a marker horizon in the outer wedge. Background bathymetry uses the same color scale as in Figure 2.2, while the color scale for the structural features is shown in the upper left corner. Note the two prominent right-lateral strike-slip faults that cut the western edge of the study area. Surface trace of the seaward OOST is shown in dark red. Location of cross section lines for Figures 2.4, 2.7, 2.5, 2.6, 2.8, and 2.13 shown in white. Motion of the Philippine Sea Plate relative to the stable interior of the Amur Plate from *DeMets et al.* [2010] shown in light gray.

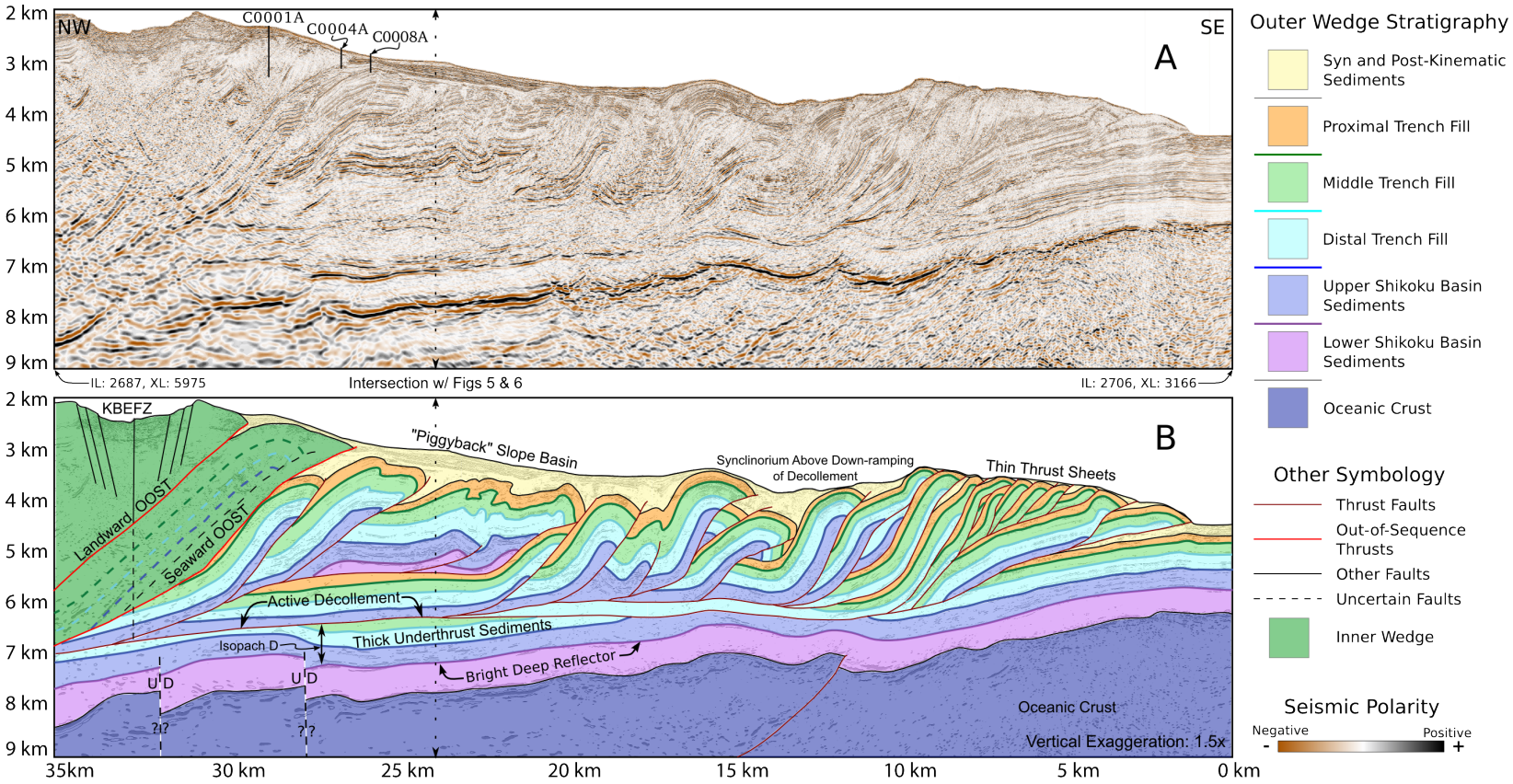

Figure 2.4: A) Depth reflection seismic profile extracted through the outer wedge along the eastern edge of the 3D PSDM volume. Location of section line shown in Figure 2.3. B) Simplified interpretation of outer wedge structures shown in (A) based on this study. Note the differences in thickness of the thrust sheets and the thick interval of underthrust sediment at the rear of the outer wedge. Out of sequence thrust sheets and the Kumano Basin Edge Fault Zone (KBEFZ) at the rear of the outer wedge are shown in dark green. The "Bright Deep Reflector" shown here was interpreted as the décollement reflector by *Moore et al.* [2007]. The interval labeled "Isopach D" is shown in Figure 2.14D.

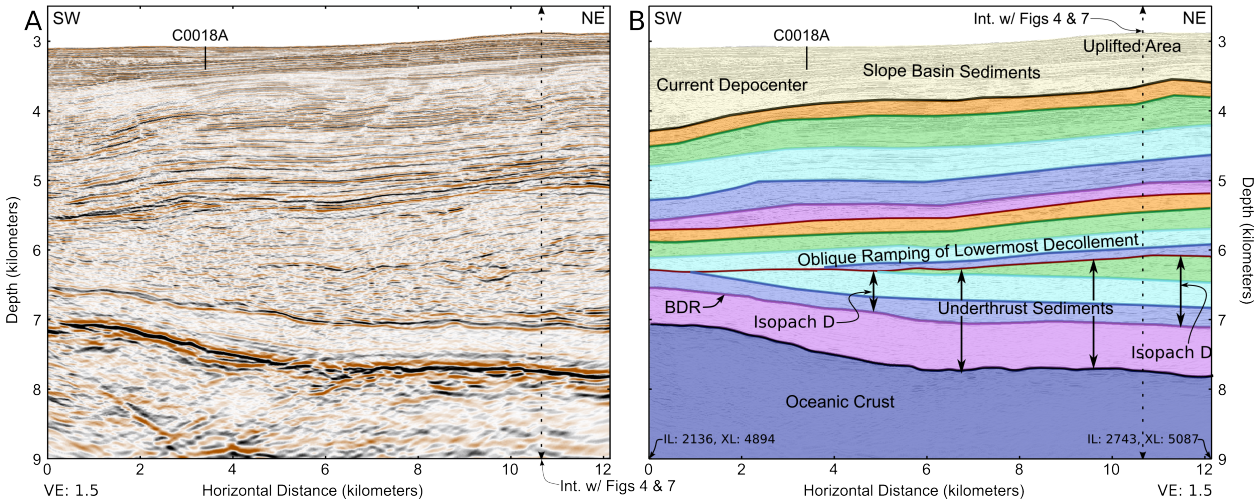

Figure 2.5: A) Depth reflection seismic profile extracted from the 3D PSDM volume parallel to the strike of structures in the outer wedge across the thickest portion of underthrust sediments. B) Simplified structural interpretation of (A) based on this study. Note that the décollement obliquely ramps upward to the northeast, producing an unusually thick sequence of underthrust sediments which thin to the southwest. "BDR" is the "Bright Deep Reflector" shown in Figure 2.4. See legend in Figure 2.4 for explanation of colorscheme and Figure 2.3 for location of section.

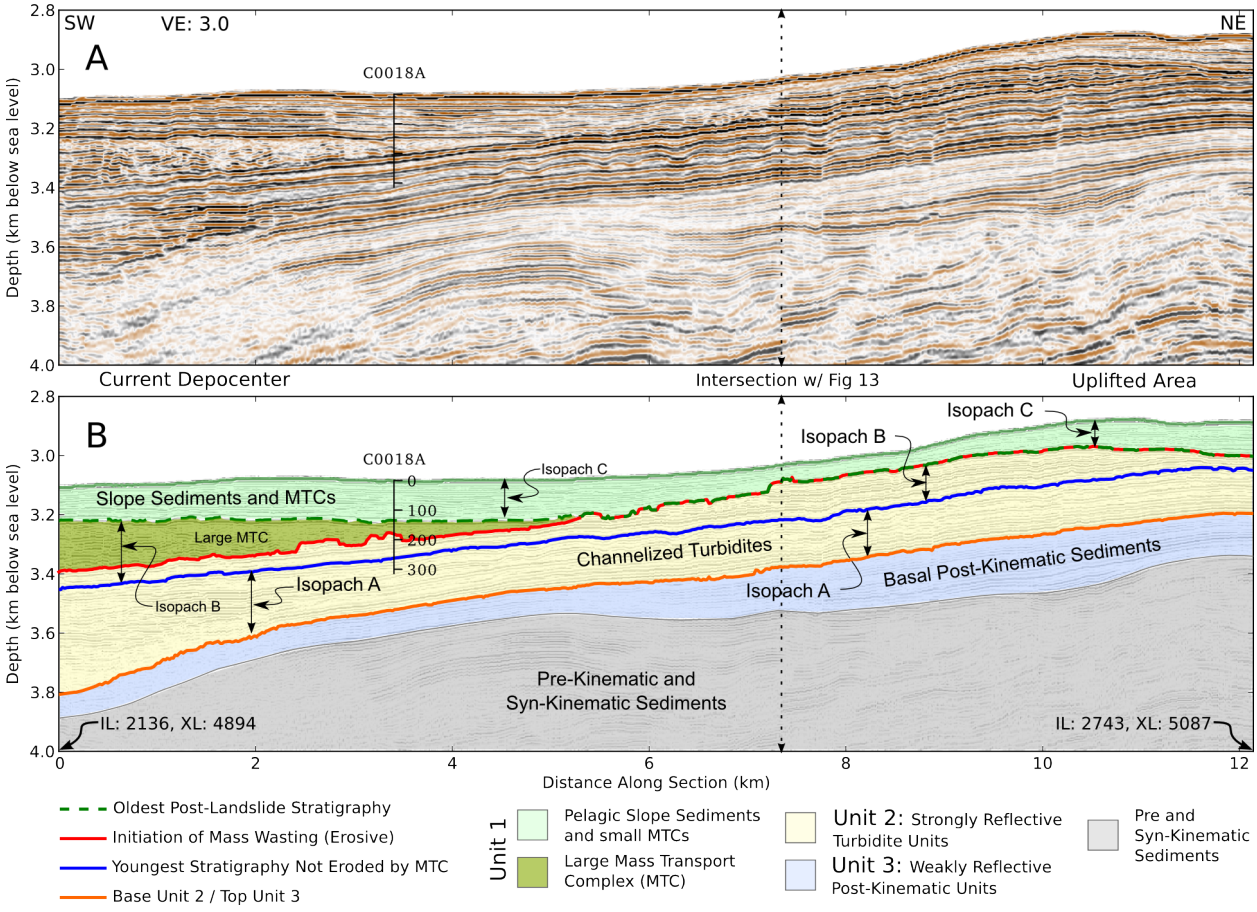

Figure 2.6: A) Shallow reflection seismic profile along piggyback basin axis extracted from 3D PSDM volume in the same location as Figure 2.5. B) Stratigraphic interpretation of (A) based on this work showing primary stratigraphic packages, the prominent mass transport complex in the southwestern portion of the basin, and the intervals used for the A, B, and C isopach maps in Figure 2.14. Note the uplift of the northeastern side of the basin.

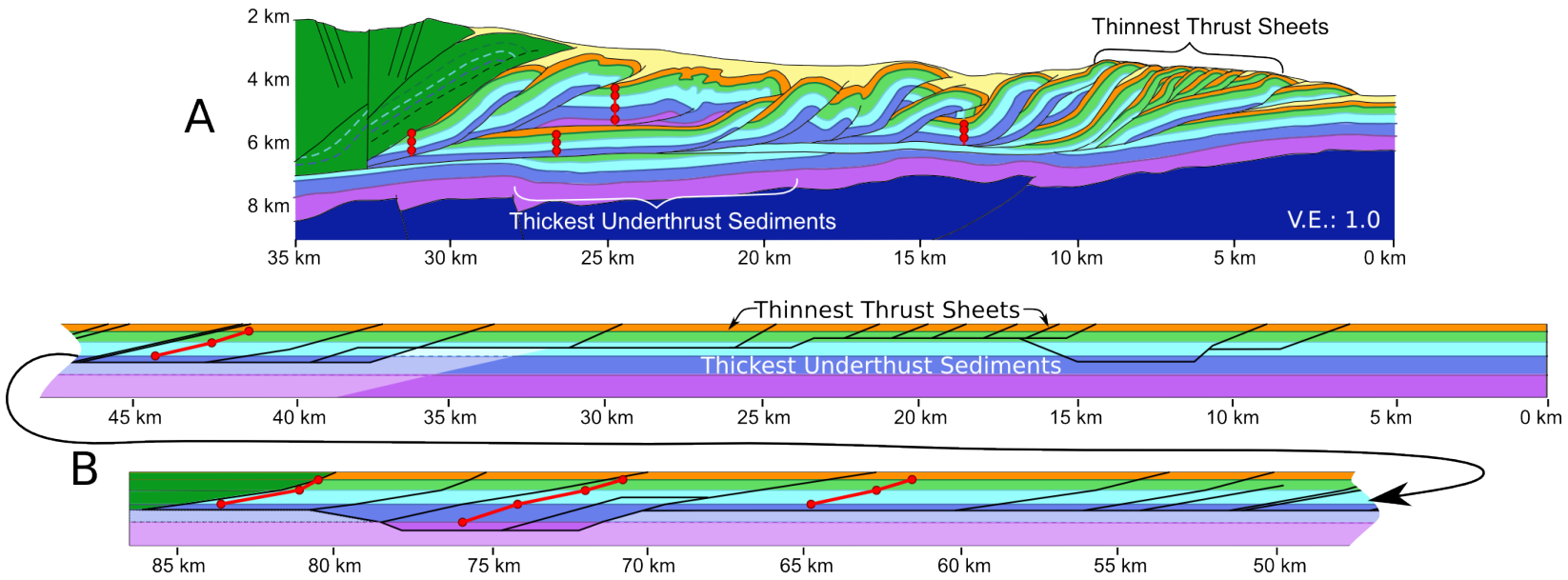

Figure 2.7: A) Structural interpretation shown in Figure 2.4 with no vertical exaggeration. B) Bed-length balancing of (A). Lighter-shaded regions indicate portions of the footwall that are beyond extent of Figure 2.4. Notice that the interpreted bed lengths place the thinnest thrust sheets above the thickest underthrust sediments (near the 20 km mark in the restored section). Therefore, we interpret that both are a result of changes in the depth of the decollement.

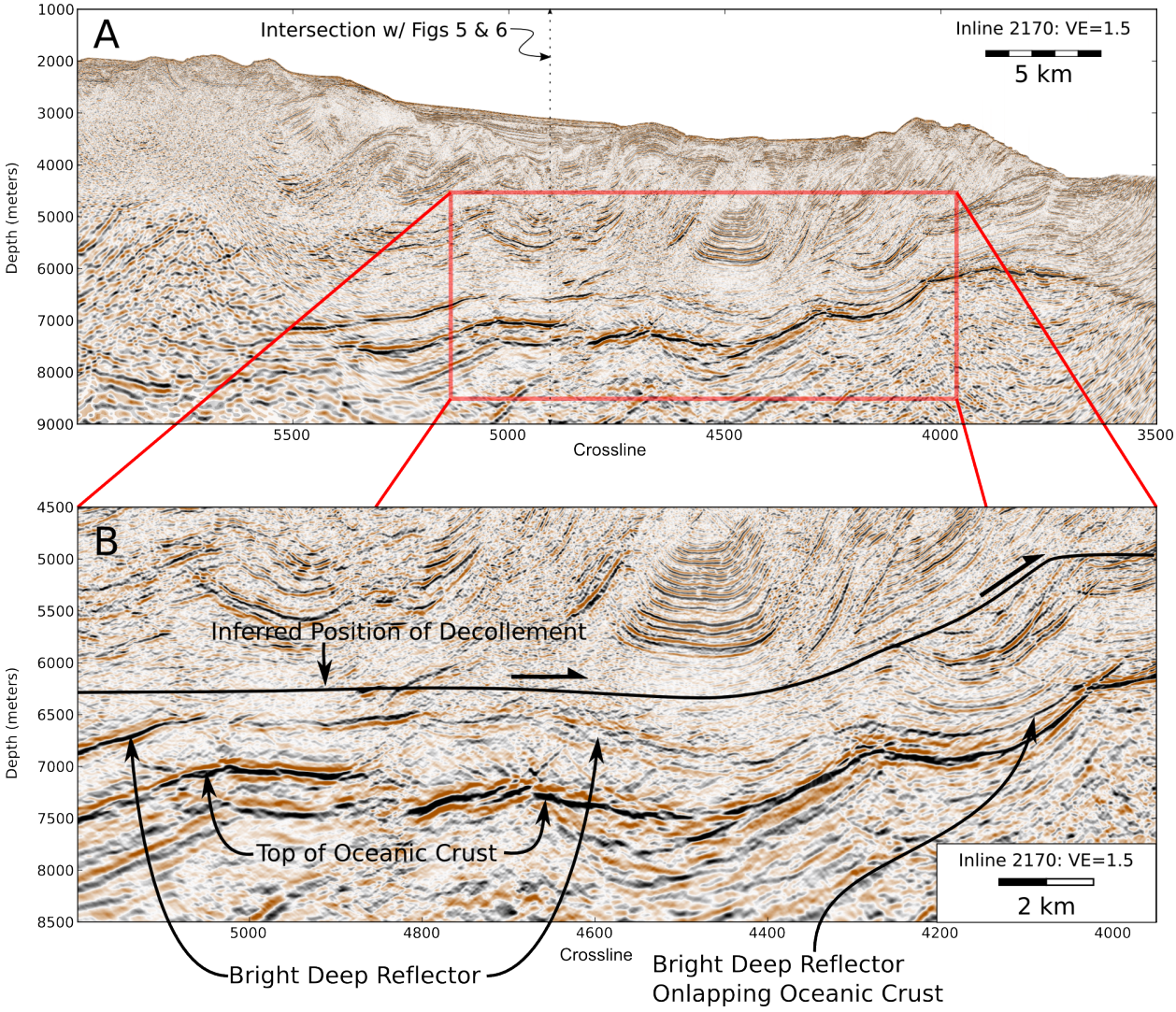

Figure 2.8: A) Inline 2170 from the 3D PSDM seismic volume near the western edge of the survey. Note the relationship of the "bright deep reflector" to the oceanic crust. B) Annotated detail from A showing the bright reflector above the oceanic crust that has been previously interpreted as the main decollement onlapping the oceanic crust. Note the relatively thin interval of underthrust sediment as compared to Figure 2.4 to the east.

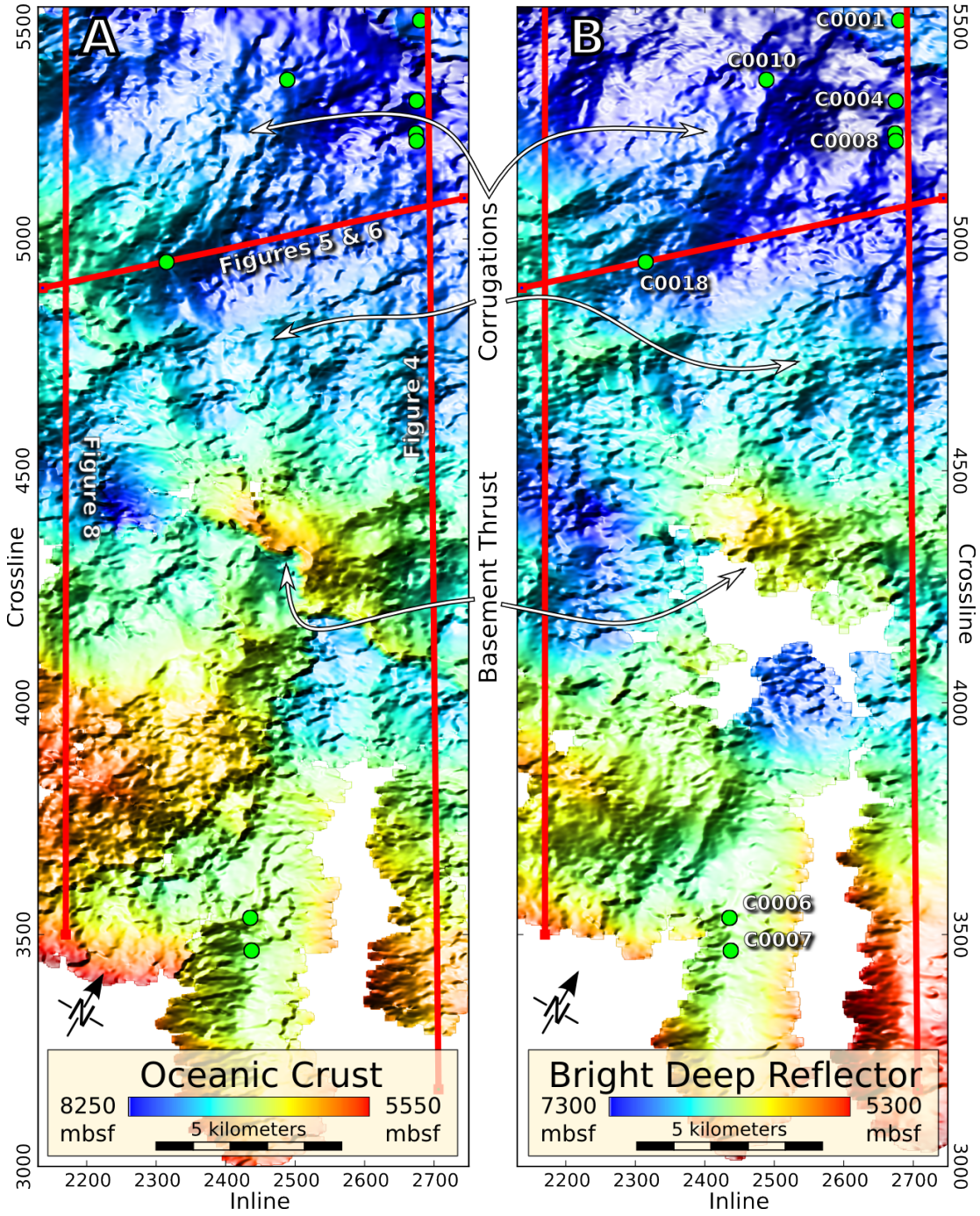

Figure 2.9: A) Map of depth to ocean crust. B) Map of depth to the "bright deep reflector". Section lines are shown in red, well locations are shown in light green. Note the similarity in structure of the two horizons, as well as the strike-parallel corrugations in the bright deep reflector that mimic the topography on the oceanic crust. Both are inconsistent with active slip on a fault surface.

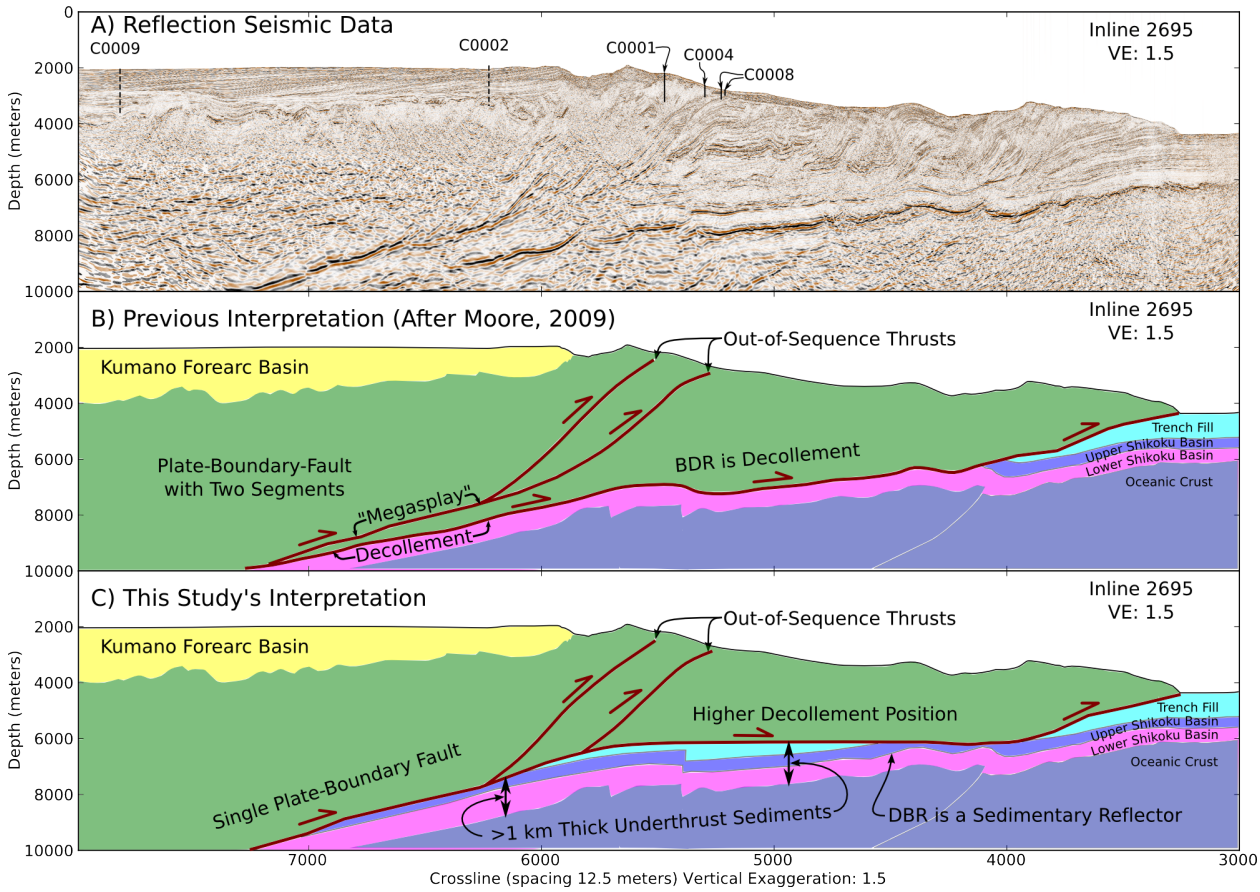

Figure 2.10: A) Inline 2695 from the 3D PSDM seismic volume near the cross section shown in Figure 2.4. IODP sites on this transect are shown with solid black lines while IODP sites nearby are shown with dashed black lines. B) Large-scale structure of the plate boundary fault as based on *Moore et al.* [2009] (similar to *Park et al.* [2002] and *Moore et al.* [2007]). C) This study's interpretation of the large-scale structure of the plate-boundary fault.

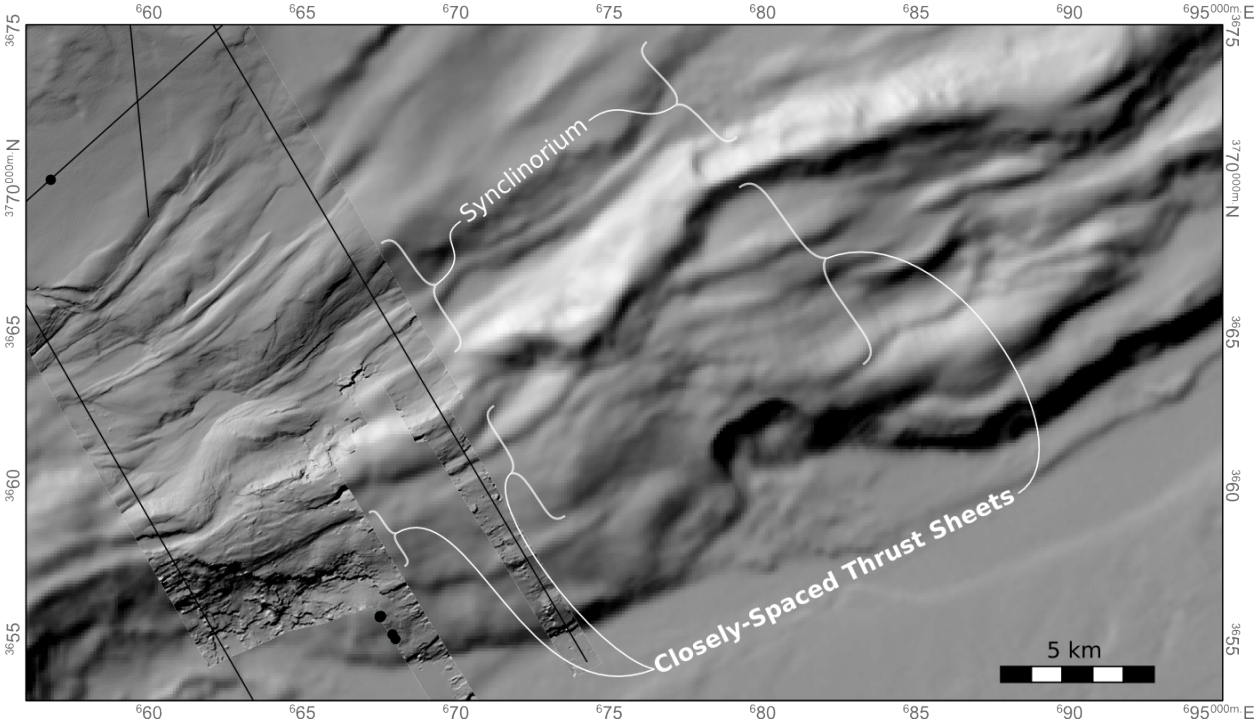

Figure 2.11: Detailed shaded relief map of bathymetry near the toe of the outer wedge. Note how the zone of closely spaced thrust sheets near the toe "pinches out" to the west. These closely spaced thrusts correspond to the thin thrust sheets shown in Figure 2.4. Extent of this map is shown by the gray box in Figure 2.2. Outline of 3D seismic volume shown by region of higher resolution bathymetry from the seafloor pick in the 3D seismic dataset. Section lines and well locations are shown in black. Map is projected in UTM Zone 53N with a datum of WGS84.

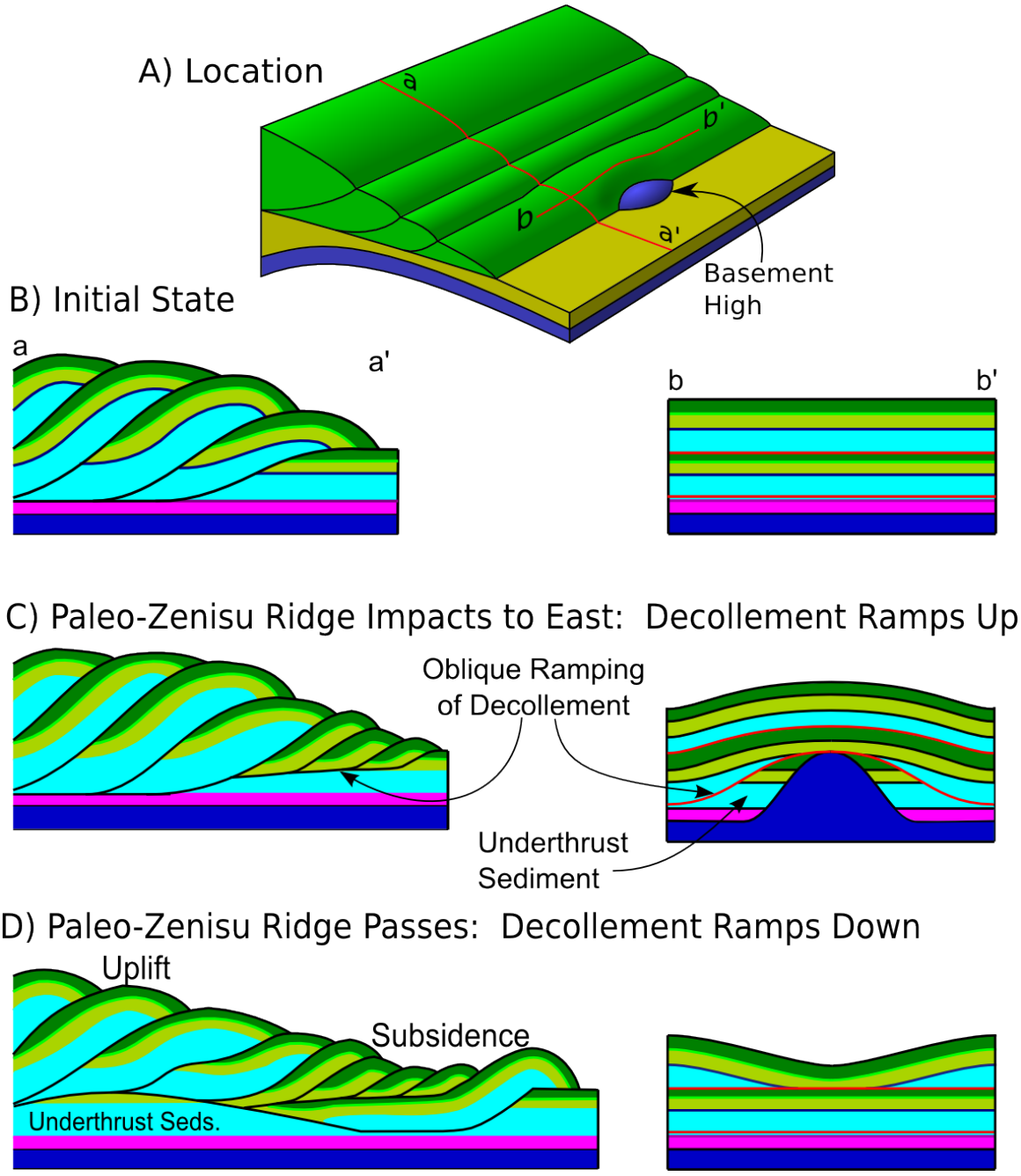

Figure 2.12: Cartoon showing model of outer wedge development as the Paleo-Zenisu Ridge passes to the east of the study area.

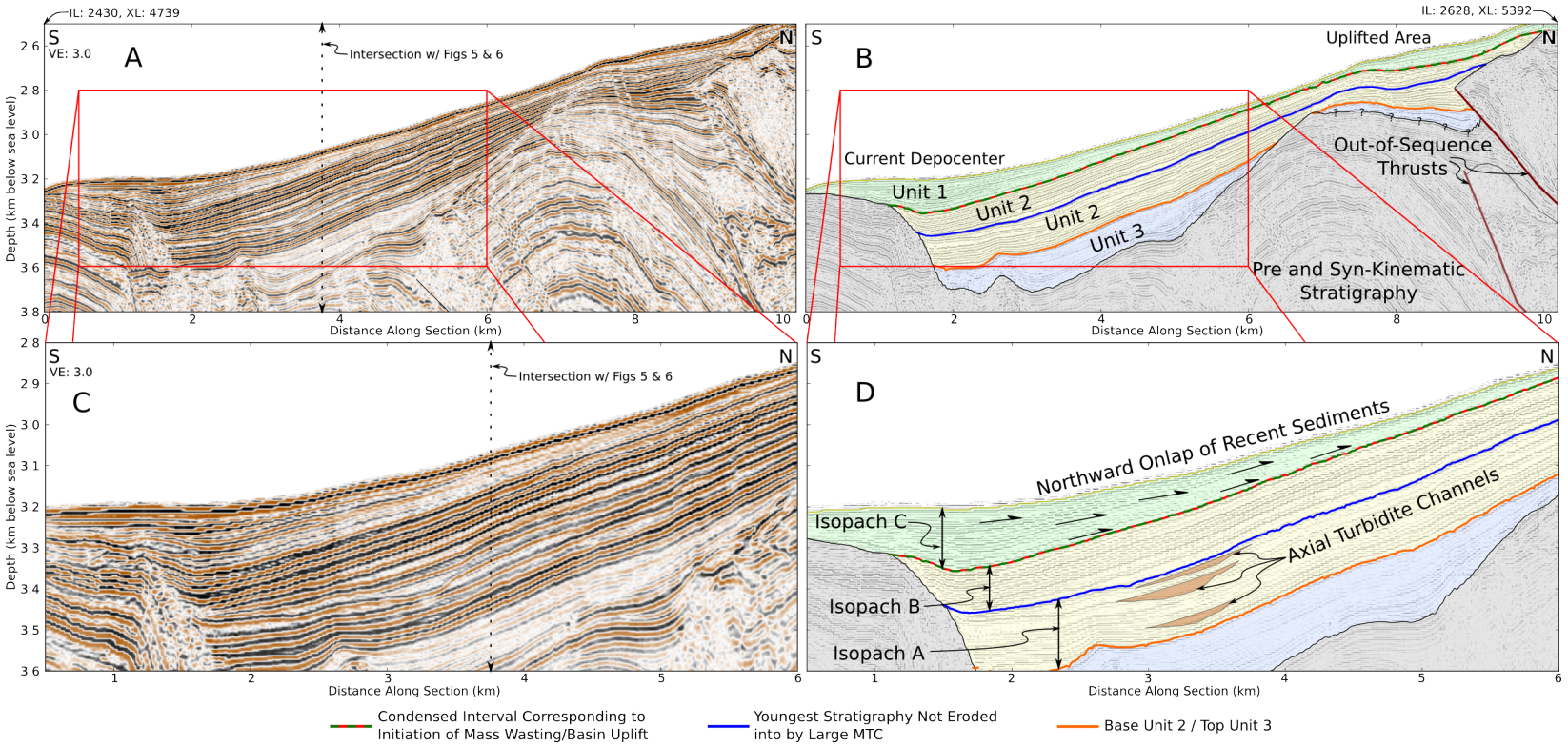

Figure 2.13: A) Shallow cross section from PSDM 3D seismic across uplifted portion of piggyback basin showing onlap of recent stratigraphy. B) Stratigraphic interpretation of (A). C) Detail of (A). D) Stratigraphic interpretation of (C). Note that the onlap surface between Units 1 and 2. This section is out of the erosional scarp for the large mass transport complex in Figure 2.6, demonstrating that Unit 1 shows onlap onto Unit 2 even where there has not been significant erosion into Unit 2. Therefore, we interpret uplift of the basin and the initiation of mass wasting to be contemporaneous. See legend in Figure 2.6 for explanation of colorscheme.

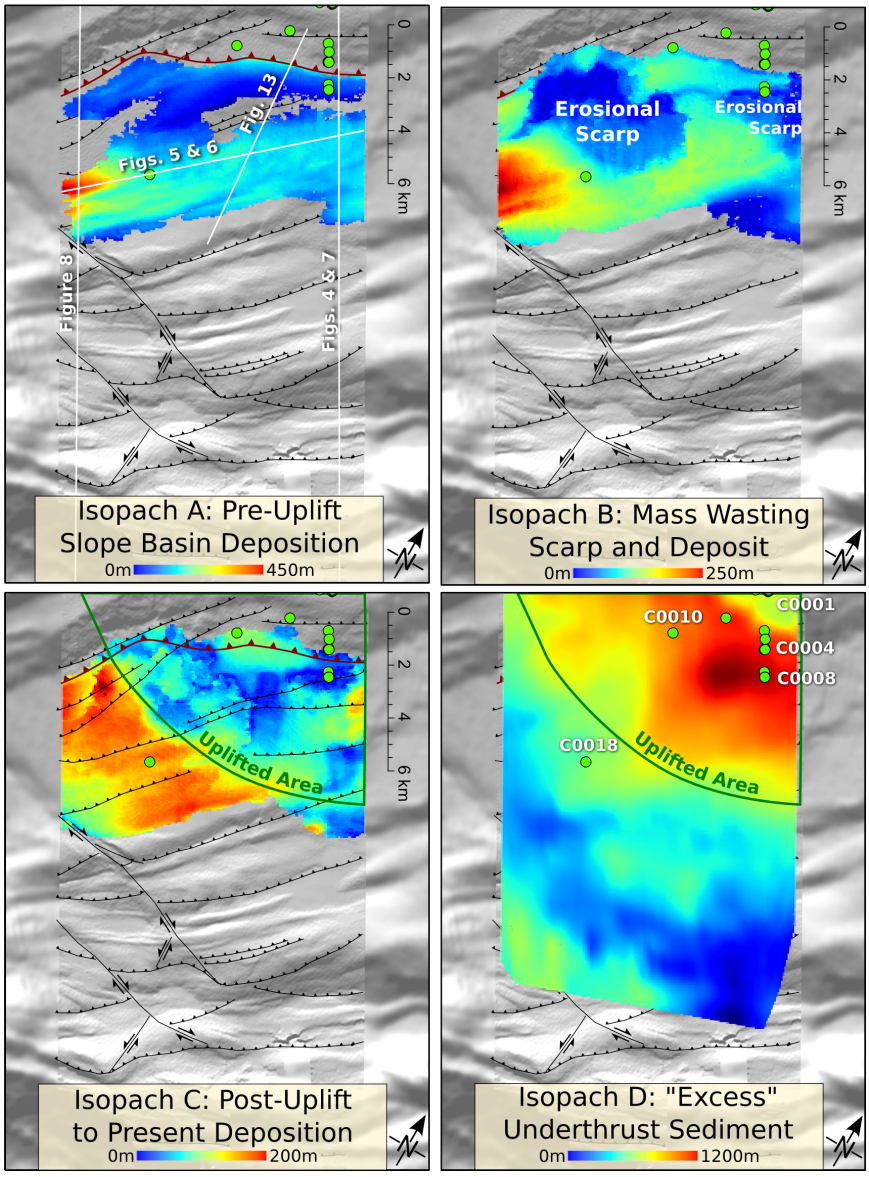

Figure 2.14: Isopachs showing sedimentation before (A) and after (C) uplift of the slope basin. Sedimentation immediately prior to and mass wasting resulting from uplift is shown in Isopach B, while the thickness of the "excess" underthrust sediment is shown in Isopach D. See Figures 2.4, 2.5, 2.6 and 2.13 for detailed vertical extents of each interval. The uplifted region of the slope basin is shown in Isopach C by the thin sediments (blue and green) deposited after the large mass wasting event. Note the differences in trend of the uplifted region and the structures underlying the slope basin. The observed pattern of uplift cannot have been produced by motion on the seaward OOST or any of the structures in the hanging wall of the décollement. However, the uplifted interval closely matches the "excess" underthrust sediment interval shown in Isopach D.

Chapter 3

Balanced Cross Sections, Shortening Estimates, and the Magnitude of Out-of-Sequence Thrusting in the Nankai Trough Accretionary Prism, Japan

Abstract

Out-of-sequence thrusting seaward of the Kumano Basin in the Nankai Accretionary Prism, Japan has been a focus of extensive recent work and two IODP expeditions. However, the amount of shortening and along strike motion accommodated by the thrusts has not been studied in detail. We constrain the total amount of shortening accommodated by the out-of-sequence thrust system in two ways. First, we compare the total shortening accommodated by all other structures in the outer wedge to the amount of shortening predicted by plate motions. Second, we use fault geometry and syn-kinematic forearc stratigraphy to model the magnitude and direction of slip on the zone's youngest structure. We then compare these two estimates to place bounds on the amount of shortening accommodated within the zone of out-of-sequence thrusting. The first method predicts 34$\pm$17 km of shortening on the entire zone, while the second predicts 14.6$\pm$1.8 km of shortening accommodated landward of the youngest out-of-sequence thrust. Additionally, kinematic modeling of the uplifted forearc basin stratigraphy constrains uplift of the forearc basin to have begun no earlier than 1.04–0.9 Ma, in contrast to previous estimates.

3.1 Introduction

Much of the recent work in the Kumano Basin region of the Nankai Trough accretionary prism, Japan has focused on the role of an out-of-sequence thrust system (OOSTS) in historic seismic events [e.g. *Park et al.*, 2002; *Moore et al.*, 2007; *Bangs et al.*, 2009a; *Strasser et al.*, 2009] (Figs 3.1 & 3.2). Understanding the role of the OOSTS in the long-term structural evolution of the outer wedge informs both site-specific work and general accretionary wedge mechanics. However, the total amount of shortening accommodated by the thrust system has not been studied in detail.

The outer wedge of the accretionary prism in the Kumano region consists of an approximately 30 km wide, predominately in-sequence fold and thrust belt [*Moore et al.*, 2009]. The OOSTS forms the boundary between the outer wedge and the forearc basin (Fig 3.2). Two prominent out-of-sequence thrusts are present in the OOSTS (Fig 3.2). Here, we term these the landward and seaward branches (Figs 3.2 & 3.3). The seaward branch of the OOSTS was penetrated at IODP sites C0004 and C0010. This fault has accommodated at least 1.9 km of shortening, beginning at $\sim$1.95 Ma, but has been inactive since $\sim$1.24 Ma [*Strasser et al.*, 2009]. However, *Gulick et al.* [2010] interpreted the edge of the forearc basin to have been uplifted over a period from $\sim$1.3 to $\sim$1.0 Ma by motion on structures within the OOSTS (Fig 3.3). The timing of forearc uplift suggests that other branches of the OOSTS, likely the landward branch, were active after activity on the seaward branch. However, while the timing of motion has been previously constrained, the magnitude of shortening accommodated by either the landward or seaward branches has not been quantified.

Previous workers have interpreted the plate-boundary fault to consist of two separate structures: 1) a "megasplay" that links to the branches of the OOSTS at 6-7 km depth and 2) a decollement that links to the deformation front at the toe of the accretionary prism [*Park et al.*, 2002; *Moore et al.*, 2009] (Fig 3.2). This interpretation is supported by the observation of two distinct, continuous reflectors: 1) a reflector beneath the forearc basin interpreted as the "megasplay" fault and 2) a separate prominent reflector beneath the outer wedge

interpreted as the décollement by *Moore et al.* [2009]. Based on analysis of hanging wall structures and the reflector's relationship with the underlying oceanic crust, *Kington et al.* [Ch. 2] hypothesized that the reflector interpreted by *Moore et al.* [2009] as the décollement is sedimentary in nature and located ∼1 km beneath the décollement. However, they did not extend their interpretation to include the region with the "megasplay" fault. Here, we extend *Kington et al.* [Ch. 2]'s interpretation beneath the forearc basin and use it as a constraint for the total shortening of the outer wedge.

We focus on two methods of estimating the amount of shortening accommodated by the OOSTS. Using the first method, we estimate the amount of shortening accommodated by the rest of the outer wedge and compare this shortening to published models of the motion of the Nankai forearc block relative to the Philippine Sea Plate to constrain shortening on the OOSTS. In the second method, we use fault geometry and the geometry of the uplifted forearc basin sediments to kinematically model the amount of shortening and direction of fault slip required to produce the observed uplift. These two methods provide independent estimates of shortening. We compare the results of these methods to constrain the role of the OOSTS in the long-term structural evolution of the Kumano outer wedge.

3.2 Method #1

The first method of estimating the amount of shortening on the OOSTS compares the present-day plate convergence rates integrated over the age of the outer wedge with the amount of shortening observed seaward of the OOSTS. Therefore, we must constrain the convergence vector between the subducting plate and the forearc basin, the age of the structures in the outer wedge, and the amount of shortening accommodated by the outer wedge. For all three of these, we rely on previously published work to provide the constraints.

3.2.1 Plate Motion Models

There are a number of different published models for the motion of the Philippine Sea Plate relative to mainland Japan (either the Eurasian Plate or the Amur Plate, depending on the model) [e.g. *Seno et al.*, 1993; *Zang et al.*, 2002; *DeMets et al.*, 2010; *Loveless and Meade*, 2010]. These models predict convergence vectors in the vicinity of the study area ranging from 301°[*DeMets et al.*, 2010] to 315°[*Zang et al.*, 2002] with rates ranging from 59 mm/yr [*DeMets et al.*, 2010] to 42 mm/yr [*Zang et al.*, 2002]. Other plate models fall between these two end-member estimates. In this study, we focus on the motion of the Nankai forearc relative to the Philippine Sea Plate. The Median Tectonic Line accommodates right-lateral strike-slip of the Nankai forearc relative to mainland Japan [e.g. *Tabei et al.*, 2003; *Loveless and Meade*, 2010]. Therefore, plate models for the motion of the Philippine Sea Plate relative to the Amur Plate likely do not reflect the convergence vector of the subducting plate relative to the forearc. For this reason, we use *Loveless and Meade's* [2010] elastic block modeling of Japan as the best available estimate of the interseismic convergence rate between the Nankai forearc and the subducting Philippine Sea Plate.

In addition to a reasonable estimate of the present-day convergence vector between the Philippine Sea Plate and the Nankai forearc, it is necessary to have an accurate estimate of the error in the convergence rate. *Loveless and Meade* [2010] provide error estimates for the location and rate of the Euler poles derived from their model, but do not provide a full covariance estimate between the parameters. Because the latitude, longitude, and rotation rate of an Euler pole representing plate motion commonly strongly co-vary, assuming no covariance between the error estimates leads to an overestimation of error in the velocity at a given location. Using *Loveless and Meade's* [2010] published Euler poles and errors predicts a convergence vector of 304°$\pm$5°with a rate of 47$\pm$5 mm/yr in the immediate vicinity of the study area. However, *Loveless and Meade* [2010] give rates of right-lateral strike-slip and reverse dip slip of 18.8$\pm$1.4 mm/yr and 44.2$\pm$2.1 mm/yr, respectively, on a fault segment in the same location with an azimuth of 236°. This yields a convergence vector of

302.8°±2.2°with a rate of 48.0±1.7 mm/yr. Due to the previously mentioned overestimation of error in the former estimate, we consider the latter estimate more realistic.

3.2.2 Age of Outer Wedge Structures

The in-sequence thrust sheets in the footwall of the seaward-most thrust branch in the OOSTS were cored at IODP site C0008, and the youngest pre-kinematic sediments date to 1.95-2.512 Ma, based on biostratigraphy [*Strasser et al.*, 2009]. However, *Strasser et al.* [2009] consider the older portion of the 1.95-2.512 Ma age interval a more reasonable estimate for the age of the oldest in-sequence structures seaward of the OOSTS. Therefore, we consider the thrust sheets seaward of the OOSTS to have formed since 2.3±0.2 Ma in our calculations.

3.2.3 Balancing of Outer Wedge Structures

To estimate the amount of shortening accommodated seaward of the OOSTS, we use the interpretation of *Kington et al.* [Ch. 2] (Fig 3.4). We focus on a single section along the eastern edge of the 3D seismic survey, as this avoids out-of-plane complications due to right-lateral tear faults that offset and interfere with many of the folds in the outer wedge.

3.2.3.1 Using Bed Length as a Strain Estimate

Bed-length (or "line") balancing of cross sections provides a reasonable minimum estimate of shortening, despite being an over-simplification of the complex deformation that occurs in fold and thrust belts [*Dahlstrom*, 1969; *Woodward et al.*, 1989]. However, bed-length balancing assumes no volume loss, and sediments in accretionary prisms commonly undergo extensive volume loss during deformation and deform through both ductile and brittle processes [*Bray and Karig*, 1985; *Morgan and Karig*, 1995; *Screaton et al.*, 2002; *Moore et al.*, 2011]. In order to use bed-length balancing as an integrated strain measurement, we need to estimate the lateral volume loss during deformation and the amount of ductile shortening within the thrust sheets. We define the term α as a measure of the sum of these

effects:

$$\alpha = \frac{T_s}{F_s} - 1 \tag{3.1}$$

where T_s is the total amount of shortening, F_s is the shortening accommodated by fault slip, with α expressed as a fraction. Therefore, we can estimate the total shortening from the observed shortening on discrete structures as

$$T_s = (1 + \alpha)F_s \tag{3.2}$$

Based on data from the Muroto region of the Nankai trough near ODP Site 808, *Morgan and Karig* [1995] and *Moore et al.* [2011] have suggested that brittle shortening, such as that estimated from bed-length balancing, may account for $< \frac{1}{3}$ of the overall shortening accommodated by structures in the accretionary prism, implying $\alpha > 200\%$. However, these estimates exceed the local rate of plate motion by a significant factor. Given that the age of pre-kinematic sediments at site 808 is constrained to be <0.28 Ma [*Pickering et al.*, 1993; *Olafsson*, 1993], the estimate of shortening accommodated by the structures seaward of and including the thrust sheet at site 808 from *Moore et al.* [2011] (2.43 km) is considerably larger than the ~1.5 km of plate motion estimated over the same time [*Loveless and Meade*, 2010]. *Morgan and Karig* [1995] do not give shortening estimates for individual thrust sheets, but calculate similar total shortening estimates as *Moore et al.* [2011]. Because these shortening estimates are larger than the total plate motion, we consider the α values derived from them to be unrealistically large. *Butler and Paton* [2010] estimate 18%-25% lateral volume loss for similar deep-water sediments in a gravitationally-driven fold and thrust belt, yielding α values of 22%-33%, Therefore, we assume an α value of 30±10% for this study.

3.3 Results of Method #1

The component of the convergence vector from *Loveless and Meade* [2010] parallel to the section in Figure 3.2 (azimuth: 330°) is 42.9±2.1 cm/yr. Based on the interpretation of IODP results by *Strasser et al.* [2009], we estimate that the structures seaward of the OOSTS have formed in the last 2.3±0.2 Ma. Integration of the convergence rate over this timeframe

predicts 99±10 km of total shortening parallel to the section shown in Figure 3.2 (Fig 3.5). The results of *Kington et al.* [Ch. 2] suggest that the restored length of the outer wedge is 82±2 km (Fig 3.4). We include ±10% of this length as an estimate of the interpretation error. The deformed length of the section is 32 km (Fig 3.4), yielding a total shortening estimate of 50±10 km (Fig 3.5). Applying an α value of 30±10% yields a total of 65±14 km of shortening accommodated by the outer wedge structures (Fig 3.5). Therefore the OOSTS has likely accommodated 34±17 km of shortening measured parallel to the section in Figure 3.2.

3.4 Method #2

The second method of estimating shortening on the OOSTS uses kinematic modeling of forearc uplift using the 3D geometry of the landward branch of the OOSTS imaged in 2D [*Taira and Curewitz*, 2005] and 3D [*Moore et al.*, 2007, 2009; *Bangs et al.*, 2009a; *Park et al.*, 2010] seismic reflection data. We invert for the amount and direction of shortening on the landward branch required to restore each uplifted horizon to horizontal. In doing so, we are explicitly assuming that all of the observed forearc uplift is due to motion on the landward branch of the OOSTS. While there is localized deformation within the forearc that cannot be attributed to movement on the landward branch (e.g. near crossline 7500 on Figure 3.3), we consider this negligible. Unlike method #1, this method constrains only shortening accommodated by the landward branch of the OOSTS. Therefore, we can estimate the amount of shortening on the seaward branch of the OOSTS by combining methods #1 and #2.

3.4.1 Syn-kinematic Stratigraphy

Gulick et al. [2010] identified twelve key intervals in the Kumano forearc basin, and numbered them in reverse-stratigraphic order (increasing age) 1–12. We use a similar horizon naming strategy as *Gulick et al.* [2010] for ease of comparison. Using post-stack depth-migrated 3D reflection seismic data, we define 3D surfaces throughout the forearc basin for the top and bottom of *Gulick et al.* [2010]'s intervals 1–7 (Fig 3.3). We then number

these horizons 1–7 where each numbered horizon is the bottom of the corresponding interval in *Gulick et al.* [2010] (Fig 3.3). In addition to the top and bottom of each interval, we sub-divide intervals 2–4 and number these horizons based on the horizons above and below them. For example, horizon 3.5 is between horizons 3 and 4, and corresponds to the center of *Gulick et al.* [2010]'s interval 4 (Fig 3.3). This yields a total of ten 3D horizons that can be used to constrain the direction and amount of slip of the fault, when coupled with the fault's geometry.

3.4.2 Fault Geometry

3.4.2.1 Fault Surface Irregularities

The landward branch of the OOSTS is imaged by 2D and 3D seismic down to its intersection with the main plate-boundary fault [*Park et al.*, 2002; *Moore et al.*, 2007, 2009]. Therefore, we can confidently interpret a 3D fault surface throughout the study area (Fig 3.6). In order to accurately model motion, we extend the surface down-dip along the main plate-boundary fault to the depth limits of the 2D seismic data. The fault has a broad ridge parallel to its overall dip near the western edge of the 3D seismic volume (Fig 3.6). Because of this and other along-strike geometric variations in the fault, we can distinguish components of dip-slip and strike-slip based on the geometry of the syn-kinematic forearc stratigraphy.

3.4.2.2 Depth Conversion

In order to constrain the strike-slip component of any motion on this fault from deformed forearc stratigraphy imaged within the 3D volume, we need to constrain the geometry of the fault surface over an area larger than the stratigraphy is imaged over. Otherwise, any strike-parallel motion of the horizon will be unconstrained by the fault's geometry. To do this, we combine the available 2D and 3D seismic data in the study area. Kinematic models of deformation caused by movement on a fault require true depths to the fault's surface. However, while post-stack depth-migrated (PSDM) 3D data is available [*Moore et al.*, 2009], we have the 2D data only in post-stack time form. Therefore, we used the PSDM velocities

for the 3D seismic data [*Park et al.*, 2010] to build a simplified 1D velocity model matching sub-seafloor travel-time to the fault reflector to the depth equivalent in the 3D volume. Because it is not representative of portions of the accretionary prism other than the forearc basin and inner wedge, this model is used *only* to match the fault geometry in time over the area covered by the 2D seismic lines to the fault geometry in depth, and is not used to depth-convert the 2D seismic as a whole for interpretation. Nonetheless, it accurately matches the fault reflector imaged in 2D seismic to the PSDM 3D data and should provide a reasonable constraint on fault geometry outside the 3D seismic volume.

3.4.3 Kinematic Model

To model the uplift resulting from movement along the fault, we implemented a homogeneous inclined shear method [*White et al.*, 1986]. We followed the methods described in *Egan* [1999] and *Kerr et al.* [1993] for implementing inclined shear in three dimensions, but we supplied a fault geometry and inverted for fault slip, rather than inverting for a fault geometry as in *White et al.* [1986] and *Kerr et al.* [1993]. The homogeneous inclined shear method was developed for, and is most often applied in, extensional settings. Although other models *Suppe* [e.g. 1983] are more commonly applied to compressional settings, homogeneous inclined shear is generally applicable and yields reasonable geometries for reverse faulting [*White et al.*, 1986]. Furthermore, inclined shear kinematic models are computationally faster and simpler to implement in 3D than flexural-slip models such as *Suppe* [1983]. The computational speed of the fault kinematic model is important in this study because we iteratively invert for fault slip. Therefore, flexural-slip models are impractical for the purposes of this study and homogeneous inclined shear is better suited to our problem.

3.4.3.1 Simplifying Assumptions

In addition to choosing an appropriate kinematic model, we must make some simplifying assumptions. Homogeneous inclined shear assumes that deformation is the result

of a single slip vector along the fault which does not vary with depth [*White et al.*, 1986]. In general, the magnitude of the slip vector could be allowed to vary perpendicular to its direction in 3D. However, we model the slip as constant everywhere along the fault to simplify the inversion process. Furthermore, we neglect the effect of sedimentary compaction on the geometry of syn-kinematic sediments. As the uplifted sediments at the seaward edge of the forearc have not been deeply buried, the effect of compaction on the overall geometry of the horizon should be relatively small. We also restrict the shear angle through which the hanging wall deforms to lie in the direction of slip. We invert for slip direction and magnitude, both of which are allowed to freely vary, but we impose this restriction so that the hanging wall does not deform out of the plane of slip.

3.4.4 Inversion of Fault-Slip Vector

We use a non-linear conjugate-direction method [*Powell*, 1964] to invert the observed 3D geometry of uplifted horizons for a 2D slip vector along the fault surface using inclined shear as a kinematic model. We assume each horizon was deposited horizontally, and therefore we minimize the variance of the horizon's elevation. We invert for the offset required to flatten each syn-kinematic horizon independently, with a starting guess of zero movement.

3.4.4.1 Estimation of Shear Angle

Homogeneous inclined shear [*White et al.*, 1986] requires an estimate for the shear angle by which the hanging wall deforms (see *Egan* [1999] for a graphical depiction). In general, this angle may vary over a 360° range in azimuth, as well as over a 90° range in plunge. To reduce the parameter space over which we are inverting we restrict this angle to lie along the plane of slip. This restricts the shear angle to range between -90° and 90° in a vertical plane. Due to numerous local minimums, most standard non-linear inversion techniques did a poor job of finding both the shear angle and offset that best flattened the syn-kinematic stratigraphy without a starting guess. Therefore, we used a grid search

to find the single shear angle that best flattened all syn-kinematic stratigraphy. For each trial shear angle, we inverted for the offset and azimuth that best flattened each horizon and summed the resulting variances. The grid search resulted in a maximum reduction of variance at a shear angle of 70°, equivalent to distributed back-thrusting on faults dipping 20°seaward. We assume the same shear angle with respect to vertical for all syn-kinematic stratigraphy, though we allow its azimuth to vary with the inverted slip vector for each horizon.

3.4.4.2 Estimation of Offset and Slip Direction

Each syn-kinematic horizon yields an independent estimate of the offset vector required to restore it to horizontal. Because we have a sequence of syn-kinematic stratigraphy, we can use the stratigraphic order of the horizons in two ways: 1) The stratigraphic order provides an independent test of our solution. Older syn-kinematic horizons should require progressively more offset to be restored to horizontal. 2) We can use the differential offset between each restored horizon as an estimate of the slip direction on the fault during the deposition of the interval between each horizon. This allows us to constrain how the azimuth of slip on the fault has evolved through time.

We assess the error in the offset vector for each horizon using 200 trials of bootstrapping with replacement. We resample both the horizon and fault surfaces in each trial, resulting in 200 estimates of the offset vector required to restore each horizon to horizontal. The error in each measurement can then be estimated from the resulting distribution.

3.5 Results of Method #2

Because each horizon is independently inverted for an offset vector, the stratigraphic order of the horizons provides a test of our results. As expected, each horizon restores to a progressively larger offset, with the oldest horizons requiring the greatest offset to be flattened (Fig 3.7). Horizons 5–7 restore to horizontal at approximately the same position (Fig 3.8). They have almost identical dips (Fig 3.9) and the difference between their restored

positions is less than 500 meters. We therefore consider the difference between their restored positions negligible, implying that horizons 5–7 are pre-kinematic.

Thus, we can use the average restored positions of horizons 5–7, including their individual errors based on bootstrapping, as an estimate of the total shortening accommodated on the landward branch of the OOSTS. This yields 15.4±2.0 km of shortening at an azimuth of 321°(Fig 3.8). This amount of shortening produces 11 km of heave along the fault at an azimuth of 300°, providing a minimum bound on of the amount of shortening (Fig 3.8). The total estimated shortening results in 14.6±1.8 km of shortening parallel to the section in Figure 3.2 (Fig 3.8).

3.6 Discussion

3.6.1 Timing of Forearc Uplift

The results of method 2 require almost all of the motion on the landward branch of the OOSTS to have occurred after the deposition of horizon 4—dated to ∼0.9-1.04 Ma based on biostratigraphy at IODP site C0002 [*Expedition 314 Scientists*, 2009; *Gulick et al.*, 2010]. Furthermore, because the required displacements are all non-zero, all but the youngest forearc strata appear to have been uplifted and tilted since their deposition. This suggests that motion on the landward branch of the OOSTS may have continued up until the present or recent geologic past. Although no age constraints are available for the youngest forearc basin stratigraphy, horizon 3 corresponds to the surface S1 identified at IODP site C0009 by the *Expedition 319 Scientists* [2010] and must be younger than 0.5 Ma based on biostratigraphy [*Expedition 319 Scientists*, 2010]. Therefore, we infer that forearc uplift began ∼0.9 Ma and continued until sometime <0.5 Ma, possibly continuing to the present.

In addition to the results of kinematic modeling from method 2, the timing of tilting of the forearc basin stratigraphy is constrained by differences in present-day dips of the horizons. Horizons 5–7 all consistently dip ∼4.5°, while horizons 1–2.5 dip ∼1°(Fig 3.9). Furthermore, horizons 3, 3.5, and 4 show the most abrupt changes in dip, requiring that the

majority of forearc tilting occurred during deposition of interval 4, from ∼0.9 Ma–<0.5 Ma (Fig 3.9).

These results contradict previous interpretations of the timing of forearc uplift. *Gulick et al.* [2010] interpret the forearc stratigraphic intervals 8–12 to pre-date development of the landward branch of the OOSTS, intervals 5–7 to be syn-kinematic with movement on the landward branch, and intervals 1–4 to be post-kinematic (Fig 3.3). *Gulick et al.* [2010] use the age of the base of interval 4 (∼0.9 Ma) as the termination of forearc tilting. However, their isopach maps (e.g. Figure 4f in *Gulick et al.* [2010]) and cross sections (e.g. Figure 2 in *Gulick et al.* [2010]) demonstrate that most of the tilting in the forearc occurred during the deposition of interval 4 and that little or no tilting occurred during the deposition of the intervals they interpret as syn-kinematic with tilting. Therefore, we conclude that our results are compatible with their data, although our interpretations differ.

3.6.2 Structural Interpretation

While our structural interpretation is based on *Kington et al.* [Ch. 2], we have extended their interpretation to include the geometry of the plate boundary fault beneath the forearc basin (Fig 3.2). Based on both 2D and 3D reflection seismic data, previous workers [e.g. *Park et al.*, 2002; *Moore et al.*, 2009] interpreted the plate-boundary to be partitioned into two separate faults that connect at ∼8-9 km depth, beneath the forearc basin. The upper and most steeply dipping of these they termed the "megasplay"; they interpreted the lower fault as the primary decollement beneath the outer wedge (Fig 3.2). However, the reflector interpreted as the lower décollement, termed the "bright deep reflector" by *Kington et al.* [Ch. 2], is likely below the active decollement beneath the outer wedge and most likely corresponds to a sedimentary reflector in the interval underthrust beneath the decollement [*Kington et al.*, Ch. 2] (Fig 3.2).

Following *Kington et al.* [Ch. 2], we interpret the "bright deep reflector" as underthrust Middle Shikou basin sediments, with the decollement above this reflector (Fig 3.2). This interpretation requires the decollement to directly connect to the reflector interpreted as

the "megasplay" by *Moore et al.* [2009] seaward of IODP site C0002 (Fig 3.2). The resulting geometry implies that there is only a single plate-boundary fault and that there is no "megasplay" fault separate from it. We therefore interpret the OOSTS as a system of out-of-sequence thrusts that directly sole into the plate-boundary fault, rather than connecting to a "megasplay" system that then connects to the plate-boundary fault (Fig 3.2). This leads to a simpler and more mechanically compatible geometry than previous interpretations.

The Kumano Basin Edge Fault Zone's (KBEFZ) age of initiation and relationship to other structures are poorly constrained [*Martin et al.*, 2010]. However, it appears to be active today [*Martin et al.*, 2010], and its geometry is incompatible with motion on the OOSTS. Therefore, we infer that the KBEFZ probably crosscuts the OOSTS. Based on this interpretation, the KBEFZ likely connects directly to the plate-boundary fault at depth (Fig 3.2). This is supported by *Kamei et al.* [2012]'s observation of a vertically oriented low velocity zone (LVZ_3 in *Kamei et al.* [2012]'s Figure 4b) beneath the surface expression of the KBEFZ. This low velocity zone extends to a depth of $\sim$6 km, similar to our interpretation of the plate-boundary fault's position at this location (Fig 3.2).

3.6.3 Comparison of Estimates

Bed-length balancing (method #1) and inversion of syn-kinematic stratigraphy (method #2) yield compatible estimates for the amount of shortening accommodated on the OOSTS (Fig 3.10). Bed-length balancing and plate motion estimates predict that the OOSTS has accommodated a total of 34$\pm$17 km of shortening parallel to the section line in Figure 3.2 (Fig 3.5). Restoration of uplifted forearc basin stratigraphy suggests that the landward branch of the OOSTS has accommodated 14.6$\pm$1.8 km of shortening in this direction (Fig 3.10). Based on *Strasser et al.* [2009], the seaward branch accommodated at least an additional 1.9 km, but may have accommodated significantly more. Therefore, we consider the estimate of total shortening on the OOSTS from method #1 and the estimate of shortening on the landward branch from method #2 to be internally consistent, as method #2 does

not estimate more than method #1 or less than the minimum constraint from *Strasser et al.* [2009].

Because the two methods yield compatible measurements of total OOSTS shortening and the shortening of the landward branch, we use them to constrain the shortening on the seaward branch of the OOSTS. Subtracting estimated shortening on the landward branch (14.6±1.8 km) from the total estimated shortening on the OOSTS (34±17 km) yields an estimate of 19±17 km of shortening on the seaward branch of the OOSTS (Fig 3.10). This suggests that the landward and seaward branches accommodated similar amounts of shortening at different times, though the uncertainty in the amount of shortening on the seaward branch is almost as large as its magnitude.

3.6.4 Obliquity of Slip

Our kinematic modeling suggests that the overall slip vector on the landward branch of the OOSTS has an azimuth of 321°, ∼10°oblique to the dip of the fault and ∼15°oblique to plate motion (Fig 3.8). However, the incremental slip vector during the main phase of forearc tilting has an azimuth of ∼305°, subparallel to plate motion (Fig 3.8). This suggests that the obliquity of convergence was accommodated by oblique slip on the out-of-sequence thrusts. Therefore, strain was likely not partitioned onto separate strike-slip structures landward of the OOSTS during activity on the landward branch from ∼0.9 Ma to <0.5 Ma.

3.6.5 OOSTS Influence on Outer Wedge Development

3.6.5.1 Forward Imbrication vs. Out-of-Sequence Shortening

The OOSTS accommodated large portions of the total shortening across the prism during two different periods. Based on our results, the OOSTS accommodated 35%±18% of the total shortening in the outer wedge over the last ∼2.0–2.5 Myr. However, our results suggest that during the period when the landward branch was active (∼1.04–∼0.5 Ma), it accommodated 63%±9% of the total plate convergence vector. Similarly, although the uncertainty is very large, our results predict that the seaward branch of the OOSTS accommodated 62%±56%

of the total plate convergence vector from ∼1.95–1.24 Ma, based on ages from *Strasser et al.* [2009]. *Strasser et al.* [2009] argued that the seaward branch accommodated only 15-22% of the overall plate convergence vector during its most rapid stage of growth in this time interval. However, they use heave as a direct estimate of shortening accommodated by the fault, and we therefore consider this an under-estimate. The total shortening accommodated by the seaward branch must have been considerably larger, as the hanging wall clearly deformed during movement on the fault. Therefore, similar to *Strasser et al.* [2009], we infer that movement on a branch of the OOSTS dominated shortening in the outer wedge during the time when it was active, and that forward imbrication of thrust sheets at the toe may have slowed or temporarily ceased.

3.6.5.2 Cause of Out-of-Sequence Thrusting

Our new results for the timing of motion on the landward branch of the OOSTS may have implications for the cause of out-of-sequence thrusting in the outer wedge. There is a gap of ∼0.3 Myr between the last motion on the seaward branch and the initiation of motion on the landward branch of the OOSTS. This suggests that the outer wedge shifted from forward imbrication to out-of-sequence shortening from 1.95–1.24 Ma, then back to forward imbrication from 1.24 to 1.04–0.9 Ma, and then back to out-of-sequence shortening at around 1.04-0.9 Ma. This sequence of shifts suggests that some discrete events perturbed the outer wedge fold and thrust belt system, resulting in a change in the critical taper angle. Based on *Kington et al.* [Ch. 2], the Paleo-Zenisu Ridge may have impacted the outer wedge to the east of the study area at approximately 1 Ma. This basement topographic high may have resulted in a higher effective basal friction along the decollement. Higher basal friction leads to a larger critical taper angle, causing out-of-sequence thrusting as the outer wedge thickens [*Dahlen et al.*, 1984].

3.7 Conclusions

Based on our results, the in-sequence portion of the outer wedge has accommodated 99±10 km of shortening, while the out-of-sequence thrust system (OOSTS) accommodated 34±17 km of margin perpendicular shortening. 15±2 km (minimum of 11 km) of this occurred on the landward branch of the OOSTS. This is 34%±15% of the total 99±10 km of shortening predicted by the convergence vector between the Nankai forearc and the subducting Philippine Sea Plate [*Loveless and Meade*, 2010]. However, during the individual periods when the landward and seaward branches were active, they accommodated up to 65% of the total plate convergence vector. This suggests that out-of-sequence thrusts dominate shortening along convergent margins during the relatively short periods when they are active.

Our forearc modeling results suggest that the uplift and tilting of the forearc basin, and therefore motion on the landward branch of the OOSTS, began 1.04–0.9 Ma and continued until sometime <0.5 Ma, possibly until essentially the present. This timing suggests that there was a ∼0.2–0.3 Myr period of forward imbrication between motion on the seaward branch of the OOSTS and motion on the landward branch. Furthermore, the initiation of motion on the landward branch of the OOSTS may correspond to the nearby subduction of the Paleo-Zenisu Ridge, suggesting a link between basement topography and out-of-sequence thrusting.

Acknowledgements

This work was funded by NSF grant BLAH. Seismic interpretation was preformed in Geoprobe® Volume Interpretation Software [*Landmark*, 2003], which was generously provided by Halliburton, Inc. To visualize and display the seismic interpretation, including figures in this work, we wrote software in Python [*van Rossum and Drake*, 2006] using Numpy [*Oliphant*, 2007], Matplotlib [*Hunter*, 2007], and SciPy [*Jones et al.*, 2001]. The inclined shear method for restoring forearc stratigraphy (the `fault_kinematics` Python library [*Kington*,

2012b]) was implemented in Python using Numpy and SciPy. Code and fault data used in this paper are available at `https://github.com/joferkington/oost_paper_code`.

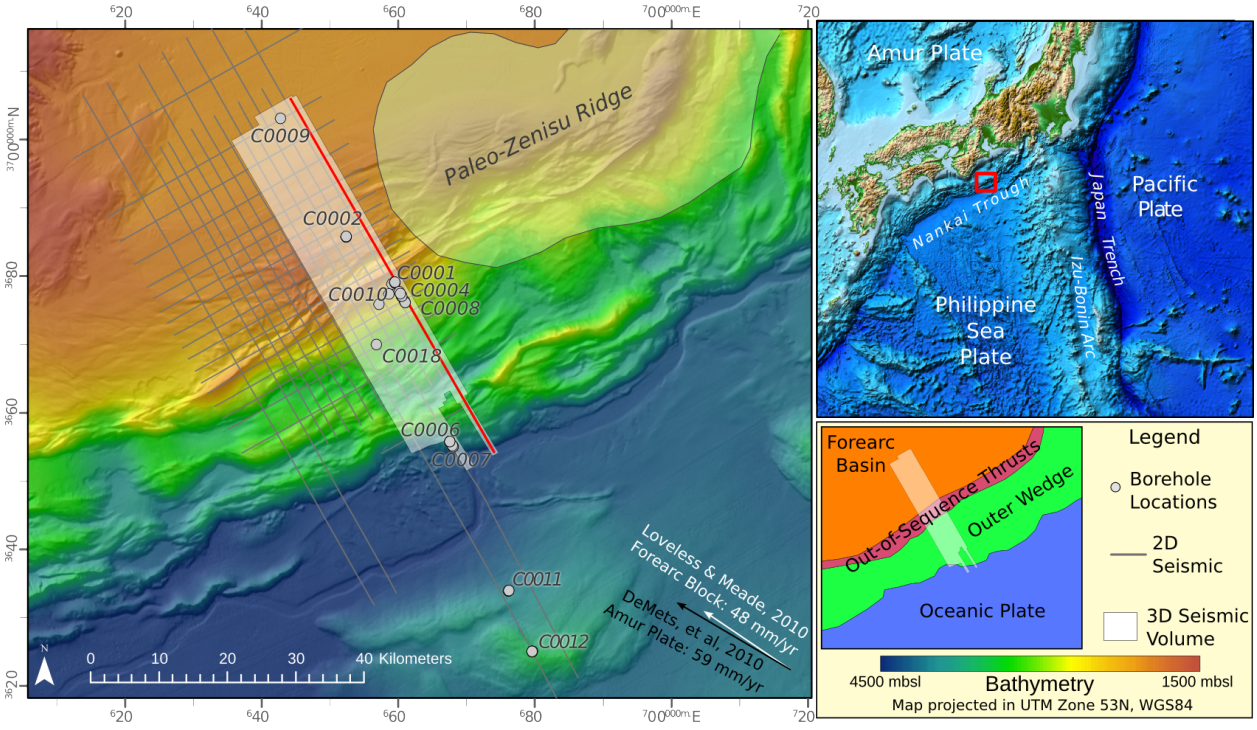

Figure 3.1: Location of study area. The Out-of-Sequence Thrust System (OOSTS) lies immediately seaward (southeast) of the KBEFZ (see inset in lower right). The OOSTS forms a steep topographic break between the forearc basin and the outer wedge. 2D seismic data used in this study [*Taira and Curewitz*, 2005] are shown by dark gray lines, and the transparent white box shows the extent of the 3D seismic volume [*Moore et al.*, 2007]. Arrows in the lower right corner of the figure show motion of the Philippine Sea plate relative to the stable Amur plate (*DeMets et al.* [2010], shown in black) and the Kumano forearc block (*Loveless and Meade* [2010], shown in white). The extent of the subducted Paleo-Zenisu Ridge (based on *Park et al.* [2003]) is shown in pale white.

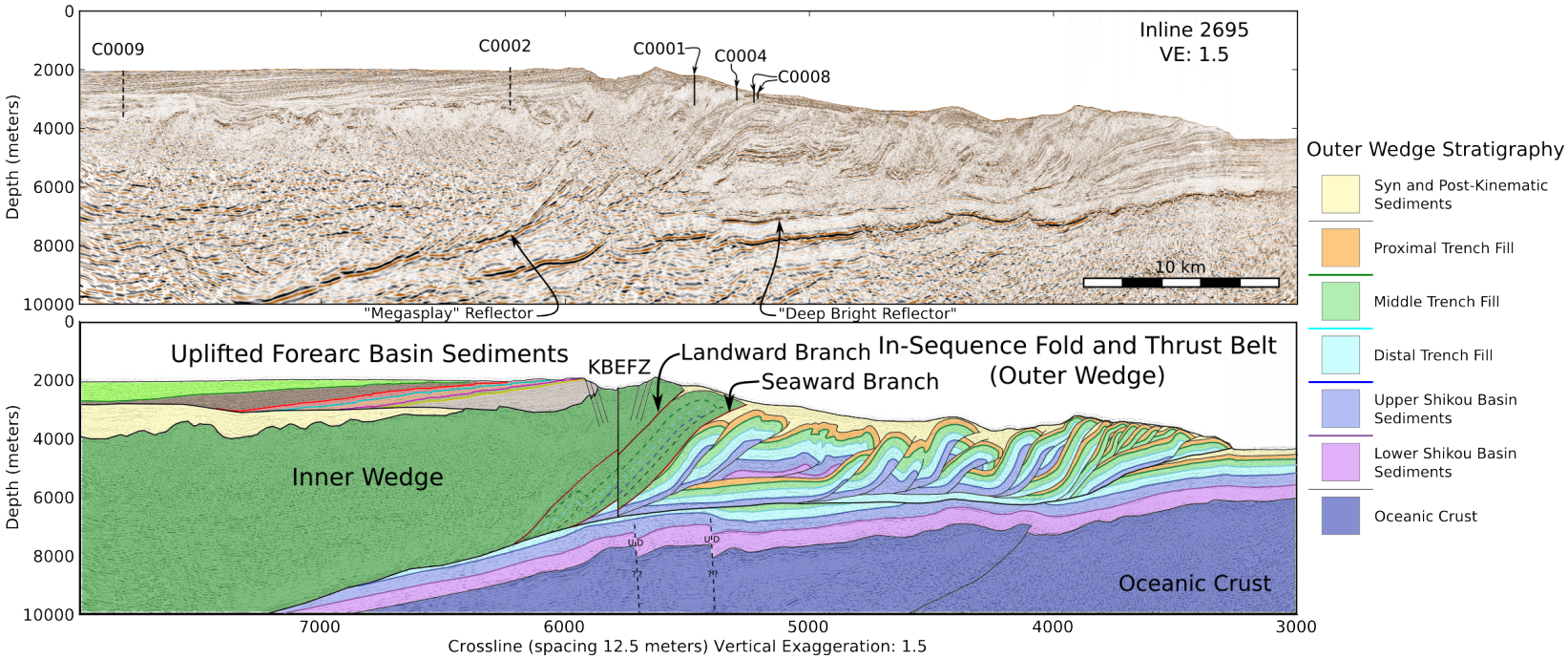

Figure 3.2: Cross section along the eastern portion of the 3D seismic volume showing the structural interpretation [*Kington et al.*, Ch. 2] used to calculate shortening accommodated seaward of the Out-of-Sequence Thrust System (OOSTS). The seaward and landward branches of the OOSTS are shown in dark red near crossline 5500. Note that we interpret the structures in the OOSTS to connect directly to the plate-boundary megathrust instead of connecting to a "megasplay". We also interpret the Kumano Basin Edge Fault Zone (KBEFZ) to crosscut the OOSTS based on the vertical low velocity zone observed by *Kamei et al.* [2012].

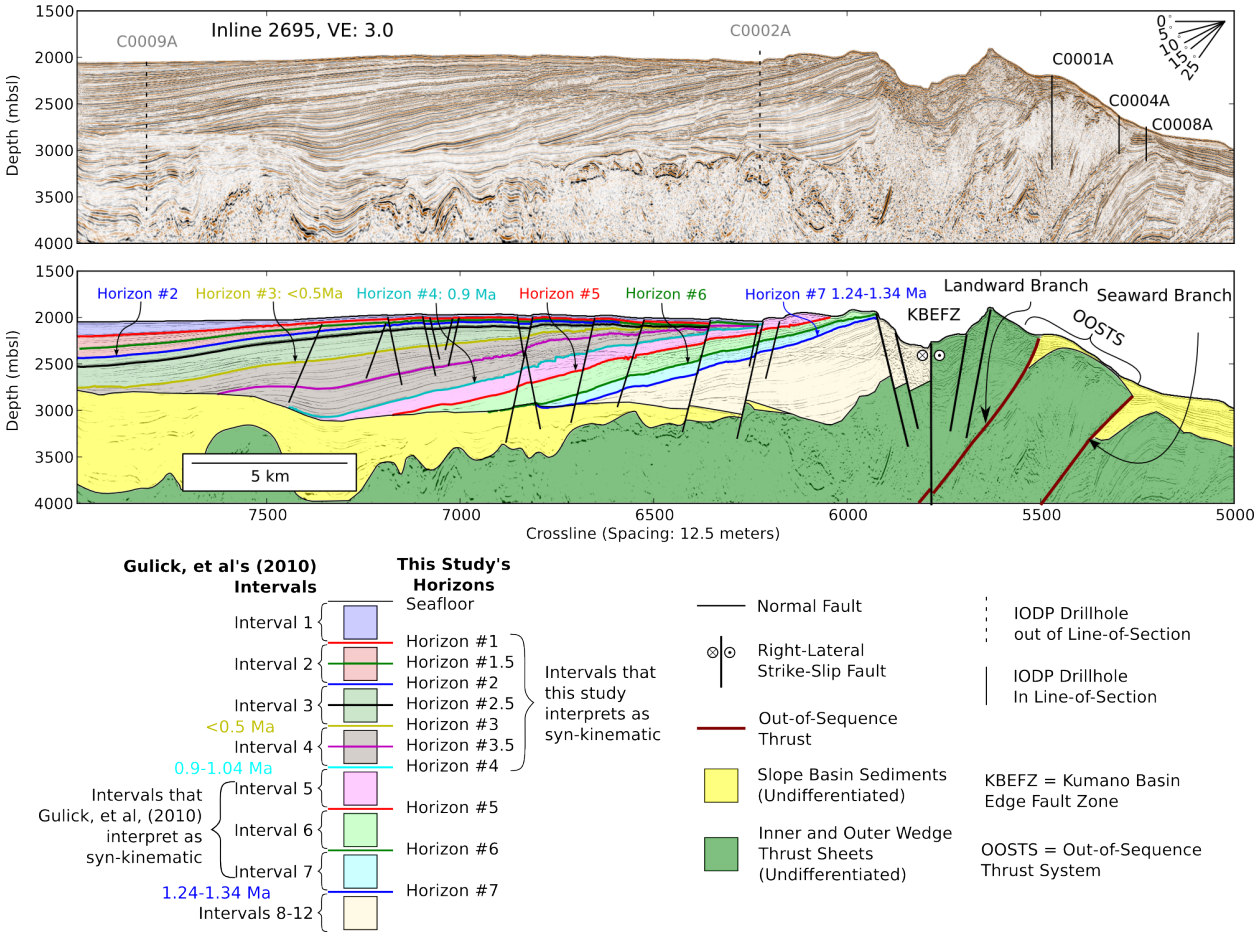

Figure 3.3: Cross section through uplifted forearc stratigraphy used in method #2. Naming follows conventions in *Gulick et al.* [2010] with the horizon number corresponding to the bottom of the intervals in *Gulick et al.* [2010]. Note the change in dip between horizons 3 & 4 (over interval 4). This change is shown quantitatively in Figure 3.9. Based on the change in dip and the differences in restored positions of the horizons (Fig 3.8), we interpret intervals 4 and younger as syn-kinematic. This implies that the majority of forearc tilting did not occur until after ∼0.9 Ma, consistent with *Gulick et al.* [2010]'s data, but contrary to their interpretation.

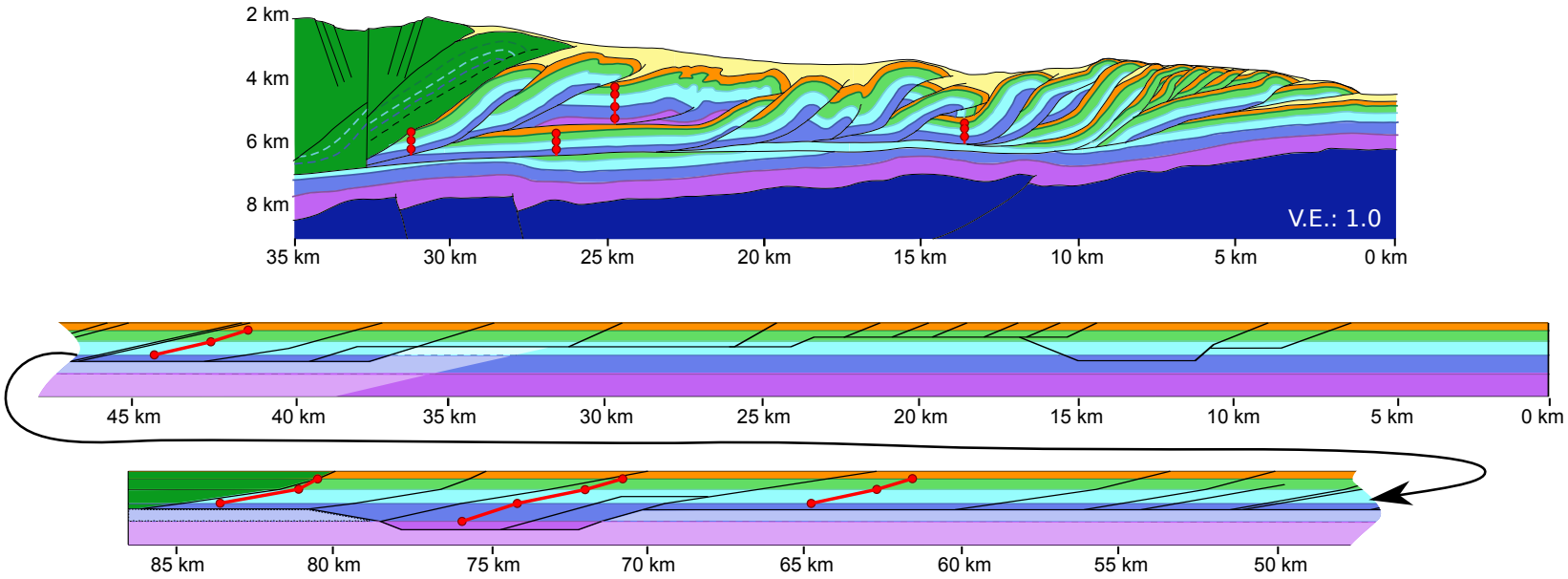

Figure 3.4: Bed-length balancing of the outer wedge interpretation shown in Figure 3.2. The restored length of the section seaward of the last pin line is 82±2 km. We assume a 10% interpretation error in this measurement, yielding a restored length of 82±10 km. This yields a shortening estimate of 50±10 km, based on the present-day length of the deformed section (32 km). This shortening estimate does not account for volume loss or bed-length changes during deformation and is therefore a minimum estimate. We apply an additional correction for volume loss (See Figure 3.5).

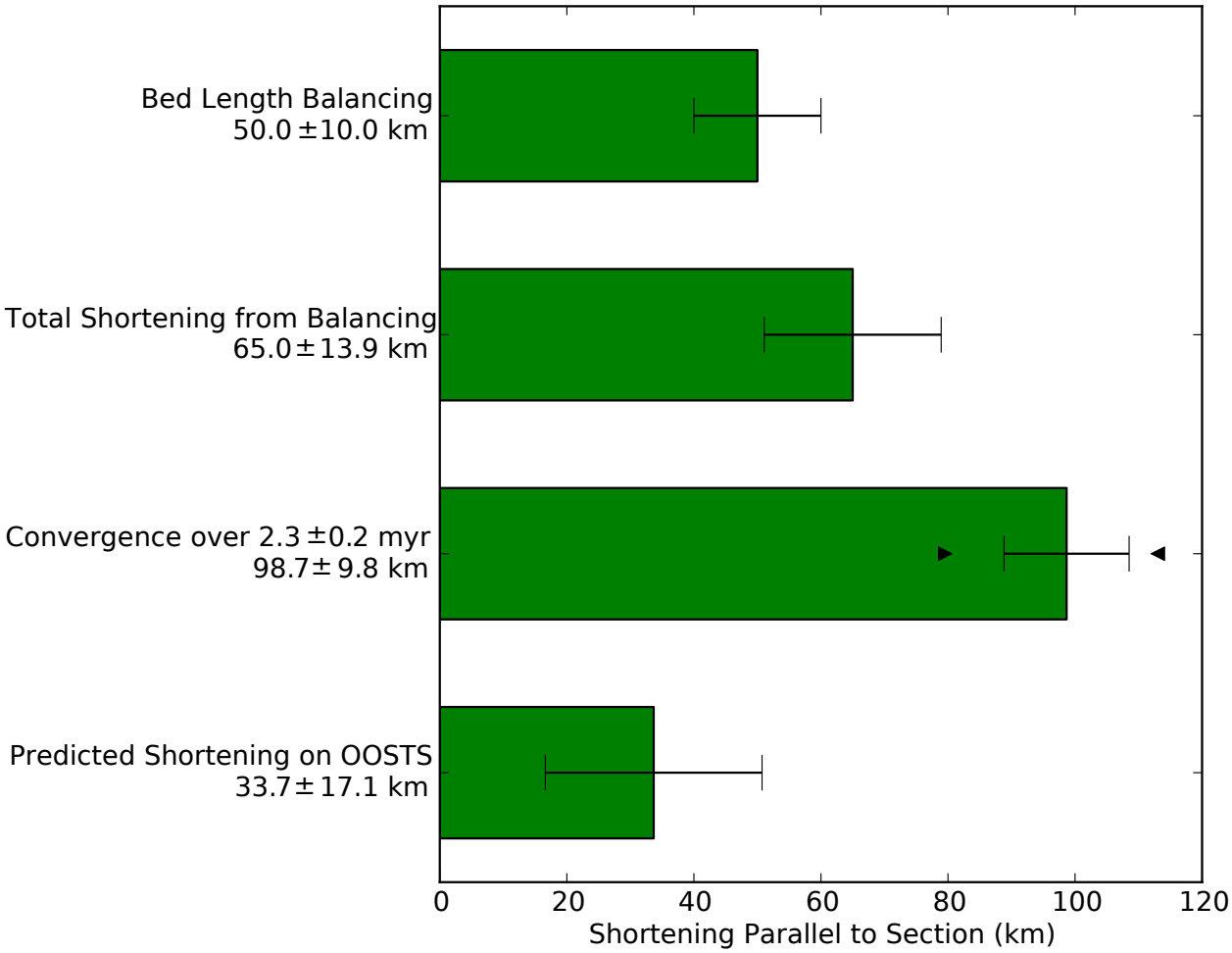

Figure 3.5: Results of method #1. Error bars indicate 2 standard deviation (σ) errors while triangles indicate minimum and maximum constraints. We correct the minimum shortening estimate from Fig 3.4 (top bar) for volume loss and ductile deformation by applying a correction factor of $\alpha = 30 \pm 10\%$. This yields an estimate for the total amount of shortening seaward of the Out-of-Sequence Thrust System (OOSTS) of 65±14 km (second bar). Based on *Strasser et al.* [2009], we model the age of the structures immediately seaward of the OOSTS as 2.3±0.2 Ma, with hard upper and lower limits of 1.95 Ma and 2.54 Ma. Integrating motion of the Kumano forearc block relative to the subducting plate from *Loveless and Meade* [2010] over these ages yields an overall shortening estimate of 99±10 km, with upper and lower bounds indicated by the triangles on the third bar. We assume that all deformation between the forearc and the subducting plate is accommodated in the outer wedge or on the OOSTS. Therefore, the difference between plate convergence and the shortening accommodated seaward of the OOSTS yields an estimate of 33±17 km for the total shortening accommodated by the OOSTS, as shown by the fourth bar.

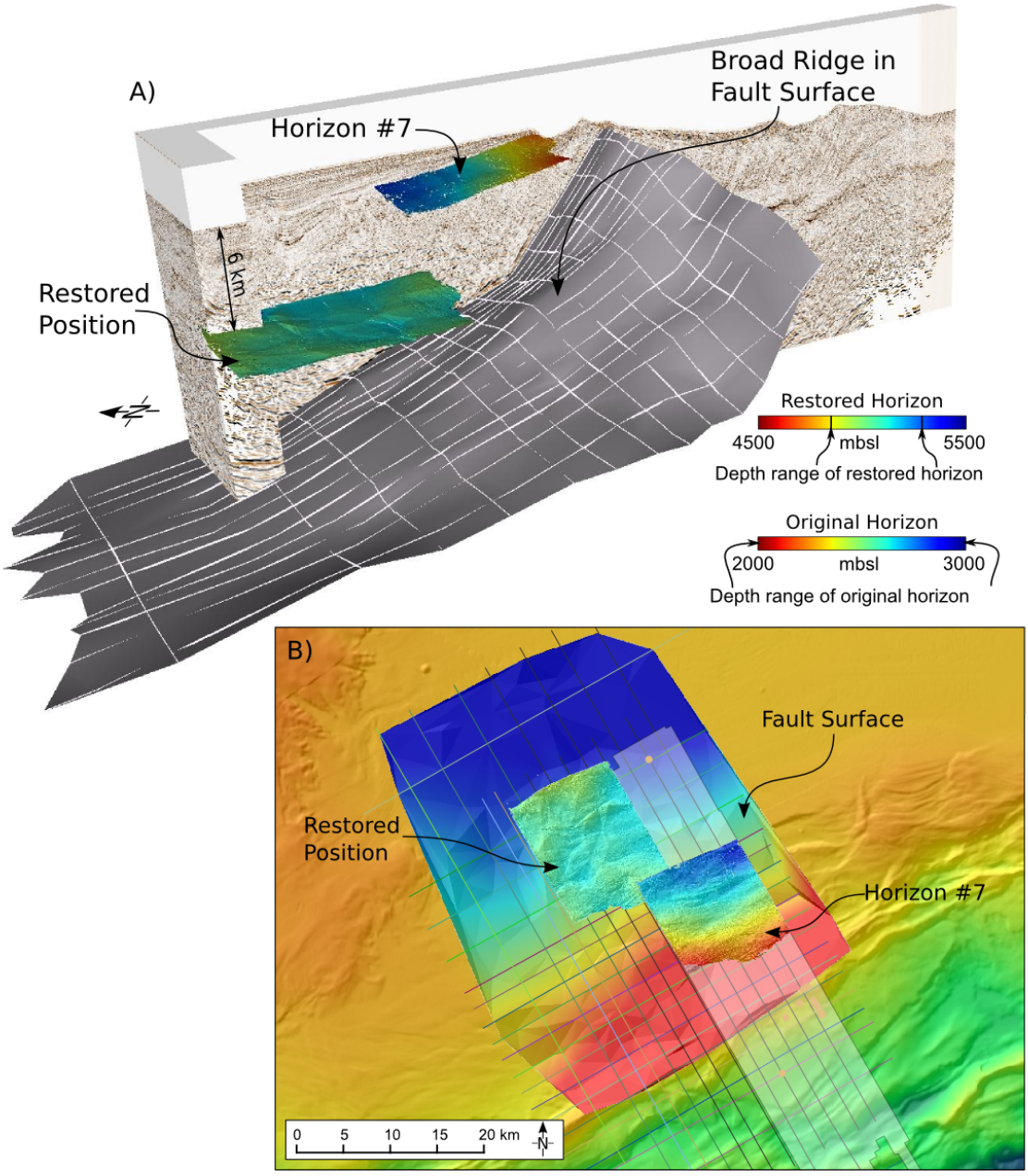

Figure 3.6: Geometry of the landward branch of the OOSTS shown with the present-day and restored positions of horizon 7 in a 3D view (A) and in map view (B). We use the present-day horizon geometry and the interpreted fault geometry to invert for the amount of slip along the fault to restore the horizon to horizontal. Outside of the 3D seismic volume, the fault's geometry is interpreted from regional 2D seismic. Note the broad ridge in the fault surface (A) which makes the inclined shear restoration sensitive to the along-strike component of fault slip. The color palettes of the present-day and restored horizons are shown with the same range (∼1 km) in depths to visually demonstrate the flattening of the horizon.

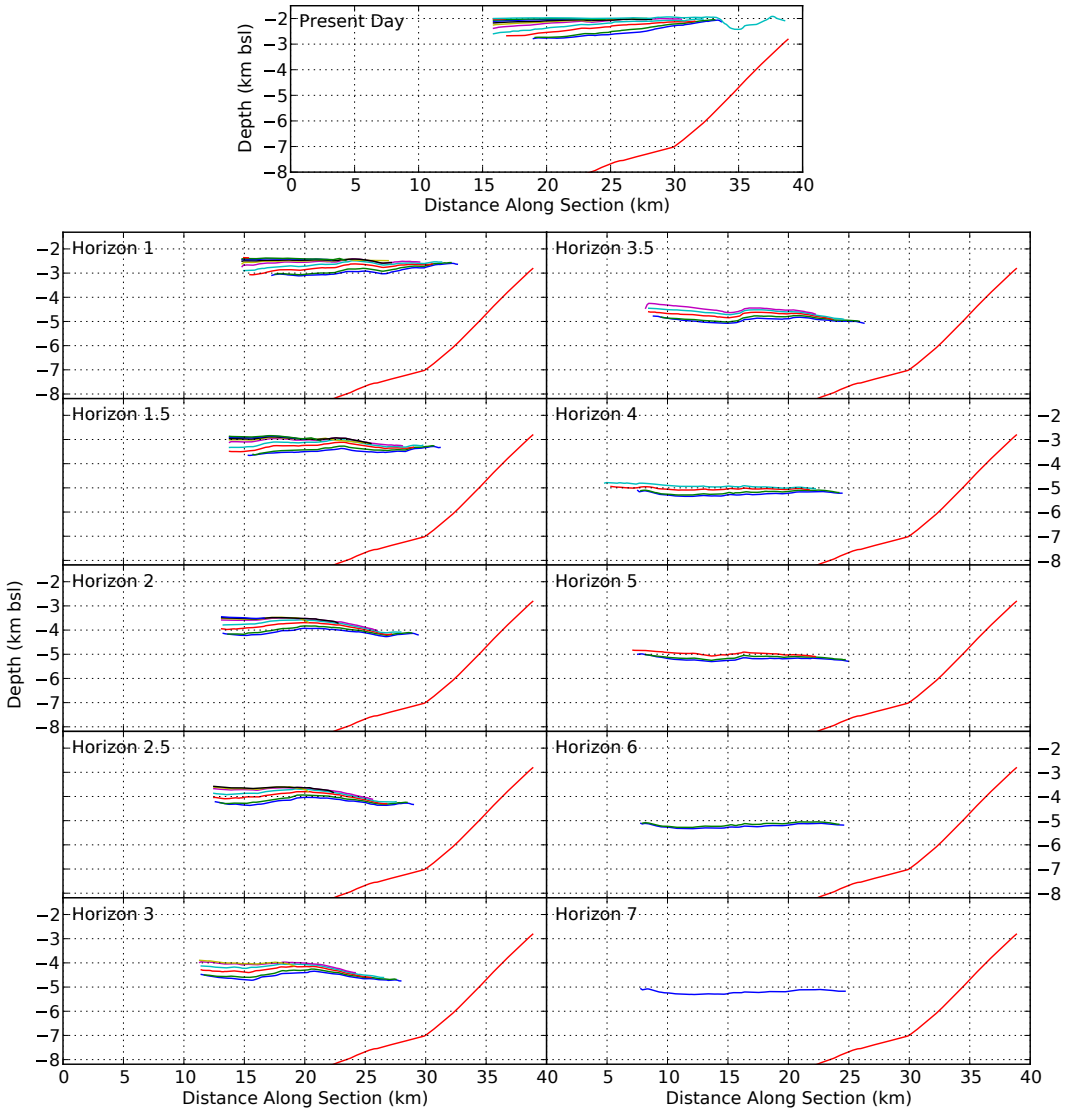

Figure 3.7: Progressive restoration of forearc stratigraphy.

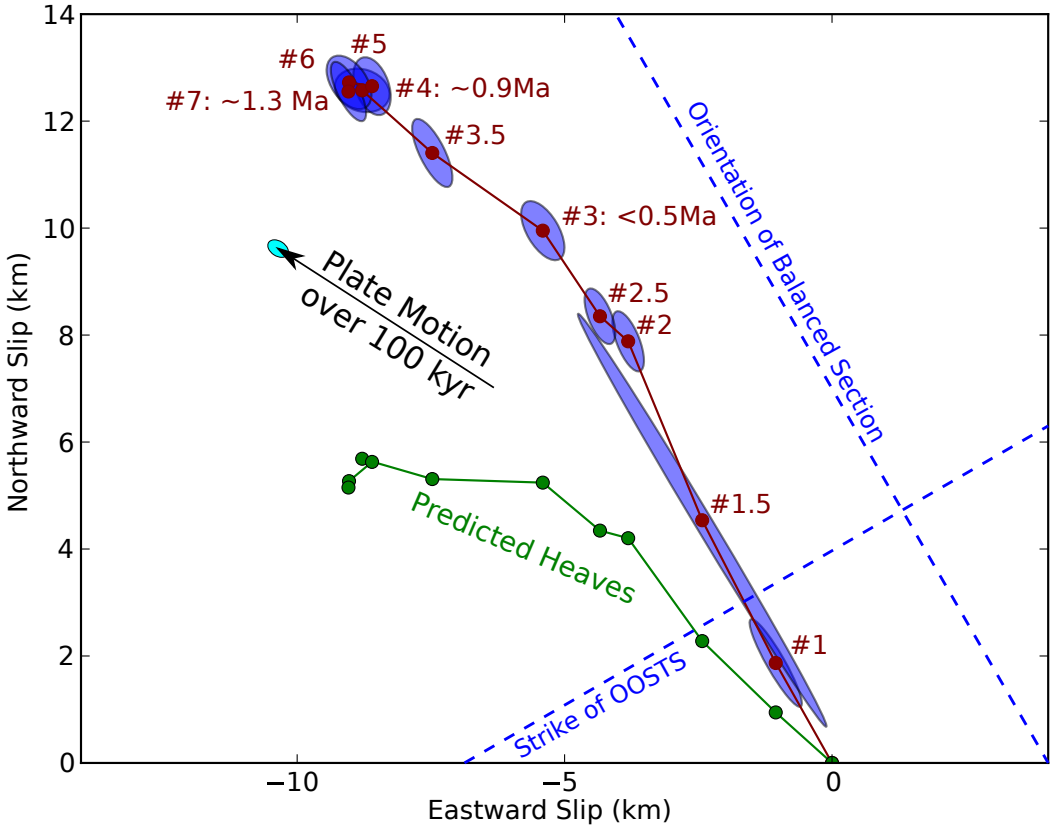

Figure 3.8: Shortening (in map view) along the landward branch of the OOSTS required to restore each horizon to horizontal. Each ellipse represents an independent estimate of shortening since the deposition of the horizon. Shortening estimates derived using inclined shear modeling are shown in red, while the heave predicted from each offset is shown in green. Note that horizons 5–7 all restore to the same position, while younger horizons restore to progressively lower offsets. Plate motion over 100 kyr is shown in black with a light blue (2σ) error ellipse [*Loveless and Meade*, 2010]. Error in shortening estimates (2σ blue error ellipses) was estimated through bootstrapping with replacement of both the fault and horizon geometries.

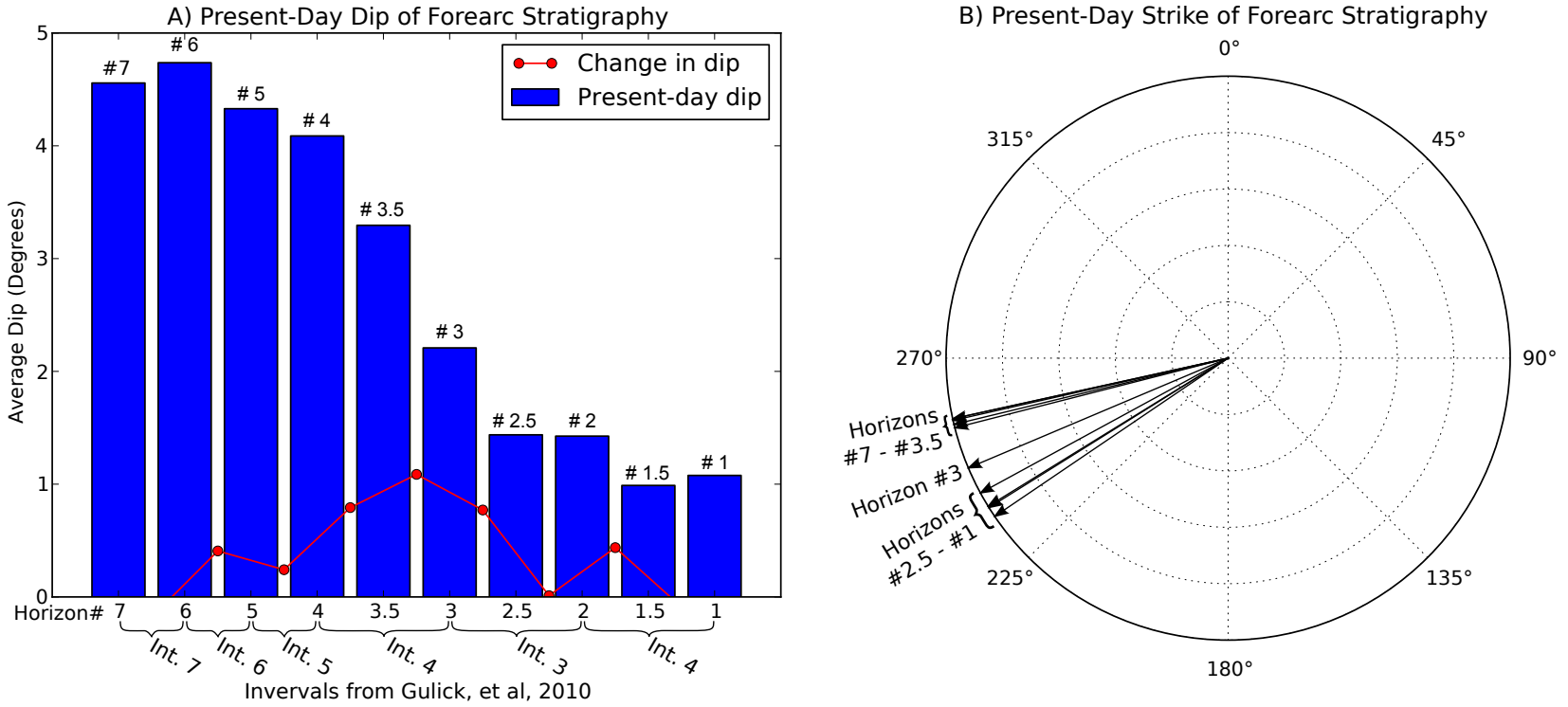

Figure 3.9: Present-day dip (A) and strike (B) of the uplifted forearc basin stratigraphy. The rate of tilting is shown in red. Notice that Horizons 7–4 have very similar dips, while the dip changes significantly between horizons 4–2.5. This suggests that tilting, and therefore motion on the landward branch of the OOSTS, occurred during the deposition of intervals 4 and younger, contrary to *Gulick et al.* [2010]'s interpretation. Strikes (shown in B) follow the right-hand rule to indicate dip direction: *i.e.* all stratigraphy dips to the northwest.

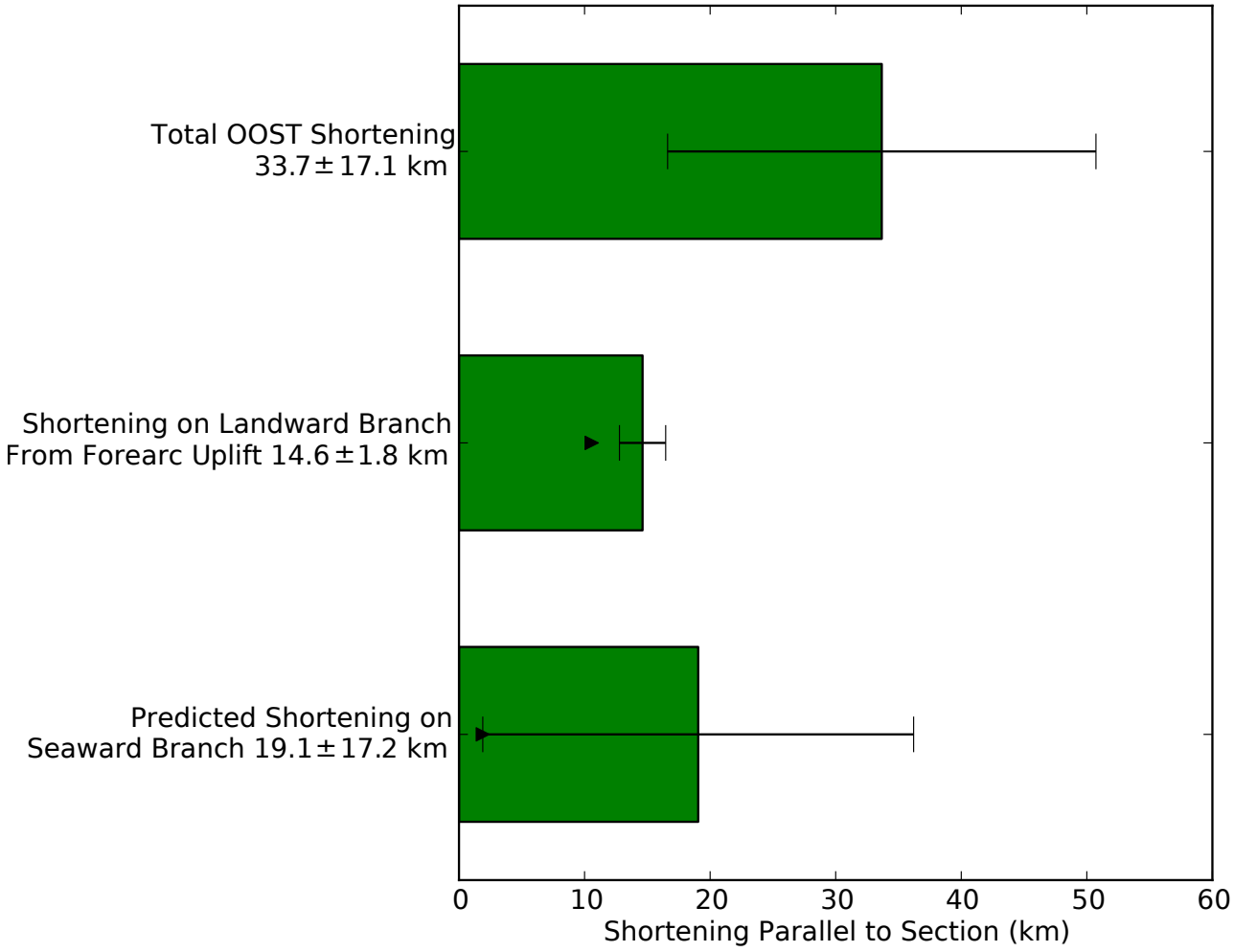

Figure 3.10: Comparison of method #1 and method #2 for estimating shortening on the OOSTS parallel to the section shown in Figure 3.2. Error bars show 2 standard deviation error estimates, and triangles show minimum bounds. Top bar shows shortening on the entire OOSTS estimated from method #1, using bed-length balancing and plate motion estimates. Middle bar shows shortening on the landward branch of the OOSTS estimated from forearc stratigraphy. Bottom bar shows estimate of shortening on the seaward branch derived from subtracting the results of method #2 from method #1. The minimum bound on the bottom bar is from *Strasser et al.* [2009].

Chapter 4

Using 3D Seismic Imaging to Constrain the Spatial and Temporal Variation in the Stress State of the Outer Wedge of the Nankai Trough Accretionary Prism

Abstract

Recent observations of borehole breakouts and extensional failure in drilled sections of the Kumano Basin region of the Nankai Trough have led to speculation that the entire accretionary prism may be in an extensional or transtensional stress regime. However, that work was limited to constraining the stress state near specific IODP sites. Here, we use 3D seismic data to document the distribution of recent faulting and constrain recent stress states in the upper ∼1 km of the outer wedge. Dynamic analysis of the faulting within the area confirms that the observed faults are consistent with nearby borehole-based estimations of the in-situ stress state. The different fault populations within the seismic volume exhibit consistent orientations of the principal axes of shortening, but differ in their relative magnitudes, resulting in differing Andersonian faulting regimes. This suggests that principal stress orientations are dominated by the far-field tectonic convergence, but their relative magnitudes reflect localized effects and/or temporal variability. Furthermore, we observe strike-slip failure throughout most of the outer wedge, whereas normal faulting is restricted to discrete regions. All but two of these regions are likely perturbed by a nearby major active strike-slip fault. The other two regions of normal faulting are within a recently uplifted area, suggesting that normal faulting in the area is due to local topographic effects.

In both cases, normal faulting is not representative of the majority of the outer wedge, and likely represents local perturbations of the "regional" stress state.

4.1 Introduction

As part of the Nankai Trough Seismogenic Experiment (NanTroSEIZE) and associated IODP expeditions, there has been considerable interest in the stress state and recent kinematic history of the outer wedge in the Kumano Basin region of the Nankai Trough [*e.g. Bangs et al.*, 2009a; *Kitamura et al.*, 2010; *Strasser et al.*, 2009; *Screaton et al.*, 2009; *Martin et al.*, 2010; *Park et al.*, 2010]. Constraining the *in situ* stress state of different portions of the Kumano accretionary prism is a major objective of NanTroSEIZE [*Tobin and Kinoshita*, 2006; *Tobin et al.*, 2009]. The *in situ* stress state provides insight into accretionary prism dynamics and the strength of the plate boundary fault [*Wang and Hu*, 2006].

IODP expeditions 314, 315, 316, 319, 322, and 333 drilled at 12 locations within the Kumano Basin area [*Tobin et al.*, 2009] (Figs 4.1 & 4.2). Borehole and core data constrain the age and lithology of the sediments and rocks at each location, providing key information on the kinematic history of the accretionary prism. Additionally, the present-day direction of maximum horizontal stress can be precisely determined at drilling locations through a variety of methods. Several workers have focused on the *in situ* stress state at IODP locations using: borehole breakouts and drilling-induced tensile fractures [*Tobin et al.*, 2009; *Chang et al.*, 2010; *Liu et al.*, 2010; *Song et al.*, 2011] (Figs 4.1 & 4.2) and anelastic strain recovery [*Byrne et al.*, 2009]. Additional constraints from non-borehole data have come from very-low frequency (VLF) earthquakes [*Ito et al.*, 2009] and shear wave splitting [*Tsuji et al.*, 2011]. For locations in the outer wedge (i.e. IODP sites C0001, C0004, C0006, C0007, C0008, and C0010), all results show consistent maximum horizontal stress orientations at an azimuth of $\sim$330°, perpendicular to the margin. However, many of these results indicate that the drilled sections are in an extensional stress state, with normal faults accommodating along-strike extension [*Byrne et al.*, 2009; *Tobin et al.*, 2009; *Chang et al.*, 2010]. This has led to conflicting interpretations of the significance of the extensional stress state

Measurements of the *in situ* stress state from borehole and core data have led to a variety of interpretations. Observations of core-scale normal faults at IODP sites C0001, C0002, C0004, and C0008 have led to speculation that the entire outer wedge may be in a state of extensional failure due to a weak décollement produced by extensive sediment underthrusting [*Byrne et al.*, 2009]. This interpretation is supported by anelastic strain recovery measurements on core collected at C0001, C0002, and C0006 that indicate an extensional stress state [*Byrne et al.*, 2009]. More recent analyses (*e.g. Chang et al.* [2010]) have suggested that the outer wedge is mostly in transpressional failure, and that only the uppermost sediments are under an extensional stress state. In addition, very low frequency earthquakes detected in the area show focal mechanisms consistent with a transpressional stress state in the deeper portions of the outer wedge [*Ito and Obara*, 2006b; *Ito et al.*, 2009]. *Chang et al.* [2010] hypothesize that differences in stress state between the shallow and deeper portions of the outer wedge is a result of decoupling between recently deposited sediments and the more competent accretionary prism rocks below.

However, borehole-based data alone cannot constrain the temporal or spatial variability in stress state. The stress state at any given point may be perturbed by a number of localized effects, including the effect of surface topography, rheologic boundaries, and nearby active faults. Therefore, it is important to understand how the stress state within the outer wedge spatially and temporally varies in order to understand where local factors perturb the "regional" stress state. It is possible that normal faulting in the area is due to local effects. If so, it is unlikely that the presence of normal faults in the outer wedge has significant implications for the present-day dynamics of the entire accretionary prism.

3D seismic imaging of small faults within the outer wedge can place constraints on the stress state at the time of fault initiation if the faults are in their original orientation and have not been reactivated. There is an approximately one kilometer thick piggyback basin of relatively undeformed sediments located just seaward of a zone of out-of-sequence thrusts that divide the outer wedge from the forearc basin (Fig 4.2). The piggyback basin blankets currently inactive thrust sheets in the outer wedge (Fig 4.2). These sediments are

cut by numerous small faults with offsets of less than 100 meters [*Moore et al.*, 2009]. Several of these faults appear to cut the seafloor, and almost all cut the uppermost 50 meters of sediment, suggesting that they are quite geologically recent.

We use this array of small faults in basins in the outer wedge to determine the recent deformation history, and potentially constrain the paleo-stress state, of this portion of the outer wedge. Furthermore, the spatial and temporal variation in types of faulting yields valuable information on the spatial and temporal variability of the stress state in the outer wedge.

This project focuses on 1) documenting the faulting styles in the shallow subsurface throughout the outer wedge, and 2) constraining the spatial and temporal variability of the principal shortening directions of the outer wedge based on recent faulting. Provided we can relate these shortening directions to the principal axes of the stress tensor, we can also constrain the spatial and temporal variability of the stress state in the outer wedge. The variability of the stress state in the outer wedge has implications for the response of the wedge to coseismic rupture and the strength of active faults in the accretionary prism.

4.2 Methods

4.2.1 Relating Faulting to Infinitesimal Strain

The orientations of and displacement on faults within the piggyback basin (Fig 4.2) in the outer wedge can yield the finite (brittle) strain tensor since their formation. However, although the sense of offset on most faults is clear, measuring the true displacement on each fault is generally impossible due to a lack of piercing points to constrain the along-strike component of slip. Nonetheless, if we assume that these faults did not follow anisotropies in the sediment and have not been rotated from their initial positions, the orientation and assumed slip vectors of the faults precisely constrain the orientations of the principal axes of the infinitesimal finite strain tensor at the time of fault formation [*Marrett and Allmendinger*, 1990].

Both a slip vector and a fault plane orientation are required in order to directly relate observed faulting styles and orientations to principal shortening axes. Unfortunately, any oblique slip component is difficult or impossible to measure from seismic imaging data alone. There are methods of constraining the shortening axes using only the orientation of the fault plane and its sense of throw (e.g. *Lisle et al.* [2001]). These methods rely on having a wide variety of sub-optimally oriented faults on which to observe either normal or reverse throw, and perform very poorly on a dataset of consistently oriented conjugate faults, as in this study. Instead, we make the reasonable assumption that the observed faults are either purely dip-slip or purely strike-slip, in accordance with their observed separation. Given the assumption that the observed faults formed along planes of Coulomb failure in relatively isotropic sediments, the initial slip on the fault should not have had any oblique component.

Therefore, to best satisfy these assumptions, we rely on small (<50 m offset) faults developed in recently deposited piggyback basin sediments (Faults inside yellow shaded region in Fig 4.2). This requires interpreting the extent and geometry of each fault surface and then inferring the kinematics of slip on the fault. Interpreted faults are broken into multiple, small, perfectly planar patches to accurately reflect their geometry. Each patch of the fault is then used as an independent fault orientation measurement. We assume pure dip or strike slip based on the sense of separation on the fault, yielding a slip vector for each fault patch. Given this information, we can determine the infinitesimal strain tensor and therefore constrain the orientations of the principal axes of the stress tensor. However, for many faults near minimum seismic resolution, a fault plane is clearly visible, but separation is not. In these cases, the faults were assumed to have the same sense of offset as nearby larger faults with a similar strike and dip.

In addition to faults within the piggyback basins, subsidiary faults in the hanging walls of major thrust sheets in the outer wedge can also provide information about recent kinematics (Faults outside the yellow shaded region in Fig 4.2). However, as the timing of their formation cannot be well constrained, it is difficult to distinguish between faults that

formed in their present orientation, faults that have been reactivated, and faults that have been rotated due to deformation of the hanging wall of the thrust sheet. Nonetheless, these faults do provide information about the deformation history of the outer wedge, and are used here as qualitative kinematic indicators. They are not included in any quantitative analysis.

4.2.2 Relating Infinitesimal Strain to Stress

In order to make any inferences about the stress state from faulting, we must relate the orientation of the observed infinitesimal strain tensor to the orientation of the stress tensor. In homogeneous and isotropic rocks, the infinitesimal finite strain tensor has principal axes parallel to those of the stress tensor [*Twiss and Unruh*, 1998]. Furthermore, even in anisotropic and inhomogeneous rocks the principal axes of the infinitesimal finite strain tensor are parallel to those of the stress tensor when directions of anisotropy are parallel to the principal stress directions. This scenario is actually a common case: shallowly buried, relatively flat-lying sediments. The primary anisotropies in flat-lying sediments are parallel to the x-y plane, and one of the principal stresses in shallowly buried rock is usually perpendicular to the Earth's surface [*Anderson*, 1951]. This gives the fundamental assumption required to relate the observed directions of strain to stress in this study: newly formed faults in an undeformed, relatively isotropic rock mass should form along planes predicted by Coulomb failure.

Additionally, we must assume that the features we observe have not been rotated or otherwise deformed since their formation. Otherwise, the analysis will not represent the stress state at the time of their formation. Based on IODP coring at sites C0004, C0008, C0010, and C0018, the slope sediments within the piggyback basin consist of mass transport complexes and turbidite sequences of silts, sands, and muds [*Expedition 333 Scientists*, 2011; *Ashi et al.*, 2009]. The basin has experienced minor uplift and associated mass wasting, but has undergone little deformation, and there is no reason to believe that recent faults in the basin have been significantly rotated since their formation. Furthermore, there should be no

preexisting structural fabric in undeformed and recently deposited silts, sands, and muds. Based on this, the sediments should be relatively laterally homogeneous and the primary anisotropy in the sediment sequence should be bedding, which is close to horizontal. Therefore, in shallow sediments of this basin, the orientations of the principal axes of the infinitesimal strain tensor should be the same as those of the stress tensor. This implies that we can accurately infer the orientations of the principal axes of the local stress tensor based on the orientations and slip sense of newly formed faults in the slope sediments.

4.2.3 Determining the Principal Axes of the Stress Tensor

Given the assumption of pure dip or pure strike slip on the observed faults, several methods may be used to determine the principal shortening directions. If the deformation occurs over a short time frame, the principal shortening directions approximate the principal stresses (σ_1, σ_2, & σ_3, where $\sigma_1 >= \sigma_2 >= \sigma_3$) in homogeneous rocks. Purely kinematic methods (e.g. *Marrett and Allmendinger* [1990]) directly constrain the principal shortening directions and require fewer assumptions about the conditions under which deformation is occurring. However, they yield poor results when one orientation of a conjugate set of faults is much more abundant than the other, as is likely to occur in this study. In dynamic methods (e.g. *Angelier* [1979]), one attempts to invert for a deviatoric stress tensor, as opposed to an incremental strain tensor. The underlying assumption in these methods is that observed slip on a fault is parallel to the resolved shear stress on the fault plane. They require many more assumptions about the state of deformation than purely kinematic methods, but the only additional assumption beyond those already outlined is that adjacent faults do not interfere with each other [*Pollard et al.*, 1993]. Whereas dynamic methods are typically capable of determining the ratio of $\frac{\sigma_2-\sigma_3}{\sigma_1-\sigma_3}$, in the particular case of purely dip or strike slip on an optimally oriented plane, all slip is perpendicular to σ_2 and therefore this ratio is not constrained. Nonetheless, qualitative observations of the modes of faulting in the outer wedge may yield some valuable constraints on the relative magnitudes of the three principal stresses.

4.2.4 Stress Tensor Inversion

Our methods here follow *Michael* [1984], who was the first to formulate a linear solution for the deviatoric stress tensor given a set of fault planes and observed slip directions. If we assume conditions of plane stress and strain ($\sigma_{xz} = \sigma_{yz} = 0$), implying that one principal axis of the stress tensor is vertical, as is inferred from borehole breakouts [*Tobin et al.*, 2009], *Michael* [1984]'s method reduces to:

$$\begin{bmatrix} n_{x1} - n_{x1}^3 + n_{x1}n_{z1}^2 & n_{y1} - 2n_{y1}n_{x1}^2 & -n_{x1}n_{y1}^2 + n_{x1}n_{z1}^2 \\ \vdots & \vdots & \vdots \\ n_{xk} - n_{xk}^3 + n_{xk}n_{zk}^2 & n_{yk} - 2n_{yk}n_{xk}^2 & -n_{xk}n_{yk}^2 + n_{xk}n_{zk}^2 \\ -n_{y1}n_{x1}^2 + n_{y1}n_{z1}^3 & n_{x1} - 2n_{x1}n_{y1}^2 & n_{y1} - n_{y1}^3 + n_{y1}n_{z1}^2 \\ \vdots & \vdots & \vdots \\ -n_{yk}n_{xk}^2 + n_{yk}n_{zk}^3 & n_{xk} - 2n_{xk}n_{yk}^2 & n_{yk} - n_{yk}^3 + n_{yk}n_{zk}^2 \\ -n_{z1}n_{x1}^2 - n_{z1} + n_{z1}^3 & -2n_{x1}n_{y1}n_{z1} & -n_{y1}^2 n_{z1} - n_{z1} + n_{z1}^3 \\ \vdots & \vdots & \vdots \\ -n_{zk}n_{xk}^2 - n_{zk} + n_{zk}^3 & -2n_{xk}n_{yk}n_{zk} & -n_{yk}^2 n_{zk} - n_{zk} + n_{zk}^3 \end{bmatrix} \begin{bmatrix} \sigma_{xx} \\ \sigma_{xy} \\ \sigma_{yy} \end{bmatrix} = \begin{bmatrix} s_{x1} \\ \vdots \\ s_{xk} \\ s_{y1} \\ \vdots \\ s_{yk} \\ s_{z1} \\ \vdots \\ s_{zk} \end{bmatrix} \quad (4.1)$$

Where:

$< n_{x1}, n_{y1}, n_{z1} > ... < n_{xk}, n_{yk}, n_{zk} >$ are the 1^{st} through k^{th} fault plane unit normal vectors

$< s_{x1}, s_{y1}, s_{z1} > ... < s_{xk}, s_{yk}, s_{zk} >$ are the 1^{st} through k^{th} unit slip vectors

In order to avoid over-emphasizing densely picked faults in the results, we weight each item by the squared area of the respective fault patch. This system of linear equations is overdetermined given two or more faults, and can be solved using standard least squares methods, giving the deviatoric stress tensor. Eigenvalue decomposition can then be used to determine the orientations of the principal stresses.

4.2.5 Determining Timing of Faulting

We use the correlation of seismic stratigraphy across the piggyback slope basin to constrain the relative and absolute timing of the last motion on a fault based on which

units it offsets. Ideally, we would constrain the timing of the initiation of each fault, as this is when it should represent a plane of Coulomb failure. Unfortunately, growth across the faults in the basin is usually below seismic resolution due to their small offset. Therefore, it is impossible to constrain the initiation of motion on most faults in the piggyback basin. Nonetheless, as these faults have small offsets, they are unlikely to be long-lived features. We therefore assume that initiation of motion on a given fault occurred relatively close to the time of the last motion on the fault. Hence, we assume that the fault surface approximately represents a plane of Coulomb failure at the time of its last motion as well as at its initiation.

4.3 Results

4.3.1 Modes of Faulting

The outer wedge in the Kumano Basin region is cut by multiple fault types (Fig 4.2). Strike-slip faults are prevalent throughout the area, with nearly vertical conjugate right-lateral and left-lateral strike-slip faults trending $\sim$105°and $\sim$156°on average (Figs 4.2 & 4.4). Normal faults are locally abundant within the outer wedge but are restricted to discrete regions (Fig 4.3).

4.3.2 Normal Fault Populations

Two populations of normal faults are present in the piggyback basin. The dominant population of normal faults forms conjugate sets striking $\sim$134°and $\sim$323°(following the right-hand-rule to indicate dip direction), with an average dip of 60°(Figs 4.5, 4.6, & 4.7). A secondary population of normal faults is present in a small area near a prominent slope break in the basin. This population forms conjugate sets striking $\sim$72°and $\sim$250°, with an average dip of 62°(Figs 4.8 & 4.4). As both of these fault populations cannot have resulted from the same stress state, the two are treated separately in the dynamic analysis.

4.3.3 Relative Timing of Faulting

Regions of strike-slip and normal faulting within the piggyback basin overlap (Figs 4.2 & 4.3). Within the overlapping region, strike-slip and normal faults terminate at the same units and appear to have occurred contemporaneously within seismic-stratigraphic resolution (Fig 4.7). The slope sediments within the piggyback basin are not cut by in-sequence thrust faulting, though some of the basal sediments in the basin are slightly deformed by late activity of hanging wall anticlines above subsidiary thrusts.

4.3.4 Dynamic Analysis

Dynamic analysis of fault orientation data within the piggyback slope basin sediments indicates a maximum horizontal stress of 313°(Fig 4.9). Solutions for the dominant normal fault population show orientations of principal stress axes within 5°of those derived from the strike-slip fault population. However, solutions derived from the normal fault populations require the principal stress axis to be vertical, in accordance with Andersonian mechanics [*Anderson*, 1951] (Fig 4.9). Likewise, solutions for the strike-slip fault population show the same directions of principal stress, but require the intermediate axis of stress in the vertical direction (Fig 4.9). In contrast, solutions derived from the secondary normal fault population require a maximum horizontal stress oriented at 263°.

4.4 Discussion

4.4.1 Comparison with Borehole Estimates

Our inferred maximum horizontal stress directions from faults within the piggyback basin are consistent with horizontal stress directions previously inferred from borehole breakouts at nearby IODP drilling locations C0001, C0004, and C0010 [*Tobin et al.*, 2009; *Chang et al.*, 2010; *Liu et al.*, 2010; *Song et al.*, 2011]. The strike-slip and dominant normal fault populations are compatible with nearby borehole breakouts and share approximately the same principal stress orientations, but require different relative magnitudes of principal

stresses. In contrast, the secondary normal fault population is not compatible with the other observed fault populations or nearby borehole data. It is, however, limited to a small geographic region and is therefore not representative of the majority of shallow faulting in the outer wedge.

4.4.2 Activity of Thrusts Beneath Piggyback Basin

The observed pattern of faulting within the piggyback basin sediments indicates that the landward portion of the outer wedge is presently accommodating along-strike extension. With the exception of the out-of-sequence megasplay, no thrusting is observed within the piggyback slope sediments. Conversely, sediments near the prism toe are clearly undergoing active thrusting. This requires that the landward portions of the outer wedge undergo along-strike extension contemporaneously with thrusting into the undeformed sediments at the prism toe. This suggests that the stress state within the hanging wall of the primary decollement is different from the stress state at the toe of the prism, as is expected from Coloumb wedge theory [*Davis et al.*, 1983; *Dahlen et al.*, 1984]. However, there are no other abrupt changes in recent subsidiary faulting patterns near any of the faults in the outer wedge. As an actively slipping fault should locally perturb stress conditions, this supports the conclusion that the thrusts below the piggyback basin are currently inactive.

4.4.3 Regions of Normal Faulting

Throughout the outer wedge, normal faults are confined to discrete regions, while strike-slip faults are pervasive (Fig 4.2 & Fig 4.3). Normal faults within the piggyback basin are constrained to three distinct regions (Fig 4.3, A, B, & C). Outside the piggyback basin, two regions of faulting (D & E on Fig 4.3) occur in the crests of doubly plunging anticlines, near where they are cut by major strike-slip faults. Therefore, regions D & E are likely not representative of the stress state in majority of the outer wedge.

Within the piggyback basin, one region of normal faulting (region A on Fig 4.3) lies near an active strike-slip fault with $>$1 km of right-lateral slip along the southwestern edge

of the basin (Fig 4.5). The stress state in its immediate vicinity is likely perturbed by the strike-slip fault and is not representative of the majority of the outer wedge.

Most normal faults in the outer wedge occur in the northeastern side of the piggyback slope basin (region A on Fig 4.3) (Figs 4.6 & 4.7). This area has undergone at least 600 meters of uplift since 0.9 Ma [*Kington et al.*, Ch. 2]. As evidenced by extensive mass wasting in the area, the developing topography undoubtedly has an effect on the stress state in this area. Because the direction of topographic slope is sub-parallel to the maximum horizontal shortening direction elsewhere, topographic stresses will tend to reduce the maximum horizontal stress, encouraging normal faulting. This may explain the presence of normal faults in this region.

Based on these observations, the regions of normal faults shown in Figure 4.3 most likely represent perturbations of a "background" transpressive stress state. Nonetheless, the variability in the structures observed in this area may yield information about the temporal variability of the stress state in the landward portion of the outer wedge.

4.4.4 Temporal Variability in Stress State

Given the assumptions put forth previously, the primary shortening directions should directly relate to the principal stress axes. Therefore, the observation of contemporaneous strike-slip and normal faulting with consistent directions of horizontal shortening yields key implications about the relative magnitudes of the principal stresses in the seaward portion of the outer wedge. In accordance with Andersonian mechanics, the maximum compressive stress should be vertical during normal faulting with the intermediate stress parallel to the strike of the normal fault sets [*Anderson*, 1951]. In contrast, during strike-slip faulting, the maximum compressive stress should be horizontal, and the intermediate stress should be vertical. Therefore, to yield both normal and strike-slip faulting in the same location at approximately the same time, the temporal variability in the maximum horizontal stress must be greater than the difference between the primary horizontal and vertical stresses.

A likely source for the variability in maximum horizontal stress is coseismic slip during earthquakes on the plate-boundary fault. Following the dynamic Coulomb wedge model developed by *Wang and Hu* [2006], coseismic slip and the associated postseismic response should significantly impact the stress state of the outer wedge. Accordingly, strike-slip faulting should correspond to increased horizontal stress during coseismic slip and normal faulting should dominate during the interseismic period. However, contemporaneous strike-slip and normal faulting are only observed in an uplifted region undergoing mass wasting. Due to unloading by mass wasting and local topographic effects due to a slope dipping in the same direction as the maximum horizontal shortening axis, this region likely has reduced maximum horizontal stresses relative to the rest of the outer wedge. Therefore the requirement that the temporal variability in the stress state is greater than the difference between the vertical and horizontal stresses most likely reflects locally decreased horizontal stresses rather than locally increased variability in stress state.

Because the temporal variability in stress state is only greater than the difference between vertical and maximum horizontal stresses in an area of reduced maximum horizontal stress, the temporal variability cannot be larger than the maximum devatoric stress throughout most of the outer wedge. If seismic cycles on the plate-boundary fault are the source of the temporal variability, this supports the premise of a weak plate-boundary fault. A relatively strong plate-boundary fault should result in a large temporal variation in the stress state of the outer wedge, whereas a weak plate-boundary fault should lead to lower temporal variation in stress state [*Wang and Hu*, 2006].

4.5 Conclusions

Small-scale faulting within the outer wedge in the NanTroSEIZE study area is consistent with the principal horizontal shortening directions determined from borehole and core data by previous workers. However, normal faults are constrained to isolated areas, and most of the outer wedge appears to be in strike-slip failure, in agreement with the most recent estimates of the stress state of the outer wedge [*Chang et al.*, 2010]. The observation

that normal faults are constrained to isolated areas suggests that normal failure near IODP sites C0001, C0004, C0010, and C0008 is not representative of the entire outer wedge and represents local perturbations to the overall stress state. Therefore, this region of normal faulting represents an area where the principal horizontal stress has been reduced, likely due to local topographic effects. However, the regions of normal failure and strike-slip failure within the piggyback basin overlap, and normal and strike-slip faults appear to have been active contemporaneously within the overlapping area. This indicates that the temporal variation in the stress state is larger than the difference between the principal vertical stress and the principal horizontal stress within this area. Because this only occurs in an area of locally reduced devatoric stress, the temporal variation in the stress state cannot be larger than the difference between the principal horizontal and vertical stresses in the majority of the outer wedge.

Acknowledgements

This work was funded by NSF award OCE-0800653. Seismic interpretation was preformed in Geoprobe® Volume Interpretation Software [*Landmark*, 2003], which was generously provided by Halliburton, Inc. To visualize and display the seismic interpretation, including figures in this work, we wrote software in Python [*van Rossum and Drake*, 2006] using Numpy [*Oliphant*, 2007], Matplotlib [*Hunter*, 2007], and SciPy [*Jones et al.*, 2001]. Dynamic inversion of fault data was likewise implemented in Python using Numpy and displayed using `mplstereonet` [*Kington*, 2012a]. Code and fault data used in this paper is available at `https://github.com/joferkington/stress_state_paper_code`.

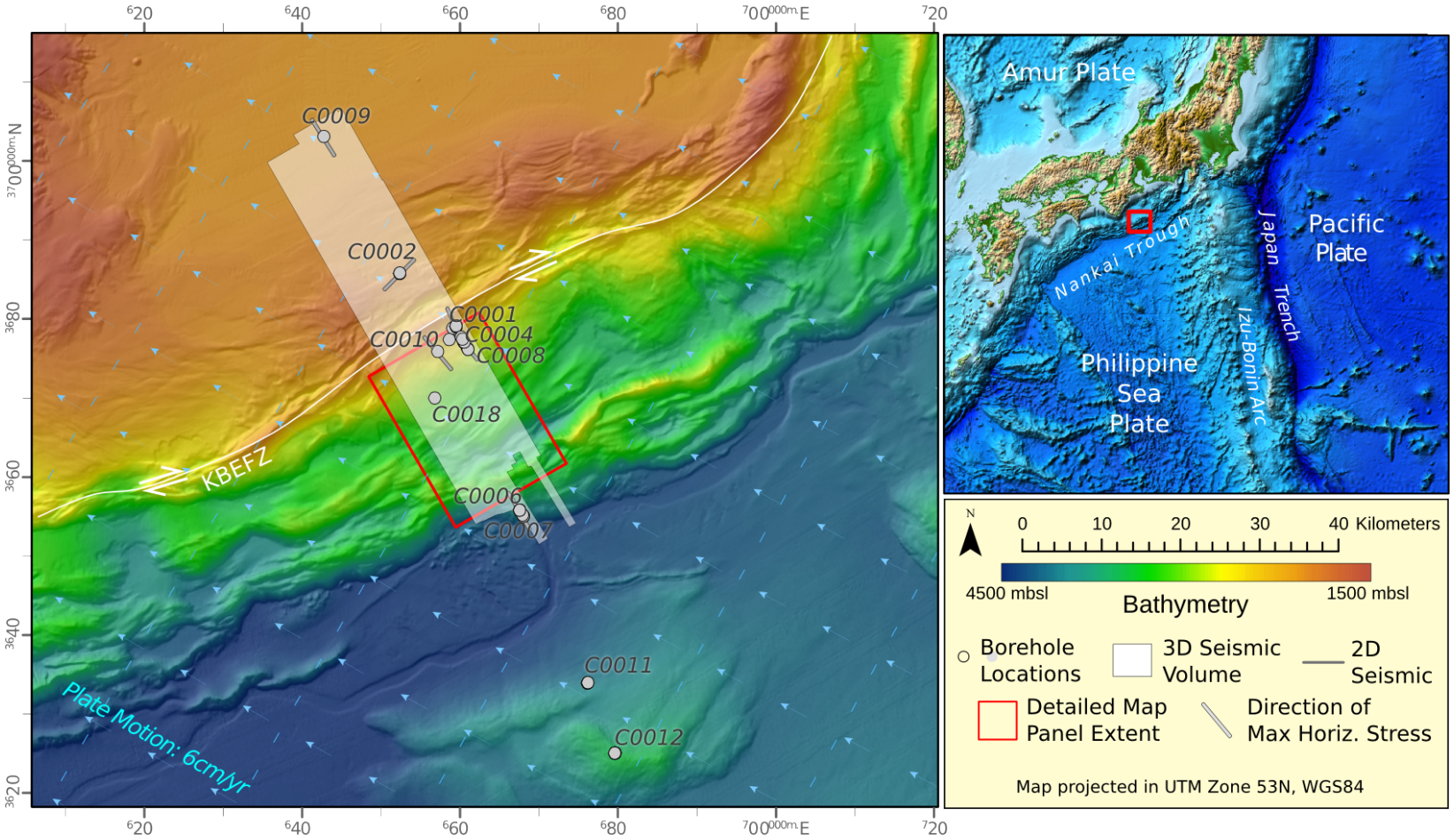

Figure 4.1: Location of study area and maximum horizontal stress orientations from borehole breakouts. Stress data are from *Kinoshita et al.* [2009] and *Saffer et al.* [2010].

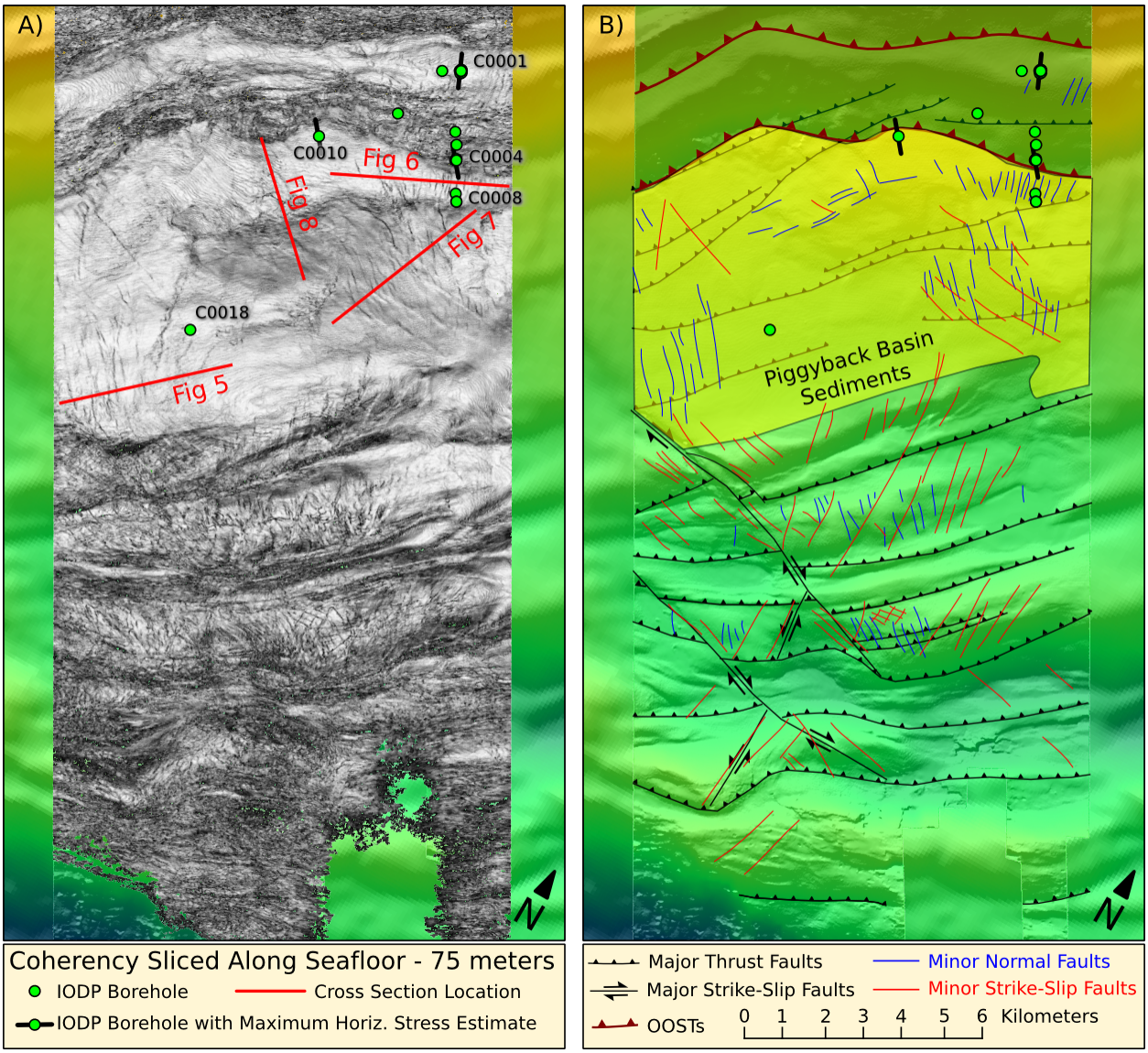

Figure 4.2: Small-scale faults in the outer wedge. Left panel shows eigenstructure-based coherency calculated from the 3D seismic dataset sliced along an irregular surface at a constant depth of 75 meters below the seafloor. Right panel shows the traces of faults interpreted in the 3D seismic volume based on both seismic amplitudes and coherency.

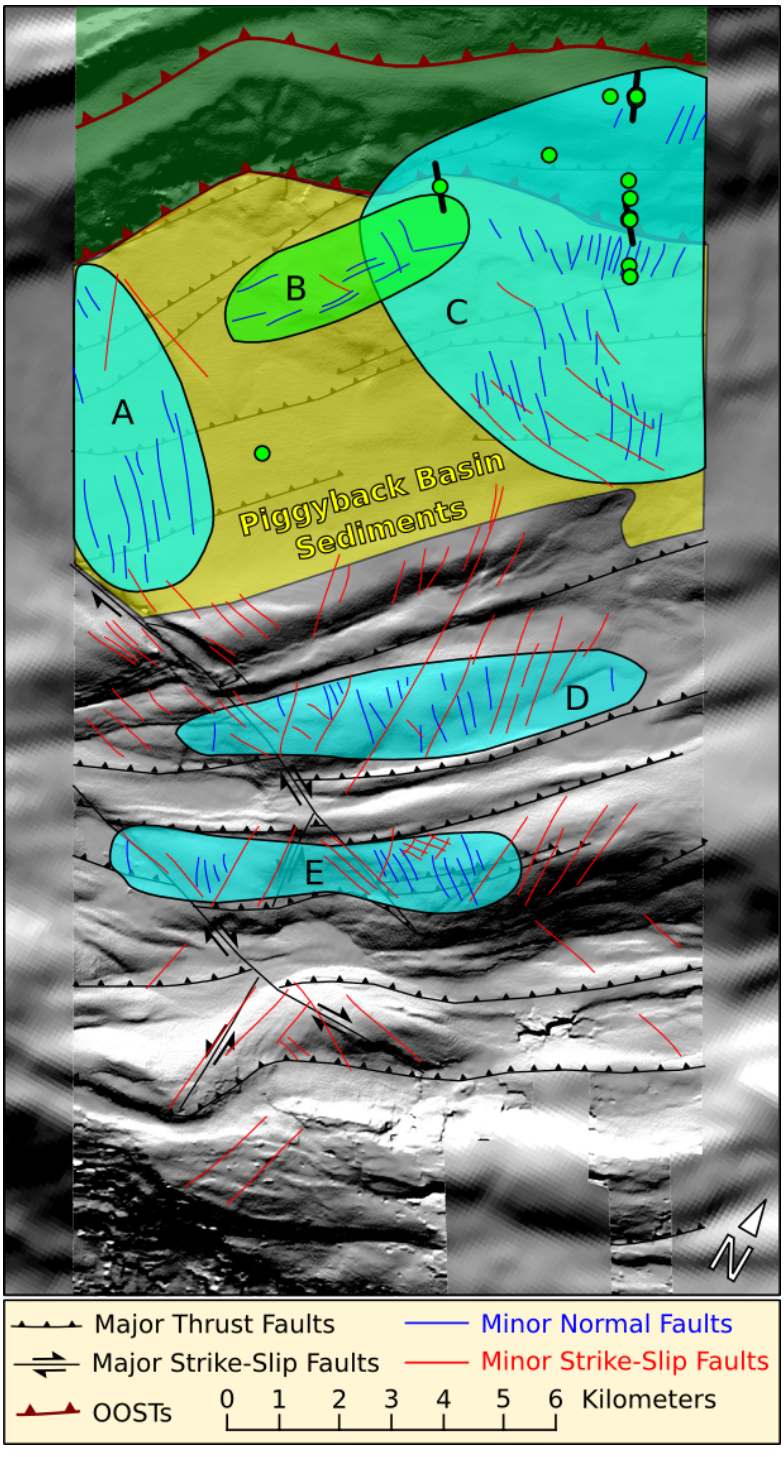

Figure 4.3: Regions of normal faulting in the outer wedge. Blue shading indicates regions of the primary normal fault population, whereas green indicates the secondary normal fault population. Extent of piggyback basin sediments is outlined in yellow. Individual study areas are lettered A–E.

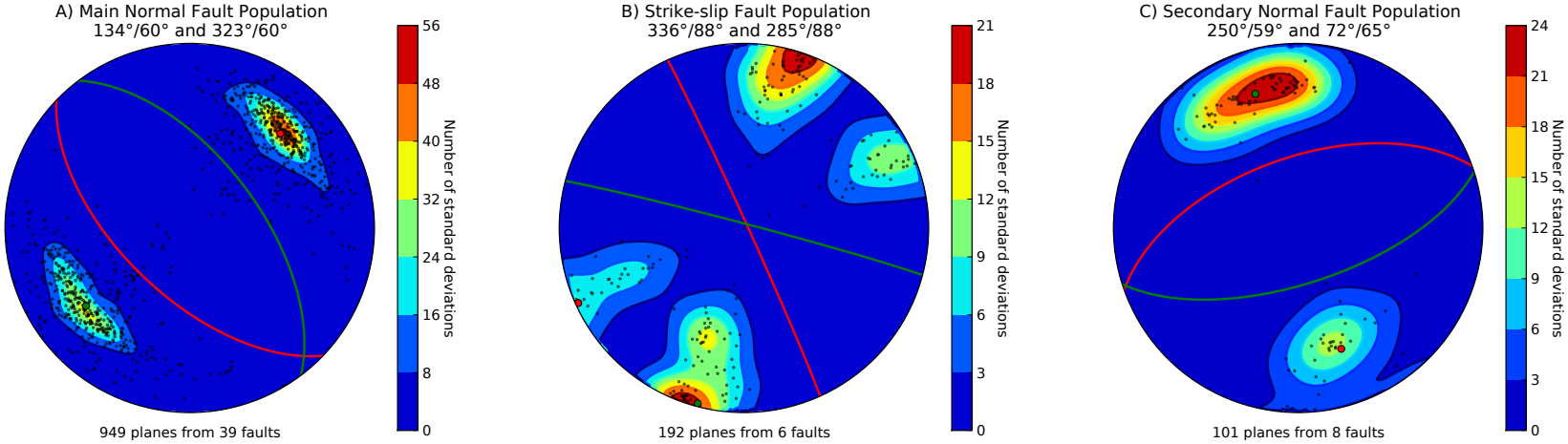

Figure 4.4: Lower-hemisphere, equal area nets showing poles to fault planes for each conjugate fault population. Mean planes and poles for each mode are plotted in red and green.

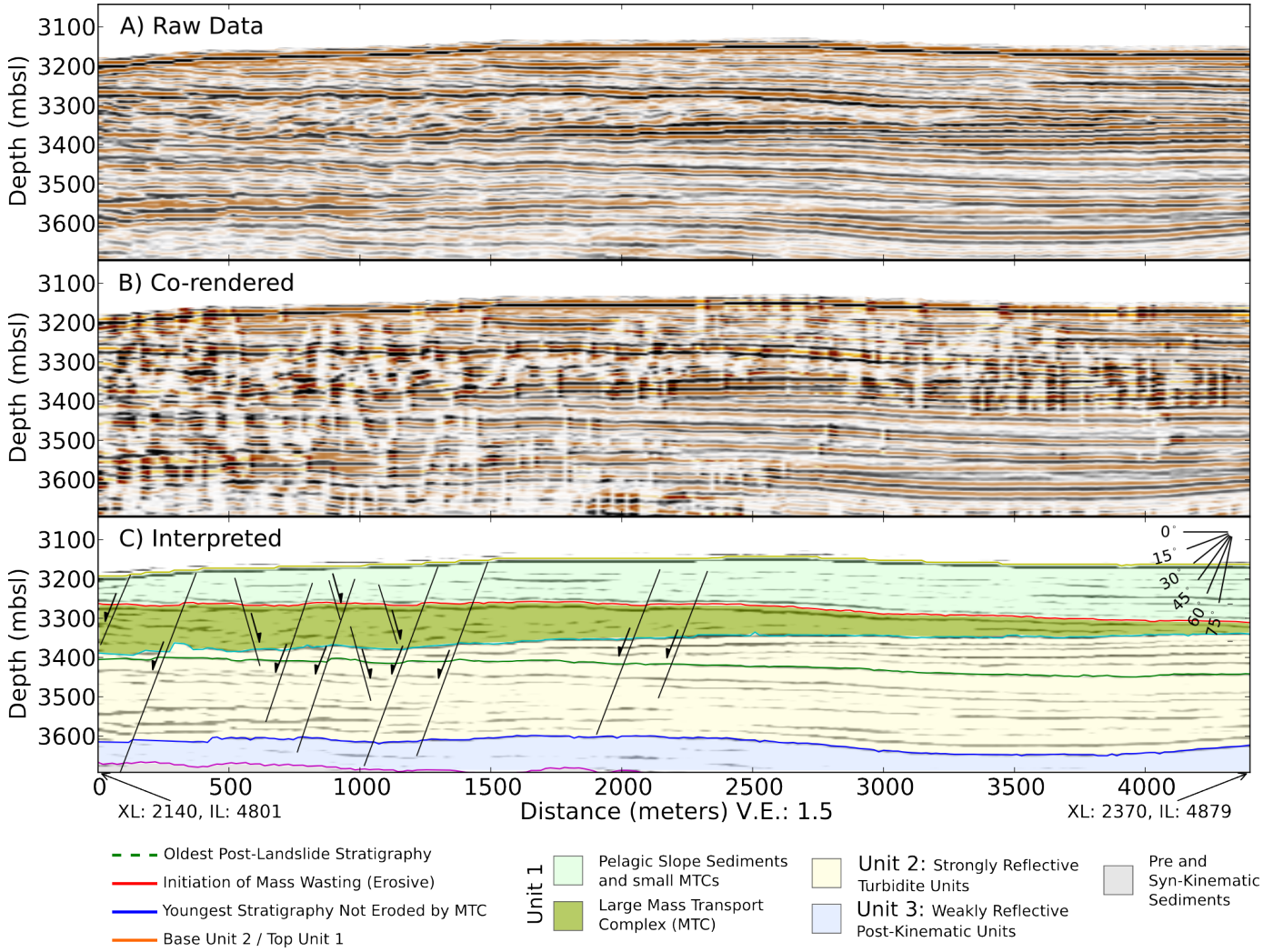

Figure 4.5: Normal faults near an active, major strike-slip fault. The major strike-slip fault is located immediately beyond the left hand margin of this cross section. Top panel (A) shows uninterpreted seismic data, middle panel (B) shows seismic data co-rendered with coherence. Co-rendering uses the coherence data shown in Figure 4.2 as input for shading (identical to "hillshading" of topographic data), which is then overlain on top of the seismic section. Bottom panel (C) shows interpreted seismic section.

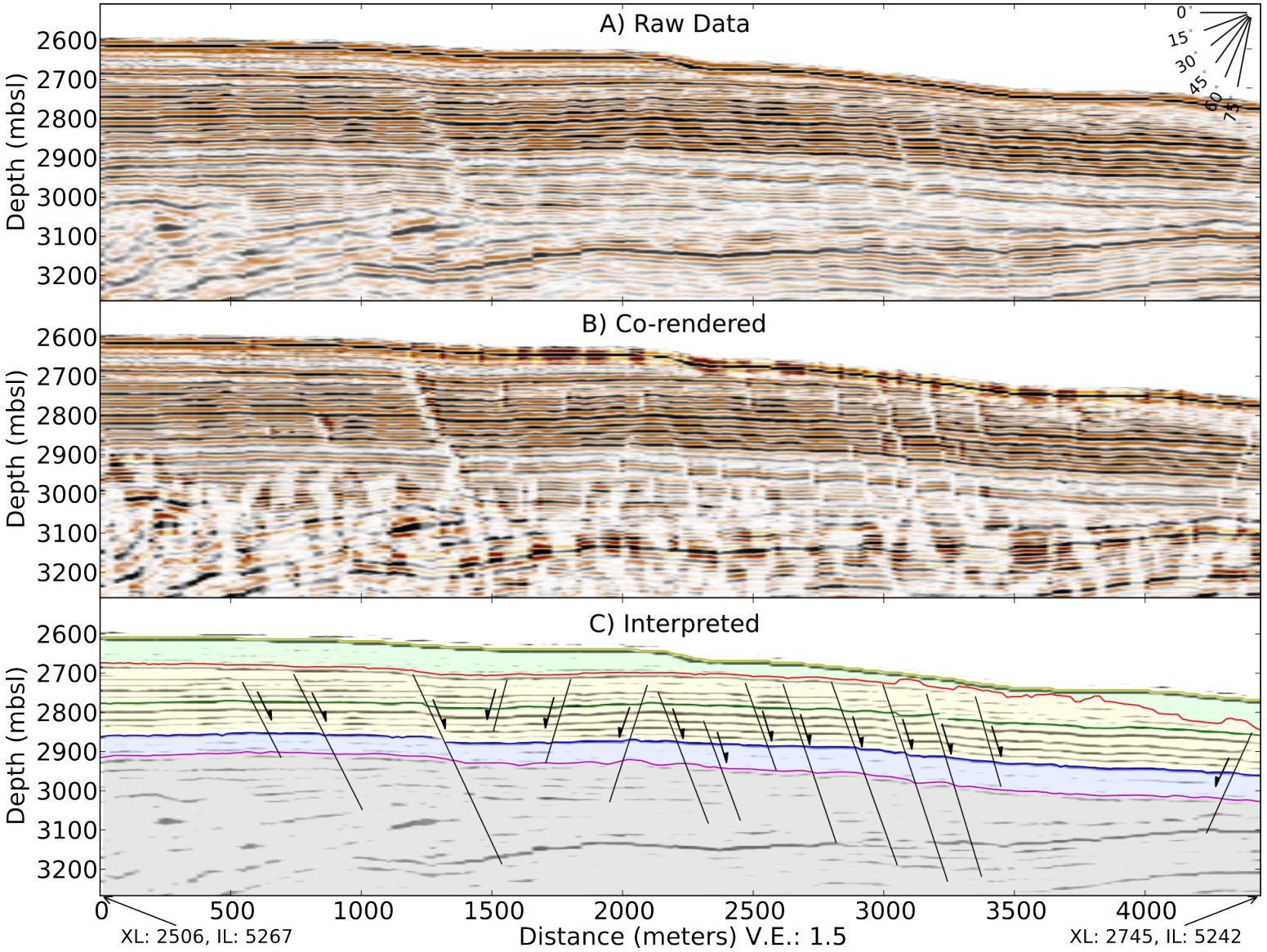

Figure 4.6: Normal faulting near IODP sites C0004 and C0008. See Figure 4.5 for legend and definition of stratigraphic units.

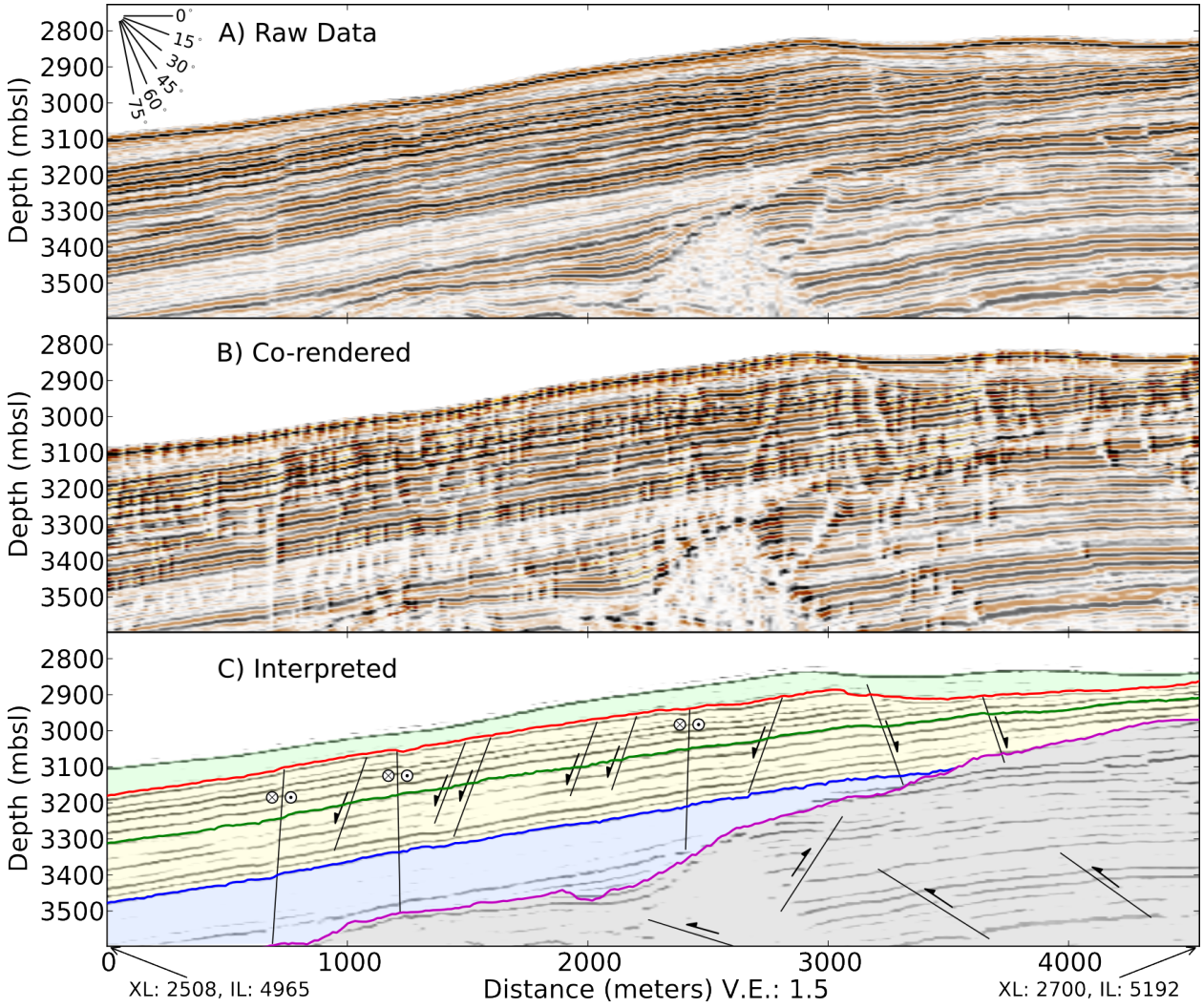

Figure 4.7: Contemporaneous normal and strike-slip faults. Note that both normal and strike slip faults extend up to and locally deform the top of Unit #2 (shown in red), but do not offset the seafloor. Therefore, we infer that both normal and strike slip faults were active during the deposition of the youngest stratigraphic unit, Unit #1. Thrusts in pre-kinematic section pre-date and do not deform the piggyback basin stratigraphy.

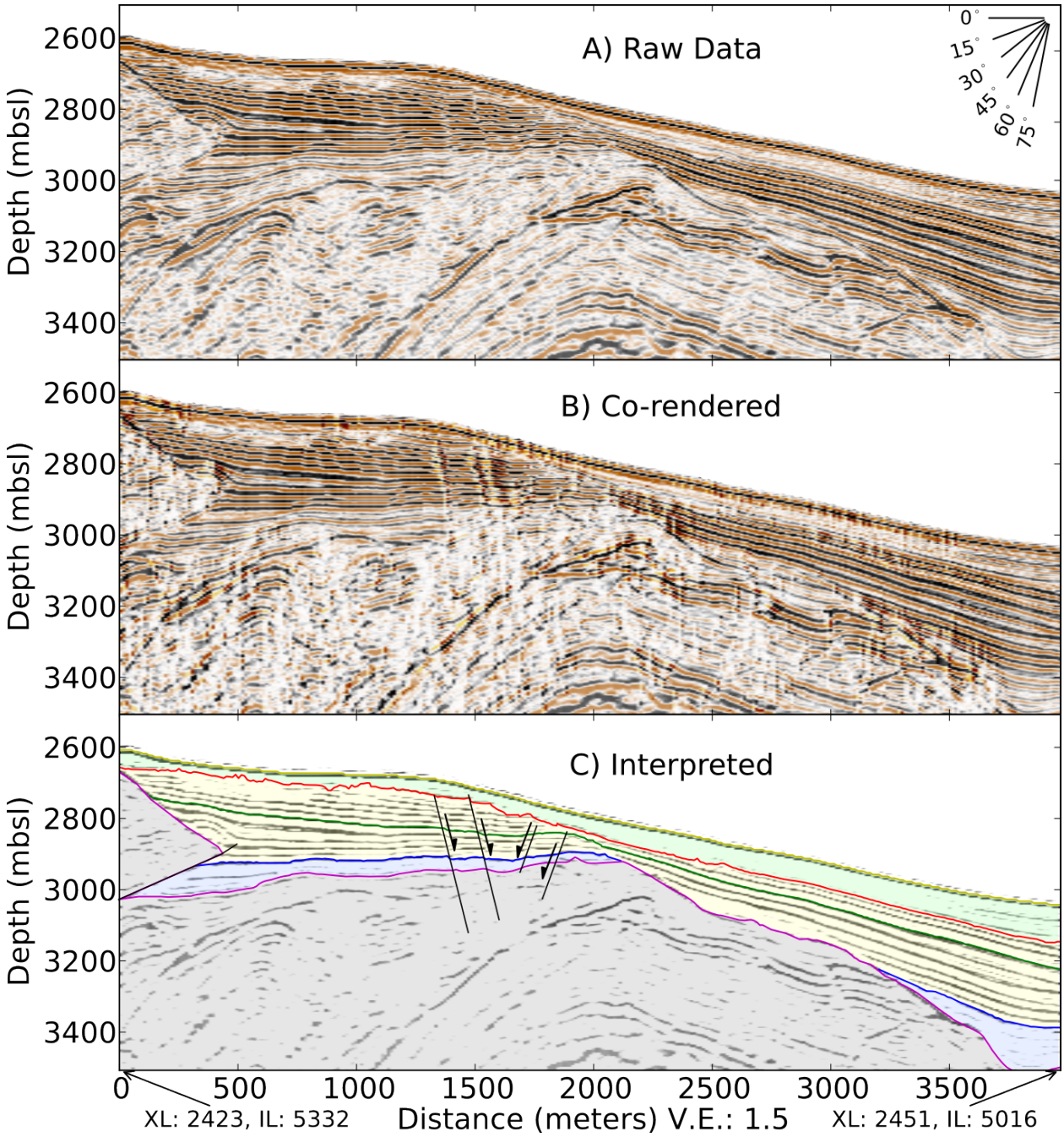

Figure 4.8: Secondary normal fault population that is approximately perpendicular to the primary normal fault population.

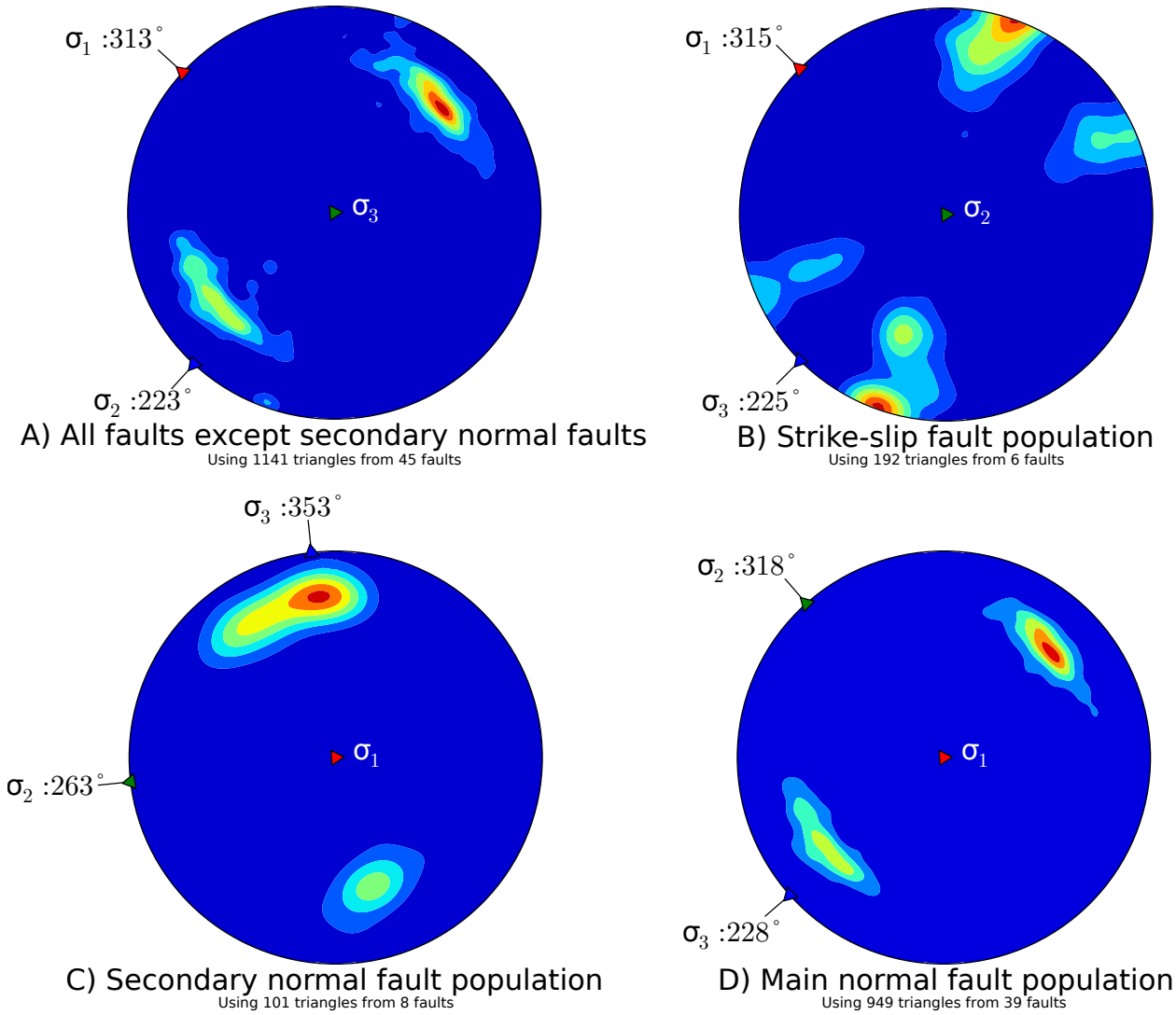

Figure 4.9: Dynamic inversion of principal stresses assuming pure strike or dip slip for all consistent faults and each fault population individually.

Chapter 5

Conclusions

5.1 Summary of Conclusions

5.1.1 Chapter 2

In the second chapter, I investigated the kinematic evolution of the fold and thrust belt in the vicinity of the Nankai Trough Seismogenic Zone Experiment (NanTroSEIZE) transect and linked this to the stratigraphic record of a piggyback slope basin within the outer wedge. Based on this work, the Kumano Basin region of the Nankai Trough accretionary prism shows evidence for a progressive thinning and abrupt thickening of thrust sheets within the outer wedge. These changes in thrust sheet thickness resulted in a thick package of underthrust sediment.

Because the pattern of uplift of the piggyback basin cannot be explained by movement on underlying or nearby thrusts, it is unlikely that an out-of-sequence thrust is causing the uplift, as hypothesized by *Kimura et al.* [2011]. Similarly, *Strasser et al.* [2011]'s hypothesis that uplift of the basin is being caused by growth of fault-propagation folds beneath the basin does not match the observed pattern of uplift. However, the geometry and extent of the uplifted region of the piggyback basin can be convincingly linked to the underthrust sediment volume. Therefore, the underthrust sediment volume likely forms an oblique footwall ramp in the décollement, which is causing uplift of the piggyback slope basin as the outer wedge rides over it.

I hypothesize that the changes in thrust sheet thickness, underthrust sediments, and uplift of the outer wedge are a result of the subduction of the Paleo-Zenisu Ridge to the

east of the study area. As this basement topographic high was subducted to the east, the décollement ramped up along strike in the study area, producing the thin thrust sheets and thick package of underthrust sediment. After the passage of this feature, the décollement ramped downward, and continued subduction of the underthrust sediment package has caused ongoing uplift of the rear of the outer wedge.

This conceptual kinematic model explains the key features of the outer wedge in terms of its structural evolution since ∼2 Ma. If similar fold and thrust belt kinematics occur elsewhere in sediment-dominated accretionary prisms, this implies that subducted basement features may produce laterally extensive regions of underthrust sediment, affecting the seismogenic properties of the nearby plate-boundary fault.

5.1.2 Chapter 3

In the third chapter, I focused on the shortening accommodated by the Nankai Trough accretionary prism over the last ∼2 million years in the Kumano Basin region. In the Kumano Basin region, the active outer wedge fold and thrust belt is separated from the forearc basin and inactive inner wedge by a zone of out-of-sequence thrusting. I used bed-length balancing [*Dahlstrom*, 1969] of structures in the outer wedge fold and thrust belt to estimate the overall in-sequence shortening. I then coupled this with plate motion estimates from *Loveless and Meade* [2010] to estimate the total out-of-sequence shortening. Finally, I investigated shortening accommodated on the landward-most branch of the zone of out-of-sequence thrusting using the inclined shear method [*White et al.*, 1986] to restore syn-kinematic forearc stratigraphy in 3D.

Based on my results, the in-sequence portion of the outer wedge has accommodated 99±10 km of shortening, while the out-of-sequence thrust system (OOSTS) has accommodated 34±17 km of margin perpendicular shortening. Slightly less than half of this, 15±2 km (minimum of 11 km), occurred on the landward branch of the OOSTS based on restoration of forearc stratigraphy. This is 34%±15% of the total 99±10 km of shortening

predicted by the convergence vector between the Nankai forearc and the subducting Philippine Sea Plate [*Loveless and Meade*, 2010]. However, during the individual periods when the landward and seaward branches were active, they accommodated up to 65% of the total plate convergence vector. This suggests that out-of-sequence thrusts dominate shortening along convergent margins during the relatively short periods when they are active.

Restoring syn-kinematic forearc basin stratigraphy suggests that the uplift and tilting of the forearc basin, and therefore motion on the landward branch of the OOSTS, began 1.04–0.9 Ma and continued until sometime $<$0.5 Ma. This timing suggests that there was a $\sim$0.2–0.3 myr period of forward imbrication between motion on the seaward branch of the OOSTS and motion on the landward branch. Furthermore, the initiation of motion on the landward branch of the OOSTS may correspond to the nearby subduction of the Paleo-Zenisu Ridge, suggesting a link between basement topography and out-of-sequence thrusting.

5.1.3 Chapter 4

Finally, in the fourth chapter, I used arrays of small faults imaged with 3D seismic to constrain the spatial and temporal variation in the stress state of the upper $\sim$1 km of the outer wedge. Small-scale faults within the outer wedge in the NanTroSEIZE study area are consistent with the principal horizontal shortening axes determined from borehole and core data by previous workers. However, normal faults are constrained to isolated areas, and most of the outer wedge appears to be in strike-slip failure, in agreement with the most recent estimates of the stress state of the outer wedge [*Chang et al.*, 2010]. The observation that normal faults are constrained to isolated areas suggests that normal failure near IODP sites C0001, C0004, C0010, and C0008 is not representative of the entire outer wedge, but instead records local perturbations to the overall stress state. Therefore, this region of normal faulting represents an area where the principal horizontal stress has been reduced, likely due to local topographic effects. However, the regions of normal failure and strike-slip failure within the piggyback basin overlap, and both normal and strike-slip

faulting appears to have occurred contemporaneously within the overlapping area. This indicates that the temporal variation in the stress state is larger than the difference between the principal vertical stress and the principal horizontal stress within this area.

5.2 Implications

5.2.1 Site-specific Implications

Due to NanTroSEIZE and related IODP expeditions, there has been considerable interest in the Kumano Basin region of the Nankai Trough over the past five years. My work focuses on integrating structural and stratigraphic observations to understand the tectonic history of the Kumano Basin region. This aids and informs other ongoing work in the region.

The interpretation of the décollement position beneath the outer wedge in Chapters 2 & 3 has implications for future drilling at IODP site C0002 during IODP Expedition 338. My interpretation suggests that the plate boundary fault in this area may be a single structure, rather than a separate "megasplay" and basal décollement as previously thought [*Park et al.*, 2002; *Moore et al.*, 2007, 2009; *Bangs et al.*, 2009a].

Chapter 2 partly focused on the recent uplift of a piggyback slope basin within the outer wedge. The uplift of and subsequent mass transport deposits within this basin have been the topic of several recent studies [*e.g. Kimura et al.*, 2011; *Strasser et al.*, 2011; *Ikari et al.*, 2011] and a focus of IODP Expedition 333 [*Expedition 333 Scientists*, 2011]. Previous workers [*e.g. Kimura et al.*, 2011; *Strasser et al.*, 2011; *Ikari et al.*, 2011] have used the uplift and mass wasting within the piggyback basin as evidence of motion on the seaward branch of the out-of-sequence thrust system after 1.24 Ma. The results of Chapter 2 suggest that they likely mis-identified the cause of uplift, and that mass wasting in the basin cannot be used as evidence for motion on the seaward branch of the OOSTS.

Based on the results of Chapter 3, forearc tilting, and therefore motion on the landward branch of the OOSTS, occurred much more recently than previously believed. *Gulick et al.* [2010] proposed that tilting occurred from ~1.3–0.9 Ma. My results clearly demonstrate that tilting began at the time than *Gulick et al.* [2010] interpreted tilting to end, and that it

has continued into the recent past. This has important implications for ongoing work in the forearc basin and for the overall structural evolution of the outer wedge in the region.

In the fourth chapter, I focus on constraining the spatial and temporal variation in the stress state of the outer wedge. Previous work (*e.g. Byrne et al.* [2009]) suggested that the entire outer wedge may be in extensional failure based on borehole observations. My results demonstrate that the outer wedge is dominated by strike-slip failure, and that normal faulting is limited to discrete regions. This emphasizes the need to use the available 3D seismic data to inform borehole results and to assess the spatial variability inherent in geologic features.

5.2.2 Broader Implications

In addition to site-specific concerns, my results have broader implications for the propagation of co-seismic slip into and potentially through accretionary frontal prisms. My interpretation of the outer wedge structures and the geometry of the plate boundary megathrust suggests a simpler geometry than previous interpretations (*e.g. Park et al.* [2002]). An interpretation with a single plate-boundary megathrust favors propagation of coseismic slip all the way to the trench axis, rather than up a more steeply dipping megasplay.

Based on the stratigraphy present within the thrust sheets of the outer wedge in Chapters 2 & 3, there is a $\sim$1 km thick section of relatively undeformed sediments being subducted along with the oceanic plate in the Kumano Basin region, similar to the conclusions of *Bangs et al.* [2009a]. However, my results show that with the exception of a single thrust sheet that is interpreted to contain the uppermost Lower Shikou stratigraphy, the entirety of the Lower Shikou Basin sediments have been subducted for the last $\sim$2–2.5 Ma. Because these sediments are being subducted to seismogenic depths, they likely influence co-seismic rupture in the region. Thick sediments carried to seismogenic depths are commonly thought to blanket irregularities in the oceanic crust, leading to a smoother plate boundary fault that may rupture over a larger area [*e.g. Ruff*, 1989]. While previous authors [*Moore et al.*, 2007; *Bangs et al.*, 2009a; *Park et al.*, 2010] have noted a relatively thick underthrust section

at the updip end of the plate-boundary megathrust. My results confirm that continuous underthrusting of sediments in accretionary prisms may persist over long timescales.

Bibliography

Anderson, E., *The Dynamics of Faulting*, Edinburgh and London, 1951.

Ando, M., Source mechanisms and tectonic significance of historical earthquakes along the nankai trough, Japan, *Tectonophysics*, *27*, 119–140, 1975.

Angelier, J., Determination of the mean principal directions of stresses for a given fault population, *Tectonophysics*, *56*, T17–T26, 1979.

Ashi, J., S. Lallemant, H. Masago, and E. Scientists, Expedition 315 Summary, *In Situ*, *314*, 2009.

Baba, T., and P. R. Cummins, Contiguous rupture areas of two Nankai Trough earthquakes revealed by high-resolution tsunami waveform inversion, *Geophysical Research Letters*, *32*, 2005.

Bangs, N., G. Moore, S. Gulick, E. Pangborn, H. Tobin, S. Kuramoto, and A. Taira, Broad, weak regions of the Nankai Megathrust and implications for shallow coseismic slip, *Earth and Planetary Science Letters*, *284*, 44–49, 2009a.

Bangs, N. L., S. P. Gulick, and T. H. Shipley, Seamount subduction erosion in the Nankai Trough and its potential impact on the seismogenic zone, *Geology*, *34*, 701, 2006.

Bangs, N. L. B., G. F. Moore, S. P. S. Gulick, E. M. Pangborn, H. J. Tobin, S. Kuramoto, and A. Taira, Broad , weak regions of the Nankai Megathrust and implications for shallow coseismic slip, *Earth and Planetary Science Letters*, *284*, 44–49, 2009b.

Bell, R., R. Sutherland, D. H. N. Barker, S. Henrys, S. Bannister, L. Wallace, and J. Beavan, Seismic reflection character of the Hikurangi subduction interface , New Zealand , in the region of repeated Gisborne slow slip events, *Geophysical Journal International*, *180*, 34–48, 2010.

Bilek, S. L., S. Y. Schwartz, and H. R. Deshon, Control of seafloor roughness on earthquake rupture behavior, *Geology*, *31*, 455–458, 2003.

Bray, C. J., and D. E. Karig, Porosity of Sediments in Accretionary Prisms and Some Implications for Dewatering Processes, *Journal of Geophysical Research*, *90*, 768–778, 1985.

Butler, R., and D. Paton, Evaluating lateral compaction in deepwater fold and thrust belts: How much are we missing from "nature's sandbox"?, *GSA Today*, pp. 4–10, 2010.

Byrne, E., M. Davis, and R. Sykes, Loci and Maximum Size of Thrust Earthquakes and the Mechanics of the Shallow Region of Subduction Zones, *Tectonics*, *7*, 833–857, 1988.

Byrne, T., and D. Fisher, Evidence for a Weak and Overpressured Decollement Beneath Sediment-Dominated Accretionary Prisms, *Journal of Geophysical Research*, *95*, 9081–9097, 1990.

Byrne, T. B., W. Lin, A. Tsutsumi, Y. Yamamoto, J. C. Lewis, K. Kanagawa, Y. Kitamura, A. Yamaguchi, and G. Kimura, Anelastic strain recovery reveals extension across SW Japan subduction zone, *Geophysical Research Letters*, *36*, 1–6, 2009.

Chang, C., L. C. McNeill, J. C. Moore, W. Lin, M. Conin, and Y. Yamada, In situ stress state in the Nankai accretionary wedge estimated from borehole wall failures, *Geochemistry Geophysics Geosystems*, *11*, 1–17, 2010.

Cloos, M., Thrust-type subduction-zone earthquakes and seamount asperities: A physical model for seismic rupture, *Geology*, *20*, 601–604, 1992.

Cummins, P. R., and Y. Kaneda, Possible splay fault slip during the 1946 Nankai earthquake, *Geophysical Research Letters*, *27*, 2725–2728, 2000.

Dahlen, F. a., J. Suppe, and D. Davis, Mechanics of Fold-and-Thrust Belts and Accretionary Wedges: Cohesive Coulomb Theory, *Journal of Geophysical Research*, *89*, 10,087–10,101, 1984.

Dahlstrom, A., Balanced cross sections, *Canadian Journal of Earth Sciences*, *6*, 743–757, 1969.

Das, S., and B. V. Kostrov, Breaking of a Single Asperity: Rupture Process and Seismic Radiation, *Journal of Geophysical Research*, *88*, 4277–4288, 1983.

Davis, D., J. Suppe, and F. a. Dahlen, Mechanics of Fold-and-Thrust Belts and Accretionary Wedges, *Journal of Geophysical Research*, *88*, 1153–1172, 1983.

DeMets, C., R. G. Gordon, and D. F. Argus, Geologically current plate motions, *Geophysical Journal International*, *181*, 1–80, 2010.

Dominguez, S., Upper plate deformation associated with seamount subduction, *Tectonophysics*, *293*, 207–224, 1998.

Dominguez, S., J. Malavieille, and S. E. Lallemand, Deformation of accretionary wedges in response to seamount subduction: Insights from sandbox experiments, *Tectonics*, *19*, 182–196, 2000.

Egan, S., Computer modelling and visualisation of the structural deformation caused by movement along geological faults, *Computers & Geosciences*, *25*, 283–297, 1999.

Gulick, S. P., N. L. Bangs, G. F. Moore, J. Ashi, K. M. Martin, D. S. Sawyer, H. J. Tobin, S. Kuramoto, and A. Taira, Rapid forearc basin uplift and megasplay fault development from 3D seismic images of Nankai Margin off Kii Peninsula, Japan, *Earth and Planetary Science Letters*, *300*, 55–62, 2010.

Henstock, T. J., L. C. McNeill, and D. R. Tappin, Seafloor morphology of the Sumatran subduction zone: Surface rupture during megathrust earthquakes?, *Geology*, *34*, 485, 2006.

Hunter, J. D., Matplotlib: A 2D Graphics Environment, *Computing in Science & Engineering*, *9*, 90–95, 2007.

Ichinose, G. A., H. K. Thio, P. G. Somerville, T. Sato, and T. Ishii, Rupture process of the 1944 Tonankai earthquake (M s 8.1) from the inversion of teleseismic and regional seismograms, *Journal of Geophysical Research*, *108*, 2497, 2003.

Ikari, M. J., M. Strasser, D. M. Saffer, and A. J. Kopf, Submarine landslide potential near the megasplay fault at the Nankai subduction zone, *Earth and Planetary Science Letters*, *312*, 453–462, 2011.

Ike, T., G. F. Moore, S. Kuramoto, J.-O. Park, Y. Kaneda, and A. Taira, Variations in sediment thickness and type along the northern Philippine Sea Plate at the Nankai Trough, *Island Arc*, *17*, 342–357, 2008.

Ito, Y., and K. Obara, Very low frequency earthquakes within accretionary prisms are very low stress-drop earthquakes, *Geophysical Research Letters*, *33*, 1–4, 2006a.

Ito, Y., and K. Obara, Dynamic deformation of the accretionary prism excites very low frequency earthquakes, *Geophysical Research Letters*, *33*, 0–3, 2006b.

Ito, Y., Y. Asano, and K. Obara, Very-low-frequency earthquakes indicate a transpressional stress regime in the Nankai accretionary prism, *Geophysical Research Letters*, *36*, 2–6, 2009.

Jones, E., T. Oliphant, P. Peterson, and S. Developers, SciPy: Open Source Scientific Tools for Python, 2001.

Kamei, R., R. G. Pratt, and T. Tsuji, Waveform tomography imaging of a megasplay fault system in the seismogenic Nankai subduction zone, *Earth and Planetary Science Letters*, *317-318*, 343–353, 2012.

Kerr, H., N. White, and J.-P. Brun, An Automatic Method for Determining Three-Dimensional Normal Fault Geometries, *Journal of Geophysical Research*, *98*, 17,837–17,857, 1993.

Kimura, G., G. F. Moore, M. Strasser, E. Screaton, D. Curewitz, C. Streiff, and H. Tobin, Spatial and temporal evolution of the megasplay fault in the Nankai Trough, *Geochemistry Geophysics Geosystems*, *12*, 1–23, 2011.

Kington, J. D., mplstereonet - Lower-hemisphere Stereonets for Matplotlib https://github.com/joferkington/mplstereonet, 2012a.

Kington, J. D., fault_kinematics - A simple 3D fault kinematics library for Python https://github.com/joferkington/fault_kinematics, 2012b.

Kington, J. D., H. J. Tobin, and G. Moore, Along-strike Influence of Subducting Basement Topography : Structural Evolution of the Nankai Trough Accretionary Prism in the Kumano Basin Region, Ch. 2.

Kinoshita, M., et al., NanTroSEIZE Stage 1: investigations of seismogenesis, Nankai Trough, Japan, *Proceedings of the Integrated Ocean Drilling Program*, *314/315/31*, 2009.

Kitamura, Y., T. Kanamatsu, and X. Zhao, Structural evolution in accretionary prism toe revealed by magnetic fabric analysis from IODP NanTroSEIZE Expedition 316, *Earth and Planetary Science Letters*, *292*, 221–230, 2010.

Kodaira, S., Cyclic ridge subduction at an inter-plate locked zone off central Japan, *Geophysical Research Letters*, *30*, 1–4, 2003.

Lallemand, E., Effects of Oceanic Ridge Subduction on Accretionary Wedges: Experimental Modeling and Marine Observations, *11*, 1301–1313, 1992.

Lallemand, S., and X. L. Pichon, Geology Coulomb wedge model applied to the subduction of seamounts in the Japan Trench, *Geology*, *15*, 1065–1069, 1987.

Lallemant, S., N. Chamot-Rooke, X. Le Pichon, and C. Rangin, Zenisu Ridge : a deep intraoceanic thrust related to subduction , off Southwest Japan, *Science*, *160*, 1989.

Landmark, GeoProbe Volume Interpretation Software, 2003.

Lay, T., C. J. Ammon, H. Kanamori, L. Xue, and M. J. Kim, Possible large near-trench slip during the 2011 M w 9.0 off the Pacific coast of Tohoku Earthquake, *Earth, Planets and Space*, *63*, 687–692, 2011.

Le Pichon, X., S. Lallemant, H. Tokuyama, F. Thoue, P. Huchon, and P. Henry, Structure and evolution of the backstop in the eastern Nankai Trough area (Japan): Implications for the soon-to-come Tokai earthquake, *The Island Arc*, *5*, 440–454, 1996.

Lisle, R., T. Orife, and L. Arlegui, A stress inversion method requiring only fault slip sense, *Journal of Geophysical Research*, *106*, 2281–2289, 2001.

Liu, Z., S. Owen, D. Dong, P. Lundgren, F. Webb, E. Hetland, and M. Simons, Estimation of interplate coupling in the Nankai trough, Japan using GPS data from 1996 to 2006, *Geophysical Journal International*, pp. 1313–1328, 2010.

Loveless, J. P., and B. J. Meade, Geodetic imaging of plate motions, slip rates, and partitioning of deformation in Japan, *Journal of Geophysical Research*, *115*, 1–35, 2010.

Marrett, R., and R. W. Allmendinger, Kinematic analysis of fault-slip data, *Journal of Structural Geology*, *12*, 973–986, 1990.

Marshak, S., and G. Mitra, *Basic Methods in Structural Geology*, Prentice-Hall, 1988.

Martin, K. M., S. P. S. Gulick, N. L. B. Bangs, G. F. Moore, J. Ashi, J.-O. Park, S. Kuramoto, and A. Taira, Possible strain partitioning structure between the Kumano fore-arc basin and the slope of the Nankai Trough accretionary prism, *Geochemistry Geophysics Geosystems*, *11*, 1–15, 2010.

Michael, A. J., Determination Of Stress From Slip Data: Faults And Folds, *Journal of Geophysical Research*, *89*, 11,517–11,526, 1984.

Moore, G. F., T. H. Shipley, P. L. Stoffa, D. E. Karig, A. Taria, S. Kuramoto, H. Tokuyama, and K. Suyehiro, Structure of the Nankai Trough Accretionary Zone from Multichannel Seismic Reflection Data, *Journal of Geophysical Research*, *95*, 8753–8765, 1990.

Moore, G. F., N. L. Bangs, A. Taira, S. Kuramoto, E. Pangborn, and H. J. Tobin, Three-dimensional splay fault geometry and implications for tsunami generation., *Science*, *318*, 1128–31, 2007.

Moore, G. F., D. Saffer, M. Studer, and P. Costa Pisani, Structural restoration of thrusts at the toe of the Nankai Trough accretionary prism off Shikoku Island, Japan: Implications for dewatering processes, *Geochemistry Geophysics Geosystems*, *12*, 1–15, 2011.

Moore, G. F., et al., Structural and seismic stratigraphic framework of the NanTroSEIZE Stage 1 transect, *Proceedings of the Integrated Ocean Drilling Program*, *314/315/31*, 2009.

Moore, J. C., and D. Saffer, Updip limit of the seismogenic zone beneath the accretionary prism of southwest Japan: an effect of diagenetic to low-grade metamorphic processes and increasing effective stress, *Geology*, *29*, 183–186, 2001.

Morgan, J. K., and D. E. Karig, Kinematics and a balanced and restored cross-section across the toe of the eastern Nankai accretionary prism, *Journal of Structural Geology*, *17*, 31–45, 1995.

Nakanishi, A., S. Kodaira, S. Miura, A. Ito, T. Sato, J.-O. Park, Y. Kido, and Y. Kaneda, Detailed structural image around splay-fault branching in the Nankai subduction seismogenic zone: Results from a high-density ocean bottom seismic survey, *Journal of Geophysical Research*, *113*, 1–14, 2008.

Olafsson, G., Calcareous Nannofossil Biostratigraphy of the Nankai Trough, *Proceedings of the Ocean Drilling Program, Scientific Results*, *131*, 1993.

Oliphant, T., Python for Scientific Computing, *Computing in Science & Engineering*, *9*, 10–20, 2007.

Pacheco, J., and L. Sykes, Seismic moment catalog of large shallow earthquakes, 1900 to 1989, *Bulletin of the Seismological Society of America*, *82*, 1306, 1992.

Park, J., T. Tsuru, Y. Kaneda, Y. Kono, S. Kodaira, N. Takahashi, and H. Kinoshita, A subducting seamount beneath the Nankai Accretionary Prism off Shikoku, southwestern Japan, *Geophysical Research Letters*, *26*, 931, 1999.

Park, J.-O., T. Tsuru, S. Kodaira, P. R. Cummins, and Y. Kaneda, Splay fault branching along the Nankai subduction zone., *Science*, *297*, 1157–60, 2002.

Park, J.-O., G. F. Moore, T. Tsuru, S. Kodaira, and Y. Kaneda, A subducted oceanic ridge influencing the Nankai megathrust earthquake rupture, *Earth and Planetary Science Letters*, *217*, 77–84, 2003.

Park, J.-O., et al., A low-velocity zone with weak reflectivity along the Nankai subduction zone, *Geology*, *38*, 283–286, 2010.

Pickering, K. T., M. B. Underwood, A. Taira, and P. Sea, Stratigraphic Synthesis of the DSDP-ODP Sites in the Shikoku Basin, Nankai Trough, and Accretionary Prism, *Proceedings of the Ocean Drilling Program, Scientific Results*, *131*, 1993.

Pollard, D., S. Saltzer, and A. Rubin, Stress inversion methods: are they based on faulty assumptions?, *Journal of Structural Geology*, *15*, 1045–1054, 1993.

Powell, M., An efficent method for finding the minimum of a function of several variables without calculating derivatives, *The Computer Journal*, *7*, 155–162, 1964.

Ruff, L., Do Trench Sediments Affect Great Earthquake Occurrence in Subduction Zones?, *Pure and Applied Geophysics*, *129*, 263—-282, 1989.

Saffer, D., L. McNeil, T. Byrne, E. Araki, S. Toczko, N. Eguchi, K. Takahashi, and E. . Scientists, NanTroSEIZE Stage 2: NanTroSEIZE Riser/Riserless Observatory, *Proceedings of the Integrated Ocean Drilling Program*, *319*, 2010.

Saffer, D. M., Hydrostratigraphy as a control on subduction zone mechanics through its effects on drainage: an example from the Nankai Margin, SW Japan, *Geofluids*, pp. 114–131, 2010.

Scientists, E. ., Expedition 314 Site C0002, *Proceedings of the Integrated Ocean Drilling Program*, *314*, 2009.

Scientists, E. ., IODP Expedition 333 Preliminary Report, *IODP Preliminary Reports*, *333*, 2011.

Scientists, E., Expedition 319 summary, *Proceedings of the Integrated Ocean Drilling Program*, *319*, 2010.

Screaton, E., D. Saffer, P. Henry, S. Hunze, and L. . S. S. Party, Porosity loss within the underthrust sediments of the Nankai accretionary complex: Implications for overpressures, *Geology*, *30*, 19–22, 2002.

Screaton, E., et al., Interactions between deformation and fluids in the frontal thrust region of the NanTroSEIZE transect offshore the Kii Peninsula, Japan: Results from IODP Expedition 316 Sites C0006 and C0007, *Geochemistry Geophysics Geosystems*, *10*, 2009.

Seno, T., S. Stein, and A. Gripp, A Model for the Motion of the Philippine Sea Plate Consistent with NUVEL-1 and Geologic Data, *Journal of Geophysical Research*, *98*, 17,941–17,948, 1993.

Song, I., D. M. Saffer, and P. B. Flemings, Mechanical characterization of slope sediments: Constraints on in situ stress and pore pressure near the tip of the megasplay fault in the Nankai accretionary complex, *Geochemistry Geophysics Geosystems*, *12*, 1–20, 2011.

Strasser, M., G. F. Moore, and E. J. Screaton, Slumping and mass transport deposition in the Nankai fore arc: Evidence from IODP drilling and 3-D reflection seismic data, *Geochemistry Geophysics Geosystems*, *12*, 1–24, 2011.

Strasser, M., et al., Origin and evolution of a splay fault in the Nankai accretionary wedge, *Nature Geoscience*, *2*, 2009.

Suppe, J., Geometry and kinematics of fault-bend folding, *American Journal of Science*, *283*, 684–721, 1983.

Tabei, T., M. Hashimoto, S. Miyazaki, and Y. Ohta, -day deformation across the southwest Japan arc: Oblique subduction of the, *Earth Planets Space*, *55*, 643–647, 2003.

Taira, A., and D. Curewitz, *CDEX Technical Report, Volume 1: Nankai Trough Seismogenic Zone Site Survey, Philippine Sea, Offshore Kii Peninsula, Japan*, Japan Agency for Marine-Earth Science and Technology, 2005.

Tanioka, Y., and K. Satake, Coseismic slip distribution of the 1946 Nankai earthquake and aseismic slips caused by the earthquake, *Earth Planets Space*, *53*, 235–241, 2001a.

Tanioka, Y., and K. Satake, Detailed coseismic slip distribution of the 1944 Tonankai earthquake estimated from tsunami waveforms, *Geophys. Res. Lett*, *28*, 1075–1078, 2001b.

Tobin, H., et al., NanTroSEIZE Stage 1 expeditions: Introduction and synthesis of key results, *Proceedings of the Integrated Ocean Drilling Program*, *314/315/31*, 2009.

Tobin, H. J., and M. Kinoshita, NanTroSEIZE: The IODP Nankai Trough Seismogenic Zone Experiment, *Scientific Drilling*, pp. 23–27, 2006.

Tobin, H. J., and D. M. Saffer, Elevated fluid pressure and extreme mechanical weakness of a plate boundary thrust, Nankai Trough subduction zone, *Geology*, *37*, 679–682, 2009.

Tsuji, T., J. Dvorkin, G. Mavko, N. Nakata, T. Matsuoka, A. Nakanishi, S. Kodaira, and O. Nishizawa, Vp/Vs ratio and shear-wave splitting in the Nankai Trough seismogenic zone: Insights into effective stress, pore pressure, and sediment consolidation, *Geophysics*, *76*, 2011.

Twiss, R. J., and J. R. Unruh, Analysis of fault slip inversions: Do they constrain stress or strain rate, *J. Geophys. Res.-Solid Earth*, *103*, 12,205–12,222, 1998.

Underwood, M. B., S. Saito, Y. Kubo, and E. Scientists, Expedition 322 summary, *Proceedings of the Integrated Ocean Drilling Program*, *322*, 2010.

van Rossum, G., and F. L. Drake, Python Reference Manual, 2006.

von Huene, R., and D. Scholl, Observations at convergent margins concerning sediment subduction, subduction, *Rev. Geophys*, pp. 279–316, 1991.

von Huene, R., C. R. Ranero, and P. Vannucchi, Generic model of subduction erosion, *Geology*, *32*, 913, 2004.

Wang, K., and Y. Hu, Accretionary prisms in subduction earthquake cycles: The theory of dynamic Coulomb wedge, *Journal of Geophysical Research*, *111*, 2006.

Watts, A., A. Koppers, and D. Robinson, Seamount subduction and earthquakes, *Oceanography*, *23*, 166–173, 2010.

White, N., J. Jackson, and D. McKenzie, The relationship between the geometry of normal faults and that of the sedimentary layers in their hanging walls, *Journal of Structural Geology*, *8*, 897–909, 1986.

Woodward, N. B., S. E. Boyer, and Suppe, Balanced Geological Cross-Sections:, *Short Courses in Geology*, *6*, 1989.

Zang, S. X., Q. Y. Chen, J. Y. Ning, Z. K. Shen, and Y. G. Liu, Motion of the Philippine Sea plate consistent with the NUVEL-1A model, *Geophysical Journal International*, *150*, 809–819, 2002.